Abstract

Title of document:	COMBINED EFFECTS OF SUNLIGHT AND TITANIUM DIOXIDE NANOPARTICLES ON DIETARY ANTIOXIDANTS AND FOOD COLORS
Directed By:	Y. Martin Lo, Ph.D., Department of Nutrition and Food Science, University of Maryland, College Park

The breakthroughs in material science have enabled industrialized fabrication and production of nanomaterials. To date, nanoscale materials have been shown to exhibit improved functionalities, providing numerous novel applications. Titanium dioxide (TiO_2) nanomaterials have been widely utilized in the food industry due to their unique properties under light. Upon light irradiation, TiO_2 nanoparticles (NPs) generate highly active reactive oxygen species (ROS) therefore can be potentially used as light tunable antibacterial packaging materials. Moreover, it has also been reported that a considerable amounts of TiO_2 NPs is found as an ingredient in food, cosmetics, personal care, and pharmaceutical products. With improved photoactivity, nano TiO_2 generates higher amounts of ROS upon light irradiation that can result in oxidative damage. The present study investigates the combined effect of sunlight irradiation and TiO_2 nanoparticles (NPs) on sensitive antioxidants and food colors. Upon simulated sunlight irradiation, TiO_2 NPs weakened the radical scavenging ability of antioxidants by photocatalytic decomposition or surface adsorption. The decomposition of a widely used food azo dye FD&C Yellow No. 5 (tartrazine) by sunlight activated TiO_2 NPs was also investigated.

The mechanism is pH dependent, involving the depletion of two main ROS species, hydroxyl radical and singlet oxygen. Compared with the photocatalyst TiO_2 sample P25, food-grade TiO_2 NPs also showed strong ROS promoting ability and resulted in the degradation of selected synthetic dyes, including tartrazine, allura red and sunset yellow, as well as the semi-synthetic food color chlorophyllin sodium copper salt. Thus, TiO_2 NPs should be used with caution when added to or used in contact with food ingredients that depend solely on the existing antioxidants and colors in the system. The ability of TiO_2 to generate ROS was found to be phase-dependent. The rutile phase TiO_2 generated the least amount of ROS when compared to anatase phase and did not lead to noticeable color degradation in the studied light irradiation period. Thus, when possible, rutile phase TiO_2 should be used in food as it provides a more stable system compared to anatase and mixed phases. The results in this study provide clear insights on setting up proper protocols for evaluating and administrating nanosized TiO_2 in food uses.

COMBINED EFFECTS OF SUNLIGHT AND TITANIUM DIOXIDE NANOPARTICLES ON DIETARY ANTIOXIDANTS AND FOOD COLORS

By

Meng Li

Dissertation submitted to the Faculty of the Graduate School of the
University of Maryland, College Park, in partial fulfillment
of the requirements for the degree of
Doctor of Philosophy
2014

Advisory Committee:
Dr. Y. Martin Lo, Chair
Dr. Abani K. Pradhan
Dr. Jun-Jie Yin
Dr. Thomas W. Castonguay
Dr. Yang Tao, Dean's Representative

Acknowledgements

Patricia Cross once said: “ The tough problem is not in identifying winners, it is making winners out of ordinary people”. Therefore, I gratefully thank my advisor Dr. Y. Martin Lo, for picking me up at the starting line and supporting me all the way to the finishing point. I would love to express my genuine gratitude for his continuous encouragement, for opening a door to the magic world of food science, and for making all my achievements possible. I am also very grateful to Dr. Jun-Jie Yin, senior research scientist at CFSAN/FDA, for his guidance on my entire project. His passion and dedication to science has always inspired me throughout my graduate career. I would like to thank the members of my dissertation committee, Dr. Thomas W. Castonguay, Dr. Abani K. Pradhan and Dr. Yang Tao, for their precious advice and direction. In addition, I am thankful to Dr. Wayne Wamer, Dr. Adrian Weisz, Dr. Weiwei He and Dr. Yi Liu, for their invaluable suggestions and comments towards my research.

I want to thank my dear labmates: Melody Ge, Haohao Wu, Dr. Yuting Zhou, Armin Norouzi, Dr. Maryam Ganjavi, Dr. Setareh Shiroodi, Dr. Arpita Mondal, Elizabeth Beck, Dr. Tong Liu, Audrey Chia Kuei and Dr. Eirene Yossa. Thank you for the great time we had, for the happiness (I mean pizza) you shared with me, for being friends and family. I would like to extend my gratitude to the faculty members and staffs in the Department of Nutrition and Food Science for all that I have learned.

Finally, I thank my mom, April Ming Zhang, the most elegant, beautiful and powerful woman in the world, for everything. I thank my family and dearest friends who are always there for me during my whole life.

Table of Contents

List of Figures

In Appendix

Abbreviations

•OH	Hydroxyl radicals
•OOR	Peroxyl radical
^{15}N-PDT	^{15}*N*-labeled 4-oxo-2,2,6,6-tetramethylpiperidine-d16-1-oxyl
$^{1}O_2$	Singlet oxygen
4-oxo-TEMP	4-oxo-2,2,6,6-tetramethyl-2-piperidone
8-OH-G	8-hydroxyguanine
AA	Ascorbic acid
AN	Anatase TiO_2 powder
AR	Allura Red
BMPO	5-methyl-1-pyrroline N-oxide
Bruker AXS	Bruker D8-Advance Diffractometer
$C_6H_7O_2$	Dihydroxyphenyl group
CAT	Catalase
CCS	chlorophyllin sodium copper salt
CFR	Code of Federal Regulations
$CHCN_3$	Acetonitrile
CPH	1-Hydroxy-3-carboxy-2,2,5,5-Tetramethylpyrrolidine
Cyst	Cysteine
DCF-DA	2′,7′-dichlorodihydrofluorescein diacetate
DEPMPO	5-diethoxyphosphoryl-5-methyl-1-pyrroline-N-oxide
DMPO	5,5-dimethyl-1-pyrroline N-oxide
DPPH•	1,1-diphenyl-2-picryl-hydrazyl radical
DPPH•	DPPH radical
e^-	Electrons
$e^{-\bullet}/h^+$	An electron-hole pair
EC	Epicatechin
ECG	Epicatechin gallate
EDS	Electron dispersive spectrum
EDX	Energy-dispersive X-ray analysis
EPR	Electron paramagnetic resonance
ESI	Electrospray ionization
ESR	Electron spin resonance
EU	European Union
FG	The food ingredient TiO_2 powder
GSH	Glutathione
h^+	Holes
H_2O_2	Hydrogen peroxide
HRTEM	High resolution TEM
HSA	Human serum albumin
HTMP	4-hydroxy-2,2,6,6-tetramethylpiperidine

MDA	Malondialdehyde
MY5	Tartrazine
NH_4OAc	Ammonium acetate
NNI	National Nanotechnology Initiative
NPs	Nanoparticles
$O^{2-\bullet}$	Superoxide radicals
P25	TiO_2 P25 powder
PBN	α-phenyl-N-tert-butylnitrone
POBN	α-(4-pyridyl-1-oxide)-N-tert-butylnitrone
PPH	4-phosphonooxy-2,2,6,6-Tetramethylpiperidine-N-hydroxyl
redox	Reduction-oxidation
ROS	Reactive oxygen species
RU	Rutile TiO_2
RV	Resveratrol
SOD	Superoxide dismutase
SOD	Superoxide dismutase
SY	Sunset Yellow
TEM	Transmission electron microscopy
TEMP	2,2,6,6-tetramethyl-4-piperidone
TEMPO	2,2,6,6-tetramethylpiperidine 1-oxyl
TEMPOH	Hydroxyl amine
TEMPONE	4-oxo-2,2,6,6-tetramethylpiperidine-N-oxyl
TEMPONE	2, 2, 6, 6-tetramethylpiperidine-N-oxyl
TEMPONE	paramagnetic 2, 2, 6, 6-tetramethyl-4-piperidone-1-oxyl
TiO_2	Titanium dioxide
TiO_2 NPs	Titanium dioxide nanoparticles
TMPD	2, 2, 6, 6-tetramethyl-4-piperidone
TMPol	2,2,6,6-tetramethyl-4-piperidinol
TZ	tartrazine
UV	ultraviolet
VE	α-tocopherol
XAN	Xanthine
XOD	Xanthine oxidase
XRD	X-ray differaction

Chapter 1 Introduction

Nanotechnology is an interdisciplinary science involving the production, engineering, fabrication, and application of materials less than 100 nm in at least one dimension. The breakthroughs in nanotechnology in the last few decades have largely influenced variety of fields, including electronic engineering, medical care and medicine, sustainable energy production, environmental remediation, transportation, communication (Buzea et al., 2007), as well as agriculture and food systems (Scott & Chen, 2012). The vast potential of nanotechnology has encouraged the burgeoning interests in the research area. In 2014 alone, more than $1.7 billion US federal budget has been provided to the National Nanotechnology Initiative (NNI) for nanotechnology related research (NNI, 2014). The data from 2008 estimated that the governments of the European Union (EU) and Japan invested approximately $1.7 billion and $950 million, respectively, in nanotechnology research and development. The governments of China, Korea, and Taiwan also invested approximately $430 million, $310 million, and $110 million, respectively (Roco et al., 2011). Being a new technology that is still at an emerging stage, commercialization of nanotechnology appears to be growing at a fast pace alongside the evolution in science. To date, 1,628 commercial products that rely on the utilization of nanoscale materials already exist in the market, among which 194 are food products. These trends suggest that the number of nanotechnology products worldwide will double every three years, achieving a $3 trillion market by 2020 (Roco et al., 2011).

The possible benefits associated with nanotechnology have been recognized in almost every step of the food supply chain, including agricultural production, food processing, packaging and storage, distribution as well as home preparation. Those examples include

agrochemical delivery (Ghormade et al., 2007), pesticide detection based on nanomaterials (Vamvakaki et al., 2007), food detection methods such as ELISA & PCR, food packaging (Echegoyen & Nerin, 2013), as well as improvements in nutrient and bioactive delivery systems including encapsulation and emulsification (Magnuson et al., 2011; Sumithra & Vasugi 2012). Nanoparticles, including titanium dioxide, zinc oxide and nano-silver, and, have been incorporated into food packaging for their antibacterial or UV protection.

One of the most important intrinsic characteristics of nanoparticles is their reduced size and increased surface area. The change in size to nanoscale renders dramatic changes in physical and chemical properties of material. When the size of a material is reduced to nanoscale, its physical and chemical properties are dramatically different from the bulk material with the same substance (Sharma et al., 2003). Among those applications, direct addition of engineered nanoparticles to food products receives lots of attention, mainly because of the elevated concerns over food safety and public health. However, there remains a void in the literature on the interaction between nanosized ingredients and other active compounds in food and/or other consumer products. Such information is critical in ushering new applications for nanomaterials as well as establishing proper protocols for risk assessments of nanotechnology.

Chapter 2 Literature review

Adapted from Li, M., Yin, J.-J., Wamer, W. G., Li, M., & Lo, Y. M.,
Mechanistic characterization of titanium dioxide nanoparticle-induced toxicity using electron spin resonance. *Journal of Food and Drug Analysis, 22,* 1, 76-85.

2.1 Introduction

Titanium dioxide nanoparticles (TiO_2 NPs) have been widely applied as a coloring agent to provide whiteness and/or opacity in paints, personal care products, as well as being used as a food additive and a drug delivery agent. Moreover, due to their excellent ultraviolet (UV) absorbance and deflecting properties, TiO_2 NPs are a commonly used functional ingredient in cosmetics or skincare products to provide protection against sunlight. In environmental engineering, titanium dioxide nanocomposites have been employed as a photocatalyst in water pollutant purification and hazardous chemical detoxification. When exposed to UV light, TiO_2 NPs absorb photons having an energy equal to or higher than its band gap (> 3.0 eV), exciting electrons in the valence band to the conduction band. Photoexcitation, therefore, results in an increased number of conduction band electrons, and consequently increased valence band holes. Electrons in the conduction band interact can reduce substrates in the chemical environment, e.g. reduction of oxygen results in the formation of superoxide radical anion. Holes in the valence band can oxidize substrates such as water or hydroxide ions and generate hydroxyl radicals (•OH) (Chen & Mao, 2007; Yin et al., 2012). Photocatalyzed chemical decomposition usually involves formation of reactive oxygen species (ROS), including superoxide radicals ($O^{2-\bullet}$) and singlet oxygen ($^1O_2$) (Nosaka et al., 2004), as well as other intermediate species such as H_2O_2 or O_2 (Chen & Mao, 2007). Because of those highly

reactive free radicals generated during UV irradiation, engineered TiO_2 NPs have also been recognized for their light-induced biocidal effects against a broad range of harmful microorganisms, including bacteria such as *Escherichia coli* (Wu et al., 2010), molds, such as *Aspergillus niger* (Yu et al., 2013), as well as protozoa such as *Giardia and Acanthamoeba* species (Sökmen et al., 2008).

Exposure to ROS derived from photoexcited TiO_2 NPs has raised concerns because ROS are believed to play an important role in many inflammatory skin disorders, skin aging, and cancer formation (He et al., 2005). Due to the ability of nano-TiO_2 to induce ROS generation when irradiated, tremendous efforts have been focused on investigating potential risks associated with human exposure to TiO_2 NPs. In addition to direct exposure through consumption of products containing TiO_2 NPs, inhalation of nanoparticles in the workplace, or through other environmental sources are possible exposure routes (e.g. emitted nanomaterials that reach the land can potentially contaminate soil and migrate to water systems) (Ray et al., 2009). To date, various nanomaterial studies have linked toxicity to the production of ROS. It is well known that generation of intercellular ROS can lead to oxidative stress, resulting in inflammation, immune response, cellular damage, and genotoxicity (Tournebize et al., 2013).

Free radicals, including ROS, are very short-lived entities, making them very difficult to detect when evaluating toxicity associated with oxidative stress. Electron spin resonance (ESR, aka EPR, electron paramagnetic resonance) has been recognized as a "gold standard" and state-of-the-art tool for detecting and quantifying ROS in chemical and biological systems. Another ESR technique, ESR oximetry, has been used to monitor lipid peroxidation induced by highly reactive radicals. This article summarizes the

advantages and recent developments using ESR as a tool to unravel the mechanism of nano-TiO_2 induced cytotoxicity and phototoxicity. In addition, immuno-spin trapping, another methodology based on the spin trapping technique to detect protein or DNA radicals, is briefly introduced. Combination of immune-spin trapping with ESR spin trapping and ESR oximetry can provide deep insight into the mechanism of ROS generation triggered by nanomaterials, as well as the subsequent oxidative damage to proteins, DNA, and lipids.

2.2 Electron spin resonance

2.2.1 ESR spin trapping

Electron spin resonance (ESR) is a spectroscopic technique used to detect chemical species with unpaired electrons. ESR has been recognized as the least ambiguous method for characterizing free radicals. Due to its high sensitivity and the ability to identify the generation of radicals *in-situ*, ESR spin trapping technique is commonly employed in nanoscience research to evaluate both the ROS scavenging capability of nanomaterials with regards to their potential applications in health promotion and cancer chemotherapy (Yin & Fu, 2009), and to investigate toxicities related to ROS generation. ESR spectroscopy has also been used for the validation of results obtained using other methods. For instance, the data from ESR spectroscopy using different spin probes 1-Hydroxy-3-carboxy-2,2,5,5-Tetramethylpyrrolidine (CPH) and 4-phosphonooxy-2,2,6,6-tetramethylpiperidine-N-hydroxyl (PPH) showed good agreement with the data from confocal fluorescence imaging using different dyes, including 2′,7′-dichlorodihydrofluorescein diacetate (DCF-DA), MitoSOX™, and MitoTracker® red

CM-H_2XRos (Kuznetsov et al., 2011). Moreover, the development of non-toxic spin traps makes it possible for the detection of free radicals both *in vivo* (Tada et al., 2004) and *ex vivo* (Guarini et al., 1996).

ROS are low-level and short-lived free radicals. They are difficult to determine in chemical and biological systems. Spin trapping agents are therefore employed to intercept the target free radical and to form a relatively stable and distinguishable spin adduct that can be quantified and identified by ESR spectroscopy (Yin & Fu, 2009). Based on their characteristic structures, spin traps can be divided into two groups: nitroso and nitrone. Nitroso spin traps are less readily used in biological studies because of high reactivity of their C-nitroso group (Kalyanaraman et al., 1979). The most commonly used nitrone spin traps include 5,5-dimethyl-1-pyrroline N-oxide (DMPO), α-phenyl-N-tert-butylnitrone (PBN) α-(4-pyridyl-1-oxide)-N-tert-butylnitrone (POBN), and 5-diethoxyphosphoryl-5-methyl-1-pyrroline-N-oxide (DEPMPO). The spin label probes 2,2,6,6-tetramethyl-4-piperidone (TEMP) and 4-oxo-2,2,6,6-tetramethyl-2-piperidone (4-oxo-TEMP) have been employed to detect singlet oxygen (Lion et al., 1976). The reaction of $^1O_2$ with 4-oxo-TEMP leads to the formation of a nitroxide radical 4-oxo-2,2,6,6-tetramethylpiperidine-N-oxyl (TEMPONE) that exhibiting a stable triplet ESR spectrum (Eq (1)):

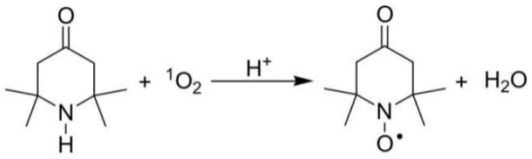

4-oxo-TEMP TEMPONE (1)

In comparison with other nitrone spin traps, DMPO is generally preferable because of its low redox activity and the ability to yield ESR spectra that are highly dependent on the radical species. However, a major drawback of DMPO is that the decomposition of DMPO/$O^{2-\bullet}$ to DMPO/•OH makes it difficult to distinguish between the formation of $O^{2-\bullet}$ and •OH (Yin et al., 2012). On the other hand, 5-methyl-1-pyrroline N-oxide (BMPO) provides an ideal solution to this problem because of the formation of a more stable BMPO/$O^{2-\bullet}$ adduct that does not decompose to BMPO/•OH (Noda et al., 1999). BMPO/•OH has an ESR spectrum similar to that of DMPO/•OH, exhibiting a characteristic set of four lines (1:2:2:1) (Yin et al., 2012). Another method to further distinguish whether the signal is from DMPO/•OH or DMPO/$O^{2-\bullet}$ spin adduct is to observe the effects of superoxide dismutase (SOD) (Wang et al., 2013) or mannitol on the ESR spectrum (Reeves et al., 2008). Since the former only scavenges $O^{2-\bullet}$, while the latter only reacts with •OH, the predominant species (•OH or $O^{2-\bullet}$) in the system can be determined by observing changes of the ESR spectra.

2.2.2 ESR spin label oximetry

As aforementioned, ESR spectroscopy detects molecules with unpaired electrons. Theoretically, the direct detection of molecular oxygen by ESR is possible because molecular oxygen is a triplet radical that possesses two unpaired electrons. However, the broadening of lines in the spectrum of oxygen in biological systems makes oxygen undetectable by ESR. This problem has been solved using a stable free radical (usually non-toxic) as a spin label in ESR oximetry (Gallez et al., 2004). ESR oximetry is based on the changes observed in the ESR spectrum of the spin label produced by collisions with molecular oxygen. ESR oximetry allows monitoring oxygen

consumption/formation in a dynamic system. Collision of the spin label with O_2 produces a spin exchange, resulting in shorter relaxation times (both T_1 and T_2) and ESR signals with broader line widths and decreasing peak height. The line broadening is caused by Heisenberg exchange between the spin label and molecular oxygen dissolved in solution (Gallez et al.,. 2004). Measurements that depend on T_1 and T_2 can both offer a direct indication of the O_2 concentration. Because it is more easily measured experimentally, investigators primarily examine changes in T_2-sensitive line width rather than T_1-sensitive saturation recovery for ESR oximetry (Altenbach et al., 1989).

ESR spin label oximetry has been applied extensively to study biological processes involving the participation of oxygen, including measuring cellular respiration rate (James et al., 1995), studying O_2 concentration across the cell plasma (Yin et al., 1999), and the detection of lipid peroxidation. It has been suggested that this method is more sensitive than the traditional thiobarbituric acid assay, especially in very early stages of lipid peroxidation (Hyde & Subczynski, 1989). It is well recognized that lipid peroxidation proceeds as a chain reaction involving continuous depletion of O_2. Thus, oxygen consumption by such mechanisms can be a direct indicator of the peroxidation rate and can be observed as a reduction in line widths and increase in peak height for the spin label. Since the area beneath the signal intensity vs. magnetic field curve remains constant, the narrowing of the ESR signal is necessarily accompanied by an increase in the peak height of the ESR spectrum (Yin et al., 2012). Therefore, the value of oxygen concentration can be obtained from a calibrated curve of the ESR line width vs. the oxygen concentration (Yin et al., 2012).

2.3 TiO_2 NPs and reactive oxygen species

2.3.1 Photogeneration of ROS

Reactive oxygen species are a group of highly reactive molecules that are intermediate products of cellular oxidative metabolism. Biologically relevant ROS include singlet oxygen ($^1O_2$), peroxides (e.g. hydrogen peroxide), and free radicals (e.g. superoxide radical ($O_2^{-\bullet}$), peroxylradical (•OOR) and hydroxyl radical (•OH)). ROS play critical roles in a variety of physiological processes in plants and animals with regard to regulation of the immune system and the development of the inflammatory response, activation of transcription factors and gene expression, and modulation of programmed cell death (i.e. apoptosis) (Brieger et al., 2012; Hancock et al., 2011). Excessive levels of ROS can oxidize cell constituents such as lipids, proteins, and DNA, and consequently pose a threat to cell integrity (Scherz-Shouval & Elazar, 2011). Mitochondria are one of the main sources of ROS in cells. In the mitochondrial respiratory chain, electrons are continuously transferred to molecular oxygen, producing ROS as a by-product of oxidative phosphorylation (Guzun et al., 2011). With the presence of TiO_2 NPs (10 ug/ml) and UVA, alteration of mitochondrial function was observed for HaCaT cells, accompanied by 14-fold increase in mitochondrial DNA damage, indicated by mitochondrial "common deletion" (Jaeger et al., 2012). Several studies have identified the intercellular oxidative stress caused by ROS as an important factor for genotoxity (Yin et al., 2012), cytotoxicity (Wang et al., 2013; Sarkar et al., 2011; Liu et al., 2010), as well as tissue damage and inflammation (Cui et al., 2011; Sun et al., 2012; Li et al., 2010).

<u>2. 3. 1. 1 Mechanism of ROS generation</u>

Generation of ROS during photoexcited TiO_2 was first discovered in the early 20th century. A study by Goodeve and Kitchener in 1938 described photobleaching of dyes by TiO_2. Photobleaching was attributed generation of active oxygen species on the surface of photoexcited TiO_2. TiO_2 absorbs light in the UVA (320 to 400 nm) and UVB (290 to 320 nm) spectral regions of the terrestrial solar spectrum. When TiO_2 absorbs photons with energy equal to or higher than its band gap (3.0 eV for rutile and 3.2 eV for anatase phase), electrons are excited from the valence band of TiO_2 to its conduction band, resulting in the formation of an electron-hole pair ($e^{-\bullet}/h^{+}$) (Chen & Mao, 2007). The holes (h^{+}) in the valence band are highly oxidizing and can react with H_2O or hydroxide ions to produce hydroxyl radicals (•OH), and the electrons in the conduction band can reduce O_2 to produce superoxide radical anions ($O^{2-\bullet}$) (Hashimoto et al., 2005). This reduction-oxidation (redox) potential of TiO_2 has a significant impact on biological systems. The fundamental process of ROS production involving photo-induced electrons and holes can be expressed as follows (Hashimoto et al., 2005; Dodd & Jha, 2011):

$$TiO_2 + hv \rightarrow e^{-}_{cb} + h^{+}_{vb} \quad (2)$$

$$O_2 + e^{-}_{cb} \rightarrow O^{2-\bullet} \quad (3)$$

$$H_2O + h^{+}_{vb} \rightarrow \bullet OH + H^{+} \quad (4)$$

$$OH^{-} + h^{+}_{vb} \rightarrow \bullet OH \quad (5)$$

$$O^{2-\bullet} + 2H^{+} + e^{-}_{cb} \rightarrow H_2O_2 \quad (6)$$

$$2\,h^{+}_{vb} + 2H_2O \rightarrow H_2O_2 + 2H^{+} \quad (7)$$

Eq. (2) describes the absorption of a photon. Eqs (3-5) are photocatalytic redox pathways involved in the generation of superoxide radical anion and hydroxyl radical. Eqs (6-7) show the possible generation of hydrogen peroxide by reductive (6) or oxidative (7) pathways. Electrons and holes generated during photoexcitation are localized at different defect sites on the surface and in the bulk material (Chen & Mao, 2007). Electron spin resonance is usually used when identifying the charge trapping center formed by UV irradiation of the catalyst (Gopal et al., 2005). The results show that electrons are trapped as Ti(III) centers, while the holes are trapped as oxygen-centered radicals, such as •OH, covalently linked to surface titanium atoms (D'Arienzo et al., 2011; Hurum et al., 2005). However, it remains unclear whether the production of ROS occurs on the surface of the TiO_2 or in the solution (Dodd & Jha, 2011).

2. 3. 1. 2 Hydroxyl and superoxide radicals

The photocatalytic mechanisms and formation of ROS of the photoirradiated TiO_2 NPs have been studied intensively using ESR spectroscopy. It has been suggested that, in general, TiO_2 photocatalytic reactions proceed mainly from the hydroxyl radicals (•OH) by the oxidation of water and superoxide radicals ($O^{2-\bullet}$) produced by the reduction of oxygen (Lipovsky et al., 2012). In aqueous solutions, the formation of •OH spin adducts have been observed using different spin traps, including DMPO, POBN, DEPMPO (Dodd & Jha, 2011), and BMPO (Yin et al., 2012). Hydroxyl radical has been recognized as the most important cause for the photogenotoxicity of TiO_2 NPs (Reeves et al., 2008). In contrast, only a few studies reported positive results on the formation of superoxide radicals (Daimon et al., 2008), while other studies using ESR spectroscopy observed no

evidence of $O^{2-\bullet}$ generation (Yin et al., 2012; Reeves et al., 2008; Dodd & Jha, 2011; Wamer & Yin, 2011).

2. 3. 1. 3 Singlet oxygen

Besides •OH and $O^{2-\bullet}$, several studies also found singlet oxygen generation during photoexcitation of TiO_2 (Nosaka et al., 2012; Yin et al., 2012). The mechanism is rather complicated and unequivocal evidences are suggested by different studies. Sterically hindered cyclic amines, including 2,2,6,6-tetramethyl-4-piperidinol (TMPol) and 2,2,6,6-tetramethyl-4-piperidone (TEMP), can be used to detect $^1O_2$, since they do not react with other oxygen radicals such as •OH and $O^{2-\bullet}$ (Lion et al., 1976; Dzwigaj & Pezerat, 1995). The reaction between these spin traps and singlet oxygen yields stable nitroxide radicals that can be monitored by ESR signals. When using TMPol as the spin trap, Reeves et al. (2008) observed that no singlet oxygen was formed on UVA irradiated TiO_2 NPs in aqueous solutions (Reeves et al., 2008). Another study by the same group of researchers reported similar results (Dodd & Jha, 2011), and argued that false positive results may have been obtained because those amines can be oxidized by other ROS such as •OH (Rosenthal et al., 1987). Interestingly, in a study conducted by Nosaka et al. (2006), electrochemical measurements revealed that sterically hindered cyclic amine 4-hydroxy-2,2,6,6-tetramethylpiperidine (HTMP) can be directly oxidized with holes (h+) in photoexcited TiO_2 to produce the TEMPOL radical. The possibility of other processes, such as reactions with singlet molecular oxygen, superoxide radical, and hydroxyl radical, was excluded from the reaction mechanism in that study.

Konaka et al. (1991) provided evidence for the direct production of singlet oxygen during photoexcitation of TiO_2 using ESR spectroscopy (Konaka et al., 1999). It was noted that the generation of $^1O_2$ originated from direct production rather than a sequential reaction involving $O_2^{\bullet-}$, based on the fact that the addition of DMPO to the reaction mixture amplified the signal of 2,2,6,6-tetramethylpiperidine 1-oxyl (TEMPO), a reaction product of spin probe TEMP and $^1O_2$. However, a completely different result has been found in a later study by Lipovsky et al. (2012) (Reeves et al., 2008). The ESR signal of singlet oxygen (using TEMP as the spin probe) was found to disappear with the addition of DMPO to the suspension of TiO_2 NPs. Under similar experimental conditions (i.e. aerated aqueous TiO_2 NPs suspension), Daimon et al. (2008) confirmed the generation of $^1O_2$ using luminal chemiluminescence probe method (Daimon et al., 2008). It was suggested that the production of $^1O_2$ could be due to an electron transfer process involving $O_2^{-\bullet}$. A two-step mechanism was thus proposed for the $^1O_2$ formation. The first step is a reduction of O_2 to $O_2^{-\bullet}$ using conduction band electrons (e^-), with the second being the oxidation of $O_2^{-\bullet}$ to $^1O_2$ using valence band holes or trapped holes (h+). Using ESR spectroscopy with TEMP as the spin probe, Yin et al. (2012) also observed similar results and successfully detected the formation of $^1O_2$ (Yin et al., 2012). Using BMPO as spin trap, only BMPO/•OH adduct was observed and no ESR signal for BMPO/ $O_2^{-\bullet}$ was found, suggested by the fact that the ESR spectrum of BMPO spin adduct did not change perceptibly when SOD is added (Fig 2-1, C &D). However, this study suggested that part of the $^1O_2$ formation proceeds via a superoxide-dependent mechanism, whereas the •OH formation is not formed via superoxide. This prediction is supported by the observation

that addition of SOD leads to a noticeable reduction of $^1O_2$ signal without effects on •OH-dependent ESR signal (Fig 2-1).

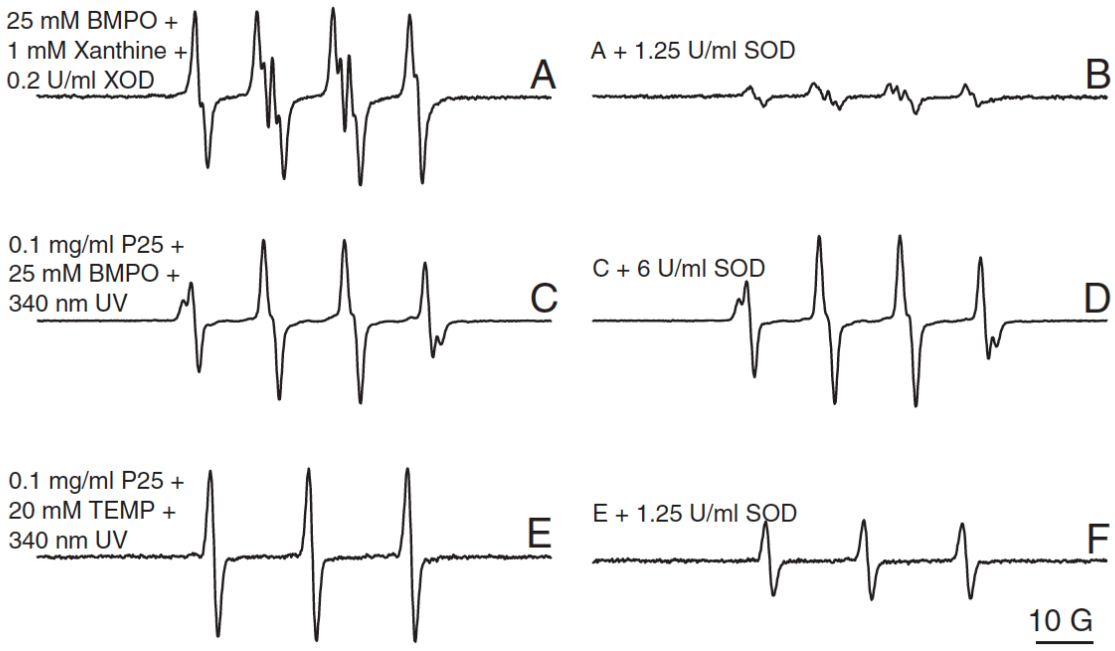

Figure 2-1 Effect of SOD on the generation of hydroxyl radicals and singlet oxygen by P25 during photoexcitation with UVA light. ESR spectra were recorded at ambient temperature 2 min after the UV light was turned on. Samples containing 25 mM BMPO and (A) without TiO_2; (B) with 0.1 mg/ml R100; (C) 0.1 mg/ml A325; (D) 0.1 mg/ml A25; (E) 0.1 mg/ml P25 and (F) same as E, but with the addition of 20% DMSO. Stars (*) indicate the ESR signal of the BMPO/•CH3 adduct. Instrumental settings: microwave power, 10mW; modulation frequency, 100 kHz; modulation amplitude, 1 G; scan range, 100 G. Reprinted with permission from ref 2. Copyright 2012 Toxicology and Applied Pharmacology.

2.3.2 Effects of intrinsic properties on ROS generation

2.3.2.1 Particle size and crystal phase

The photoreactivity of TiO_2 NPs is largely dependent on their inherent material properties, such as their particle size, shape, surface characteristics, and crystal structure (Liu et al., 2010; Sharma, 2009). Generally, nanomaterials exhibit higher reactivity

compared to the corresponding bulk material due to the increased surface area. From this standpoint, TiO_2 NPs with smaller sizes promote more ROS formation when photoexcited, which consequently may elicit more oxidative stress to biological systems (Yin et al., 2012; Nosaka et al., 2004; Xue et al., 2010). Anatase and amorphous forms of nano-TiO_2 show higher phototoxicity and cytotoxicity than its rutile form (Xue et al., 2010; Sanders et al., 2012). Furthermore, the arrangement and coordination of the surface atoms on the different crystal facets largely influence the photocatalytic activity of TiO_2 nanocrystals. Several studies have suggested that the anatase {001} face is associated with higher photocatalytic efficiency due to its highly active titanium and oxygen centers (Ma et al., 2010), whereas others found that the anatase {101} surface exhibited enhanced activity (Nagaveni et al., 2004).

Sayes et al. (2006) conducted a study on toxicity of TiO_2 NPs using human dermal fibroblasts and human lung epithelial cells (Sayes et al., 2006). Their aim was to correlate the crystal structure of nano-TiO_2 with their ability to elicit cytotoxicity and inflammatory responses. Their results suggested that the phase composition of nano-TiO_2 was strongly correlated to cytotoxicity as well as ROS generation. Anatase TiO_2 showed 100 times more cytotoxicity than rutile TiO_2 at the equivalent treatment level. In their study, ROS generation was quantified by measuring azo dye photodegradation. Using a more direct and non-destructive method, ESR spectroscopy, Yin et al. (2012) observed similar results for ROS generation in TiO_2 NPs suspensions (Yin et al., 2012). After UVA irradiation, the intensity of •OH generation for different crystal forms at the same concentration (0.1 mg/mL) followed the trend: P25 (31nm, anatase/rutile) > A25 (< 25nm, anatase) > A235 (325 mesh, anatase), while R100 TiO_2 (<100nm, rutile) in the same aqueous solution did

not show hydroxyl radical production (Yin et al., 2012). The relative efficiency of ROS generation by these four nano-TiO_2 particles was in agreement with the phototoxicity studies using human HaCaT keratinocytes, a transformed epidermal human cell line, further confirming the hypothesis that ROS production was most likely involved in the phototoxic mechanism.

2. 3. 2. 2 Synthesis method and surface coating

Both synthesis method and surface coating are critical in determining the toxicity of nano-TiO_2. Nagaveni et al. (2004) noted that under identical UV exposure, combustion-synthesized nano-TiO_2 resulted in 2 times higher initial degradation rate of phenol compared with commercial P25 TiO_2 (Nagaveni et al., 2004). This superior photocatalytic activity can be attributed to crystallinity, higher surface area, more surface hydroxyl groups, and improved optical absorption at higher wavelengths (570 and 467 nm, corresponding band gap energies of 2.18 and 2.65 eV). Using an *in-situ* sol-gel method, Kavitha (2013) synthesized anatase phase titania-chitosan NPs with spherical and irregular morphology (4.5-10.5nm) (Kavitha et al., 2013). Having tunable biocompatibility with human gastric adenocarcinoma cells and efficient antibacterial activity against *Staphylococcus aureus*, this nano-TiO_2 material might be a promising biomaterial for orthopedic and tissue engineering applications.

Using ESR spectroscopy, Sawada et al. (2010) demonstrated that TiO_2 NPs coated with fluoridated apatite (FAp-TiO_2, 100 nm) promoted ROS via photo-catalysis, and exhibited antifungal activity towards *Candida albicans* (Sawada et al., 2010). In a study by Carlotti et al. (2009), the oxidation of linoleic acid and porcine ear skin induced by UV irradiation

was investigated in the presence of different uncoated and coated titanium powders. They noted that surface characteristics largely influenced the observed oxidative damage. In their study, two types of coated TiO_2 specimens were used, namely PW Covasil S-1 and Tego Sun TS plus. While the former showed a high photocatalytic activity toward the peroxidation of linoleic acid, the latter displayed a marked protective effect (Carlotti et al., 2009).

In addition, nano-silver, the most widely employed antimicrobial nanomaterial, has been deposited onto TiO_2 NPs, a common strategy for synthesizing nanocomposites. The strong antibacterial activity of TiO_2@Ag NPs against different bacterial species has been reported under UV light (He et al., 2002), visible light illumination (Yuan et al., 2010), as well as in the dark (Allahverdiyev et al., 2013). TiO_2@Ag NPs reduced the viability of *Leishmania tropica*, and *Leishmania infantum* promastigotes 3 and 10 fold in the dark, respectively, while these rates diminished approximately 20 fold for each species in the presence of visible light. Non-visible light-exposed TiO_2@Ag-NPs were more effective against *L. infantum* parasites while visible light-exposed TiO_2-Ag-NPs exhibited nearly the same anti-leishmanial effect against both species (Allahverdiyev et al., 2013). A decrease in pH was discovered during photocatalysis using silver modified titanium dioxide nanoparticles. And such pH change has been attributed to the reduction of silver ion (Vamathevan et al., 2002).

2.3.3 Effects of environmental conditions on ROS generation

Environmental conditions, including light illumination, pH, solution composition and biological media, also influence the generation of ROS by nano-TiO_2.

2.3.3.1 UV irradiation and light illumination

Previous studies have suggested that, without UV exposure, nano-TiO_2 show little cytotoxicity (Rehn et al., 2003). It is generally agreed that ROS production of TiO_2 nanomaterials is initiated by UV irradiation. To date, there is no conclusion whether ROS can be generated on TiO_2 surface in aqueous condition without illumination. For TiO_2 NPs of different crystal forms and size, no ROS promotion was detected by ESR without exposure to light (Yin et al., 2012). Wamer & Yin (2011) conducted a study using human dermal fibroblasts to evaluate the toxicity of TiO_2 in tattoo inks. The results suggested that anatase TiO_2 was phototoxic but not cytotoxic, while the sample that only contains rutile TiO_2 was neither phototoxic nor cytotoxic (Wamer & Yin, 2011).

However, Lipovsky et al. (2012) investigated visible light-induced reactions of a suspension of TiO_2 NPs in water using ESR spin-trapping technique, and their results suggested that, without light illumination, formation of both •OH and $O_2^{-\bullet}$ were detected for TiO_2 rutile and anatase phases (50 nm NPs), but singlet oxygen was not detected in aqueous suspensions of TiO_2 NPs for either of these two crystal forms. When exposed to light in the blue part of visible spectrum (400-500 nm), increased levels of both •OH and $O^{2-\bullet}$ were detected. Singlet oxygen formation was observed with rutile NPs during irradiation (Lipovsky et al., 2012).

Without light exposure, long-term exposure to TiO_2 NPs has been proved to lead to significant alterations in the expression of various genes, and promoted production of reactive oxygen species and peroxidation of lipids, proteins and DNA in mouse lung tissue (Li et al., 2013). Exposure of zebrafish embryos to TiO_2 NPs produced

malformation and death only when the fish were also illuminated (light source: 250W blue-spectrum metal halide lamp) (Bar-Ilan et al., 2012). A similar result was obtained using a fish cell viability assay. TiO_2 alone (0.1–1000 μg/mL) had limited effect on goldfish skin cells, whereas co-exposure with UVA (0.5–2.0 kJ/m^{-2}) caused a significant dose-dependent decrease in cell viability, which was dependent on both the concentration of TiO_2 and the dose of UVA administered (Reeves et al., 2008). Using the comet assay, the same group of researchers also found that TiO_2 NPs are in fact genotoxic without UV irradiation, as all concentrations tested produced a significant increase in the level of Fpg-sensitive sites, which suggests that 8-hydroxyguanine (8-OH-G) is probably a major product of TiO_2-induced oxidative stress linked to genotoxicity. ROS promotion was also observed in toxicity studies using animal models. In a study where mice were injected with TiO_2 NPs for 45 days consecutively, accumulation of TiO_2 NPs and ROS were found in mouse spleen, accompanied by the development of congestion and lymph nodule proliferation of spleen tissue (Li et al., 2010).

2. 3. 3. 2 pH and solvents

It is notable that, when employing ESR to evaluate the ability of materials to generate/scavenge ROS, different experiment conditions, such as type of spin trap, pH and composition of solvent may lead to different results (Finkelstein et al., 1980). In early study, Jaeger & Bard (1979) have observed ESR spectra consistent with formation of both •OH and $O_2^{\bullet-}$ following absorption of UV radiation by TiO_2 (anatase) (Jaeger & Bard, 1979). However, Wamer et al (1997), using DMPO as a spin trap, observed, during UV irradiation of TiO_2, an ESR signal characteristic of DMPO/•OH spin adduct alone (Wamer et al., 1997). Dodd & Jha (2011) also reported the formation of •OH adduct in

UVA irradiated nano-TiO_2 (aerated aqueous suspension) using different spin traps including POBN, DMPO and DEPMPO, and also found no evidence of $O_2^{-\bullet}$. Their research also showed that in absence of O_2, no ESR signal was observed for PBN, DMPO, or DEPMPO. Only POBN/•OH adduct was observed under hypoxic conditions (Dodd & Jha, 2011). In a recent study to determine the phototoxicity of TiO_2 NPs with different crystal forms and molecular sizes, the generation of •OH in aqueous suspension was observed using BMPO spin trap, and no characteristic BMPO/$O_2^{-\bullet}$ was observed (Yin et al., 2012).

Hydrogen peroxide plays an important role in regulation of a wide variety of biological processes. It has been demonstrated that with the addition of H_2O_2 into aqueous suspension containing TiO_2, the concentration of $O_2^{-\bullet}$ increased with a small amount of H_2O_2 and slightly decreased at a certain concentration, and then became almost unchanged at a higher H_2O_2 concentrations (Daimon et al., 2008). The authors suggested that the first increase in $O_2^{\bullet-}$ could be attributed to the oxidation of H_2O_2 with h^+:

$$h^+_{vb} + H_2O_2 + 2OH^- \rightarrow O_2^{-\bullet} + 2H_2O$$

(8)

At the same time, the consumption of the valence band hole (h+) hinders the (e−)-(h+) recombination, and consequently accelerates the reduction of O_2 to generate $O_2^{-\bullet}$ (Eq. (2)). When the concentration of H_2O_2 is above 0.2 mM, $O_2^{-\bullet}$ decreases with the further increase of H_2O_2, which might be explained by desorption of O_2 from the TiO_2 surface, resulting from the adsorption of H_2O_2. This competition of adsorption on the TiO_2 surface was also suggested in a similar study using ethanol. Here, the addition of a small amount

ethanol resulted in the increased formation of $O_2^{-\bullet}$ yet subsequently decreased with further additional ethanol to the suspension. However, singlet oxygen decreased monotonically with additional ethanol.

2.4 TiO_2 NPs resulted cellular oxidative damage

2.4.1 Lipid peroxidation

Lipid peroxidation is an oxidative damage that leads to change of the integrity and functionality of cell membranes. It happens when free radicals abstract electrons from the lipid molecules. Nanomaterials can disrupt normal cellular function through lipid peroxidation, and reactive oxygen species have been proved to be responsible for the membrane damage that eventually leads to degeneration of cells (Sayes et al., 2006). *In vivo* studies have suggested that lipid oxidation is involved with pathogenesis of various aging related diseases, including coronary heart disease, Parkinson's disease, and cancer (Agil et al., 2006; Gago-Dominguez & Castelao, 2008; Regnström & Nilsson, 1994). Wang et al. (2013) reported a toxicity study in which the rat synovial cells were treated with different concentrations of TiO_2 NPs (0, 3, 30, and 300 mg/ml) (Wang et al., 2013). ROS were over-produced especially in the cells exposed to 30 and 300 mg/ml TiO_2 NPs. They also observed malondialdehyde (MDA), a lipid peroxidation product, as well as oxidative damage in cells. Significant decrease in activity of the endogenous antioxidant enzymes including superoxide dismutase (SOD) and catalase (CAT) was also detected.

TiO_2 NPs has been demonstrated to lead to skin peroxidation in animal models, for example, porcine skin, which is a well-accepted and readily available model for estimating damage to human skin (Carlotti et al., 2009). Oxidative stress has also been

found to occur during TiO_2 NPs dermal application on rats. In a 14 consecutive day toxicity study, different dose of TiO_2 NPs (20nm; 14, 28, 42, and 56 mg/kg) were applied to rat skin. The results of this study suggested that exposure to TiO_2 NPs increased peroxidation of lipids, and confirmed that nano-TiO_2 toxicity is associated with the oxidant generation and the resultant oxidative stress to cells (Unnithan et al., 2011). The results of these studies suggest that when investigating TiO_2 NPs toxicity, lipid peroxidation is a critical factor due to its impact on cell membranes. These studies are particularly relevant because of the use of TiO_2 NPs in many skincare and cosmetic products.

Egg PC liposome suspension were prepared as lipid membrane model to study possible oxidative damage resulting from ROS generated during exposure of TiO_2 NPs to UV light. By measuring the hyperfine structural changes of the ESR spectrum with ^{15}N-PDT as the spin label, it has been demonstrated that that ROS can produce a time-dependent peroxidation (Yin et al., 2012), and the peroxidation rate is P25>A25>A325>R100, which follows the same trend of ROS production in TiO_2 NPs suspension (Fig. 2-2).

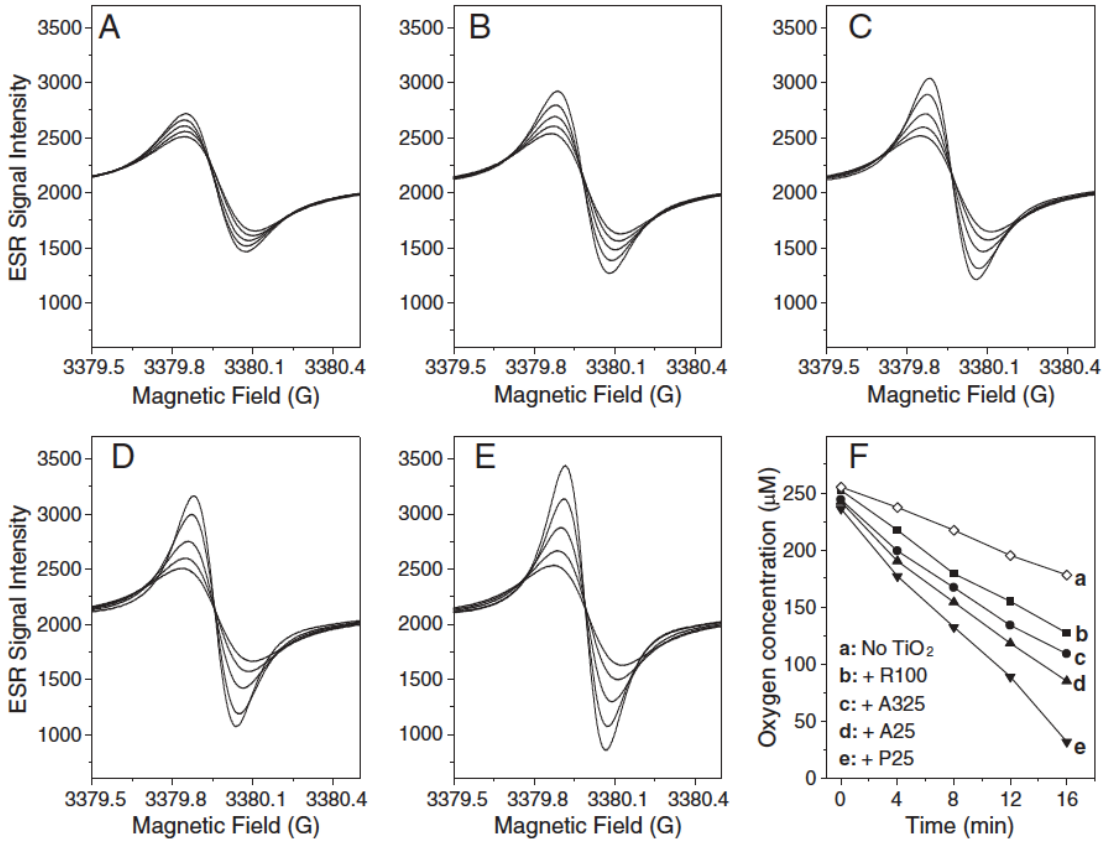

Figure 2-2 Effect of different TiO_2 samples on lipid peroxidation in liposomes. Oxygen consumption was measured in a closed chamber using liposome suspensions and the spin label ^{15}N-PDT. The liposome samples contained 30 mg/ml Egg PC and 0.1 mM ^{15}N-PDT spin label mixed with (A) no TiO_2; (B) 0.03 mg/ml of R100; (C) 0.03 mg/ml of A325; (D) 0.03 mg/ml of A25; and (E) 0.03 mg/ml of P25. Lipid peroxidation was initiated by UV (340 nm) irradiation. The ESR spectra were recorded with the low field line of the ^{15}N-PDT spin label every 4 min after the sample was sealed in a quartz capillary tube. The spectra were obtained with 0.5 mW incident microwave power and with 0.05 G field modulation at ambient temperature. The progressive increases in peak-to-peak signal intensity (and accompanying progressive narrowing of the line width) in each panel are due to time-dependent oxygen consumption resulting from lipid peroxidation, as shown in panel F. The enhancement effects of different TiO_2 nanoparticles on lipid peroxidation may be seen as bigger changes in the peak-to-peak signal intensities seen in panels B, C, D and E compared to panel A. Reprinted with permission from ref 2. Copyright 2012 Toxicology and Applied Pharmacology.

The ESR spin trap technique has also been employed for *in vivo* determination of lipid radicals, the products of lipid peroxidation, and to evaluate oxidative damage (González

et al., 2013). Here, intact *Navicula* sp. algae were suspended in 40 mM PBN stock solution with the addition of spin trap POBN (130 mM) prior to detection. The authors acknowledged the possible drawbacks for employing ESR including probe instability, interference with tissue metabolism, and lack of spin specificity. However they found this technique useful, especially when combined with other biochemical strategies.

2.4.2 Nucleic acid damage

The specificity of the reactions between nitrone spin traps with free radicals has already made spin trapping with ESR detection the most universal tool for the detection of free radicals in biological systems (Mason 2004). Based on this concept, the immune-spin trapping technique has been developed and extensively studied by Mason et al. (2004) to detect DNA or protein radicals. By trapping those radicals with DMPO, stable nitrone adducts can be formed and easily detected using an anti-DMPO serum with ELISA and Western blot assays (Mason, 2004). Using the method described by Mason et al. (2006 & 2010) (Ehrenshaft & Mason, 2006; Ranguelova et al., 2010), a significant increase in human serum albumin (HSA) protein radical was observed using DMPO as the spin trap when HSA protein was treated with P25 TiO_2 NPs and UV irradiation (Yin et al., 2012).

2.5 Concluding remarks

Concomitant with the growing uses of nanomaterials is the need to better define their safety. As the size of particles decreases, so does their surface area for the same quantity of material increase? This leads to many of the dramatic changes in the properties for nanomaterials. This change is of particular interest for nanomaterials capable of generating highly reactive oxygen species. However, detection of such short-lived

radicals remains technically challenging. ESR spectroscopy, a sensitive, nondestructive, in situ approach, is capable of unraveling the mechanisms of ROS-related toxicity of nanomaterials. The formation of ROS species (including $^1O_2$, •OH and $O^{2-\bullet}$) could be detected using different spin traps and depends on the intrinsic properties of the nanomaterials, including size, crystal phase, and surface characteristics, as well as environmental conditions. In particular, ESR spin label oximetry that detects changes in O_2 levels in a system is a reliable and effective method to monitor lipid peroxidation rate. Such an oxygen-monitoring ability is of critical importance when it comes to assessing cellular oxidative damage due to ROS that could lead to subsequent adverse health effects. Moreover, the knowledge generated from ESR studies on TiO_2 NPs could form a solid base for evaluating risk associated with nanomaterials.

Chapter 3 Research objectives

TiO_2 NPs can be activated by sunlight irradiation and consequently lead to oxidative decomposition of sensitive food compounds. The ultimate goal of the present study was to elucidate the combined effects of simulated sunlight and TiO_2 NPs toward common food antioxidant and food colors. The specific objectives include:

1) To investigate the effect of TiO_2 NPs on the free radical scavenging ability of seven major antioxidants of significance in both food matrixes and physiological systems, namely resveratrol, ascorbic acid, α-tocopherol, thiol-containing antioxidants (glutathione and cysteine), as well as polyphenols (epicatechin and epicatechin gallate) extracted from green tea.
2) To evaluate decomposition of the selected azo dye FD&C Yellow No. 5 in the presence of TiO_2 NPs that is photoactivated by simulated sunlight. During this process, ROS generation was monitored and the reaction mechanism was characterized by electron spin resonance spectroscopy and mass spectra at different pH values.
3) To characterize the ROS promoting ability of TiO_2 with regard to its phase composition, namely the anatase phase, the rutile phase and the mixed phase (P25), the degradation of representative food colors was investigated, including one semi-synthetic dye chlorophyllin copper sodium salt (E141) and three widely used synthetic food dye, namely tartrazine (E102), sunset yellow (E110), and allura red (E129).

Chapter 4 Combined effects of sunlight and TiO_2 nanoparticles on radical scavenging ability of seven selected dietary antioxidants

4.1 Introduction

A free radical is an atom, molecule or ion that bears an unpaired electron. Being extremely reactive, they are capable of engaging in rapid chain reactions that lead to destabilization of other molecules and accumulation of more radicals. In the human body, two main free radical species, reactive oxygen species (ROS) and reactive nitrogen species are generated by various endogenous systems. Those free radicals originated during body metabolism are able to adversely alter lipids, proteins and nucleic acids, and have been implicated in aging and a number of human diseases (Devasagayam et al., 2004). In living organisms, the levels of free radicals and related species are controlled by a complicated antioxidant defense system, which minimize oxidative damage to biomolecules (Aruoma & Halliwell, 1991). To maintain proper physiological function, a balance between free radicals and antioxidants is necessary (Lobo et al., 2010).

Numerous epidemiological studiess have correlated regular intake of foods containing a high content of antioxidants with a lower incidence and mortality rates due to cancer and heart diseases (Dragsted et al., 1993; Ness & Powles, 1997; Joseph et al., 1999). Typical foods with high levels of nature antioxidants including fruits and vegetables (Wang et al., 2010; Zhang &Hamauzu, 2004); tea and fruit juice as well as grains (Wennermark et al., 1994). Besides natural food materials, various dietary supplements and functional foods focusing on antioxidant functionality have emerged in the market in recent years, including vitamins and phenolics from fruit and vegetable extracts, thiol-containing

antioxidants such as glutathione and cysteine, and some other synthetic antioxidants. In addition to providing those well recognized health benefits, antioxidants are also intentionally added into a wide range of food products to ensure food stability by delaying oxidative quality deterioration.

Sunlight is an important environmental factor during storage of food products. It consists of a broad range of light wavelength including ultraviolet, visible and infrared. Even though it has been reported that the effect of sunlight on antioxidant ability is negligible during storage of products such as pomegranate juice (Perez Vicente et al., 2004) and orange juice (Solomon et al., 2000), irradiation by light reduced the antioxidant activity of phenolic compounds during the storage of olive oil (Servili et al., 2002). Exposure to sunlight promotes quality deterioration by triggering the activation of oxygen. This effect might be amplified by photoactive or photosensitive compounds in the system (Min & Boff, 2002).

Titanium dioxide (TiO_2) is a common white pigment and anti-caking agent found in food and cosmetic products. It has also shown promising applications as an active compound in sunblock lotions to provide photo protection to our skin (Hansenne & Lety, 1995). Select sunscreen products contained as high as 10% TiO_2 by weight (Weir et al., 2012). However, the use of TiO_2 has been challenged due to its high photo activity under irradiation by sunlight. It has been demonstrated that under light irradiation, TiO_2 NPs can induce generation of ROS and sequentially, lead to oxidative damage in epidermal human cell lines (Yin et al., 2012). Moreover, photoactivated TiO2 resulted in degradation of phenolics (Wang et al., 2013) and reduction of intracellular levels of GSH (Sha et al., 2013),.

In the current study, seven major antioxidants that are of great significance in both food matrixes and physiological systems have been selected. These include resveratrol, ascorbic acid, α-tocopherol, thiol-containing antioxidants including glutathione and cysteine, as well as polyphenols extracted from green tea namely epicatechin and epicatechin gallate (structures are shown in Fig 4-1). By measuring radical scavenging ability, we studied the effects of TiO_2 and sunlight on the antioxidant capacity of these antioxidants. The scavenging of DPPH radicals, hydroxyl and superoxide radicals were monitored by ESR spectroscopy with spin trapping techniques, which is a quick and reliable method for identification and quantification of short-lived free radicals (Roubaud et al., 1998).

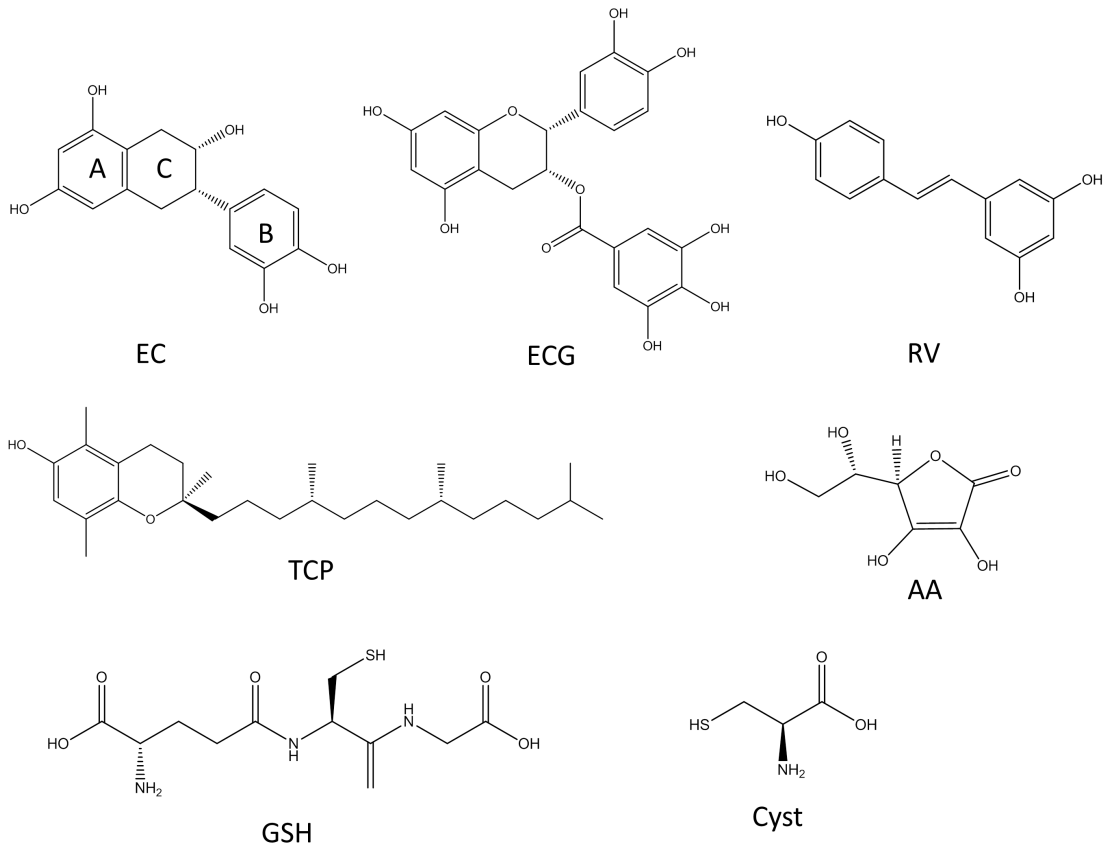

Figure 4-1 Chemical structure of epicatechin (EC), epicatechin gallate (ECG), resveratrol (RV), ascorbic acid (AA), α-tocopherol (TCP), glutathione (GSH) and cysteine (Cyst).

4.2 Materials and methods

4.2.1 Materials

The spin-trap 5-tert-butoxycarbonyl 5-methyl-1-pyrroline N-oxide (BMPO) was purchased from Applied Bioanalytical Labs (Sarasota, FL). 1-Hydroxy-3-carboxy-2,2,5,5-tetramethylpyrrolidine (CPH) was purchased from Alexis, Enzo Life Sciences, Inc. (NY, USA). 1,1-diphenyl-2-picryl-hydrazyl radical (DPPH•), ethanol, hydrogen peroxide, ammonium iron(II) sulfate heptahydrate, xanthine (XAN),

diethylenetriaminepentaacetic acid (DTPA), reduced L-glutathione (GSH), and L-cysteine (Cyst), L- ascorbic acid (AA), (−)-epicatechin (EC), resveratrol (RV), (−)-Epicatechin gallate (ECG) and α-tocopherol (VE) were all purchased from Sigma-Aldrich (Saint Louis, MO). Xanthine oxidase (XOD) was obtained from Roche Diagnostics GmbH (Mannheim, Germany). Aeroxide® TiO_2 P25 was a gift from EVONIK Industries AG (Frankfurt, Germany). Organic solvents methanol and acetonitrile ($CHCN_3$) are both from Sigma. Standard buffer solution was purchased from Sigma and treated with Chelex® 100 molecular biology grade resin from Bio-Rad Laboratories (Hercules, CA) to remove trace metal ions before use. Milli-Q water (18 MΩ cm) was used for all solution preparation.

4.2.2 ESR spectroscopy

All ESR measurements were carried out at ambient temperature (23 °C) using a Bruker EMX ESR spectrometer (Billerica, MA). Fifty milliliter aliquots of control or sample solutions were put in glass capillary tubes with internal diameters of 1 mm and sealed using Critoseal™ capillary tube sealant. The capillary tubes were inserted in the ESR cavity, and the spectra were recorded at selected times. The following parameters were used for all detection of the radicals: 20 mW microwave power, 100 G scan range and 1 G field modulation amplitude, and 100 kHz modulation frequency. The instrument was calibrated before use and data was obtained with error of less than 5%.

4.2.3 DPPH radical scavenge

DPPH radical (DPPH•) is a long-lived, stable nitrogen-centered free radical that has been commonly used to determine the radical scavenge ability of antioxidants (Zhou et al.,

2013). ESR spectroscopy is a quantitative measurement of specified radicals (Li et al., 2014). Therefore, antioxidant activity is evaluated via ESR spectroscopy on the basis that DPPH• signal intensity is inversely related to the radical scavenge ability of the antioxidant (Packer, 1999). Antioxidant stock solution were made at 100mM in water (EC, ECG, AA), 100mM in PBS buffer (pH 7.4, 100mM), or in acetonitrile (TCP and RV). Seven selected antioxidants, including EC, ECG, GSH, Cyst, AA, TCP, and RV were mixed 0.1 mg/mL TiO_2 NPs solutions, and then exposed to simulated sunlight for 30 and 60 min. Before light treatment, the initial concentration of the antioxidants was 10mM. The reaction mixtures, either without (control group) or with exposure to sunlight (experiment group), were mixed with DPPH• in ethanol to determine the radical scavenging abilities of the antioxidants. DPPH radical scavenging activity was measured according to the method described by Zhou et al. (2013) with slight modifications. Briefly, 5 uL of 500uM DPPH radical in ethanol was mixed with equivalent volume of 10mM antioxidant solutions (a) without TiO_2 NPs and not exposed to sunlight; (b) with addition of TiO_2 NPs but not exposed to simulated sunlight, (c) with 0.1mg/mL TiO_2 and exposed to simulated sunlight for 30 min and (d) for 60 min. Forty microliter water was added to make a 50uL volume final solution. After vortexing, 50 uL aliquots of the samples were collected for ESR spectroscopy. ESR spectra were collected after 5 min of mixing.

4.2.4 Superoxide radical scavenge

The superoxide radical scavenging activity assay was carried out according to Yin et al. (2008) with minor modification. Superoxide radicals ($O^{2-\bullet}$) were produced using the xanthine/xanthine oxidase (XOD) system and trapped by spin trap BMPO as the spin

adduct BMPO/ $O^{2-\bullet}$. Due to partial overlap between spin adducts of BMPO/glutathione radical and BMPO/$O^{2-\bullet}$, spin probe CPH was used to determine the superoxide radical scavenging ability of glutathione (GSH) instead of BMPO. Five microliter of the aforementioned antioxidant solutions, either with/without TiO_2 or with/without sunlight irradiation were individually introduced to freshly made XAN/XOD mixture where 0.2 U/ml XOD was added to initial superoxide radical generation. Control solution included 25 mM BMPO, 1 mM xanthine, 0.1 mM DTPA used as stabilizing agent, and 0.2 U/ml XOD in 10 mM pH 7.4 buffer. For GSH solutions, 0.1 mM CPH was used instead of BMPO. The scavenging ability on superoxide radicals was shown as the intensity reduction of superoxide radicals. ESR spectra were recorded at 2 min of mixing.

4.2.5 Hydroxyl radical scavenge

The ESR spin-trapping technique was used to evaluate the interception of hydroxyl radicals by antioxidants affected by TiO_2 NPs. The classic Fenton reaction was employed to generate the hydroxyl radicals by making a fresh reaction mixture containing 25mM BMPO, 20 mM freshly prepared $FeSO_4$ solution and 200 mM H_2O_2 with 1mM antioxidant solutions treated or without treatment of TiO_2 and simulated sunlight. Similar with DPPH and superoxide radical, the scavenging effect was determined by comparison with a solvent-treated control group. ESR spectra were recorded at 5 min.

4.2.6 Statistical analysis

Data was reported as mean ± SD for triplicate determinations. Statistical analysis was performed using Origin software (OriginPro 8.6, OriginLab). Comparison among

different treatment groups was analyzed by one-way ANOVA followed Tukey tests. Differences were considered significant at $P<0.05$.

4.3 Results and discussion

4.3.1 DPPH radical scavenging ability

Determination of the quenching effect of the stable DPPH free radical is considered one of the most convenient and reliable methods to evaluate the antioxidant activity of food materials or food ingredients (Brand et al., 1994). The scavenging capacity of the selected antioxidants before and after exposure to TiO_2 and simulated sunlight was evaluated using DPPH radical. DPPH• in 10% ethanol solution exhibits a typical one-peak ESR spectrum as shown in Fig. 4-2a. The effect of adding 1mM ECG was present in Fig. 4-2a as an example to illustrate the effect of antioxidants on DPPH• ESR signal intensity. A significant ESR signal intensity reduction (94±1% reduction) was observed after the addition of ECG. A similar phenomenon was observed when adding the ECG solutions that have been mixed with TiO_2 but not exposed to sunlight (93±1% reduction). However, when ECG was mixed with TiO_2 and irradiated by simulated sunlight for 30 and 60 min, the addition of the above ECG solution only resulted in 75±1% and 56±3% scavenging of DPPH•. Exposure to sunlight and TiO_2 NPs reduced DPPH radical scavenging of the antioxidant ECG.

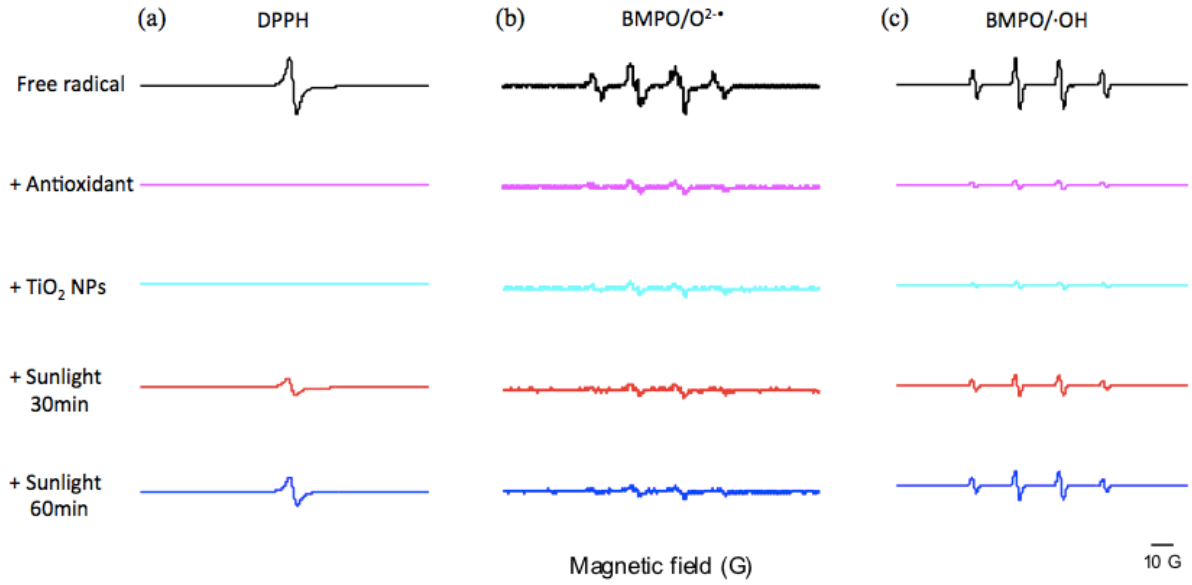

Figure 4-2 Radical scavenging ability of 1mM ECG detected by ESR spectroscopy. Control sample in panel (a) contained 50uM DPPH radical in 10% EtOH solutions; in panel (b) included 25 mM BMPO, 10 mM PBS buffer (pH 7.4), 1 mM xanthine, 0.1 mM DTPA and 0.2 U/ml XOD; (c) was a Fenton reaction system consisting of 25 mM BMPO, 0.1 mM Fe^{2+}, and 1 mM H_2O_2. The experiment groups were added by 1mM ECG (1) without TiO_2 NPs and not exposed to sunlight; (2) with addition of TiO_2 NPs but not exposed to simulated sunlight, (3) with 0.1mg/mL TiO_2 and exposed to simulated sunlight for 30 min and (4) for 60 min.

Interestingly, different results were observed for all seven antioxidants.

Fig. 4-3 summarized the DPPH• scavenging ability of these antioxidants before and after being treated with TiO_2 and simulated sunlight, including group (a) without TiO_2 NPs and not exposed to sunlight; (b) with addition of TiO_2 NPs but not exposed to simulated sunlight, (c) with 0.1mg/mL TiO_2 and exposed to simulated sunlight for 30 min and (d) for 60 min. In the time period chosen in this study, the scavenging ability of RV and GSH was not compromised by sunlight irradiation. The reduction of DPPH radical after adding

EC was 99 ±1% for group (a), 98 ±1% for group (b), 96 ±1% for group (c) and 57±4% for group (d). For TCP, the DPPH• reduction was found to be 90 ±1%, 90 ±1% for group, 70 ±1%, and 48±3% for group (a) – (d), respectively. The influence of sunlight and TiO_2 on AA and Cyst was not as significant as for EC, ECG and TCP.

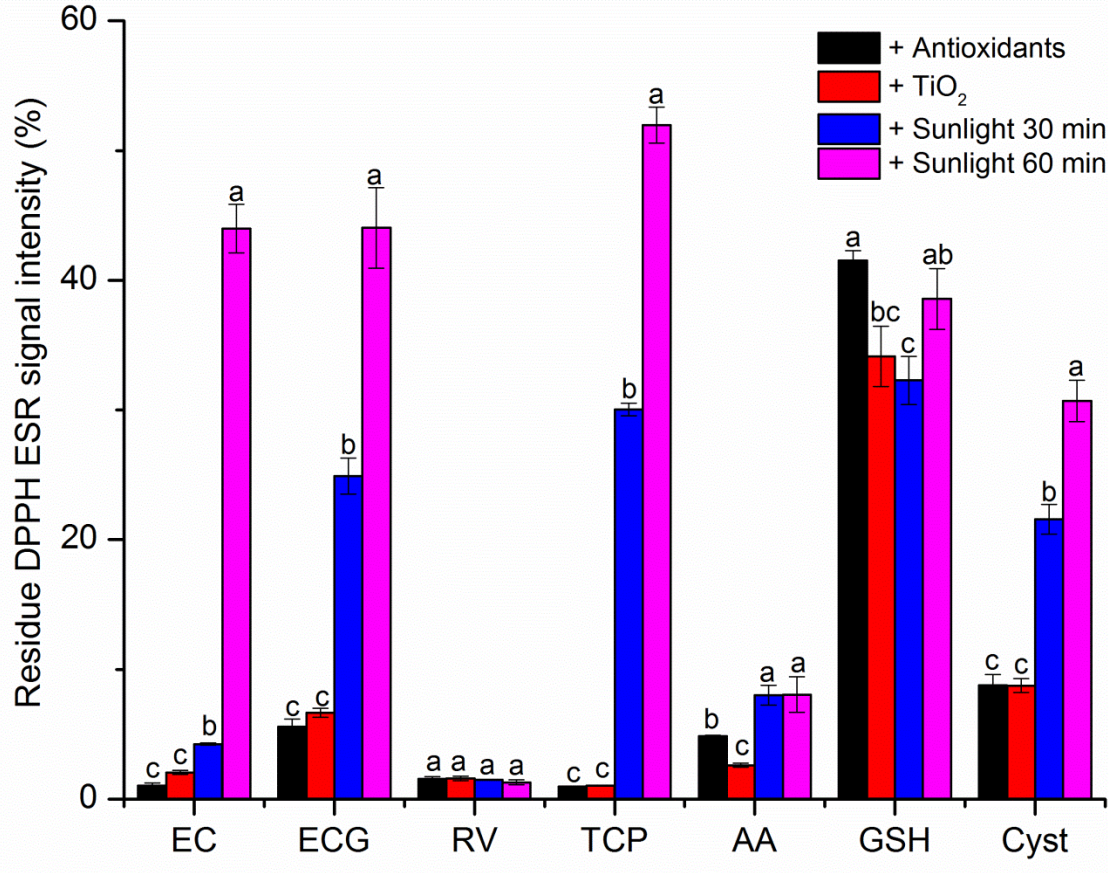

Figure 4-3 DPPH radical scavenging ability of EC, ECG, RV, TCP, AA, GSH and Cyst. Sample solutions contained 50uM DPPH radical in 10% EtOH. Y axis shows the remained radical signal intensity percentage after adding the antioxidants (1) without TiO_2 NPs and not exposed to sunlight; (2) with addition of TiO_2 NPs but not exposed to simulated sunlight, (3) with 0.1mg/mL TiO_2 and exposed to simulated sunlight for 30 min and (4) for 60 min. ESR spectra were recorded at 5 min after mixing the solutions. Means sharing the same superscript are not significantly different from each other (P<0.05).

4.3.2 Superoxide radical scavenging ability

Superoxide is another important radical that poses significance to physiological systems (Chang et al., 2007). Employing spin trap agent BMPO, we evaluated the generation of superoxide using the XAN/XOD system and the superoxide scavenging effect of the selected antioxidants, as well as the effects of sunlight and TiO_2 exposure on their superoxide radical scavenging ability. BMPO itself is ESR silent, while the spin adduct of BMPO and superoxide radical ($BMPO/O_2^{-\bullet}$) has a typical 4 line ESR spectrum with hyperfine splitting structure (a^N = 13.4 G, a^H_β = 12.1G) (Bruker, EPR Detection of the Superoxide Free Radical with the Nitrone Spin Traps DMPO and BMPO). Fig. 4-2b shows the addition of ECG to the freshly prepared reaction mixture containing XAN/XOD reduced the $BMPO/O^{2-\bullet}$ signals. After treatment with TiO_2 in conjunction with simulated sunlight, the reduction of radical signal intensity was still observed however the scavenging effect was less significant. Spin probe CPH was used instead of BMPO spin trap due to the partially overlap of BMPO/GSH radical and $BMPO/O^{2-\bullet}$ spectra. Reduction of GSH scavenging ability can be detected by ESR monitoring CP• radical generation, which is the oxidation product of CPH due to the excessive $O^{2-\bullet}$ in the solution.

Fig. 4-4 shows the effect of exposure to TiO_2 and simulated sunlight on the superoxide radical scavenging ability of those seven antioxidants. It is noteworthy to mention that, instead of reducing superoxide radical scavenging ability, treating RV with TiO_2 NPs and sunlight resulted a further decrease of BMPO/ $O^{2-\bullet}$ signal compared to untreated group. The superoxide radical scavenging capacity of RV was 64 ±2%, 63 ±2%, 77 ±2% and 77 ±3% for group (a) – (d). The superoxide scavenging capacity of the other 6 antioxidants

were reduced to different levels when exposed to simulated sunlight with the presence of TiO_2.

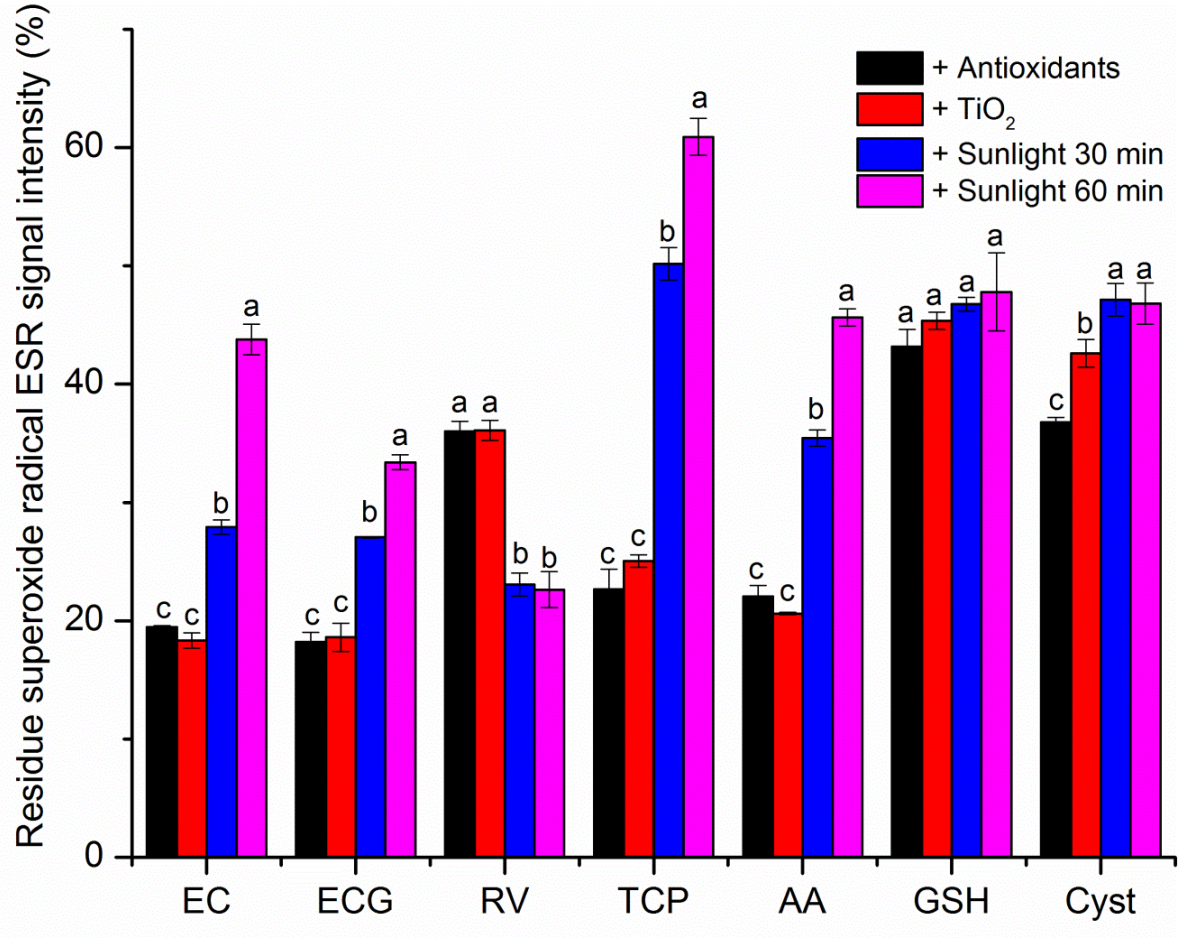

Figure 4-4 Superoxide radical scavenging ability of EC, ECG, RV, TCP, AA, GSH and Cyst. Sample solutions contained XAN/XOD system as a resource of superoxide radicals, including 25 mM BMPO, 10 mM PBS buffer (pH 7.4), 1 mM xanthine, 0.1 mM DTPA and 0.2 U/ml XOD. Y axis shows the remained radical signal intensity percentage after adding the antioxidants (1) without TiO_2 NPs and not exposed to sunlight; (2) with addition of TiO_2 NPs but not exposed to simulated sunlight, (3) with 0.1mg/mL TiO_2 and exposed to simulated sunlight for 30 min and (4) for 60 min. ESR spectra were recorded at 2 min after mixing the solutions. Means sharing the same superscript are not significantly different from each other ($P<0.05$).

4.3.3 Hydroxyl radical scavenging ability

Hydroxyl radical (·OH) scavenging capacity is an ideal indicator to estimate antioxidant property of a chemical compounds since ·OH is the most reactive ROS and it involves with a wide range of metabolism processes (Zhou et al., 2013). The hydroxyl radicals were generated using a classic Fenton reaction involving the reaction between Fe^{2+} and H_2O_2 (Yin, et al., 2009). Spin trap BMPO was used to form the stable spin adduct BMPO/·OH in order to quantitatively measure the short-lived hydroxyl radical. Fig. 4-2c showed the typical 1:2:2:1 four-line ESR signal (a^N = 13.5 G, a^H_β = 15.3 G, a^H_γ = 0.6 G) of the BMPO/·OH adducts (Zhao et al., 2001). Addition of the original antioxidants solution or antioxidants that have been surrendered to sunlight/TiO_2 treatment resulted different levels of BMPO/·OH signal reduction.

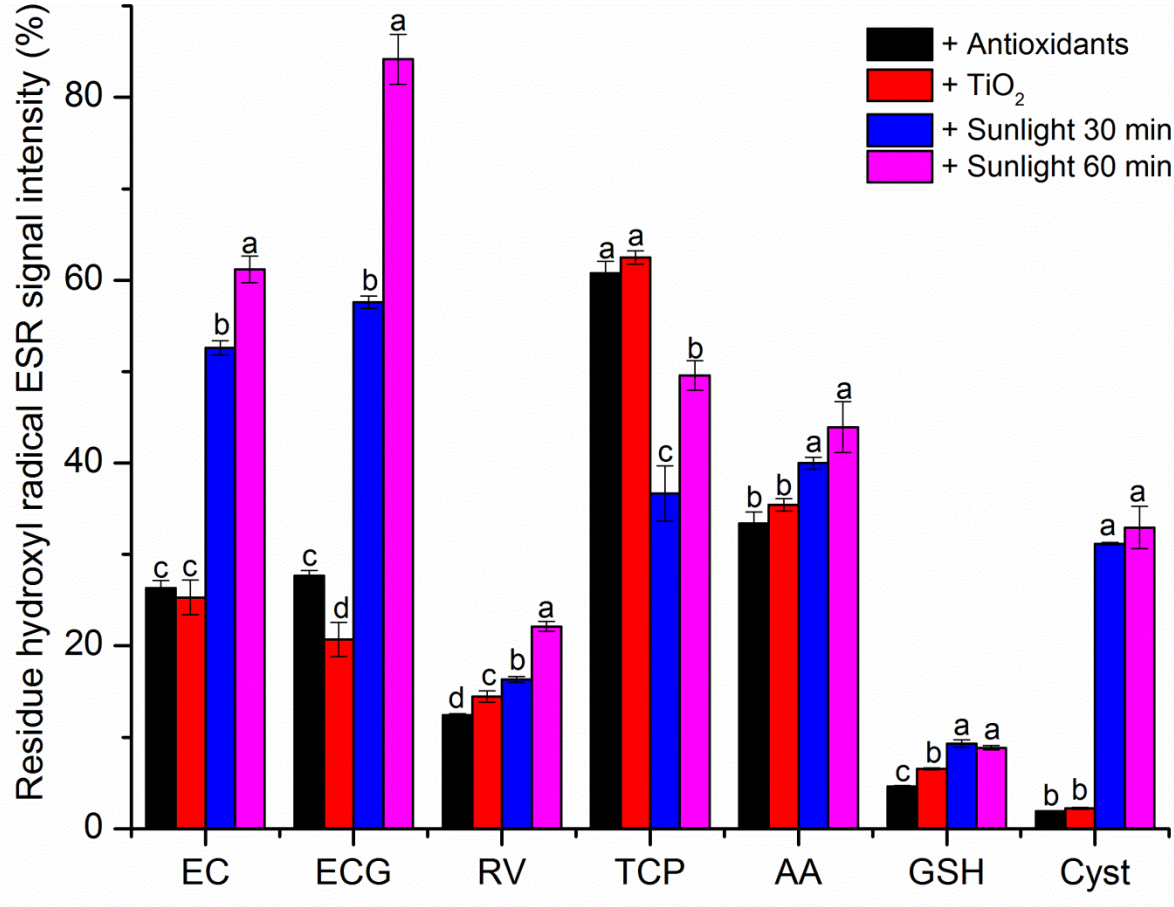

Figure 4-5 Hydroxyl radical scavenging ability of EC, ECG, RV, TCP, AA, GSH and Cyst. Sample solutions contained Fenton reaction system consisting of 25 mM BMPO, 0.1 mM Fe^{2+}, and 1 mM H_2O_2. Y axis shows the remained radical signal intensity percentage after adding the antioxidants (1) without TiO_2 NPs and not exposed to sunlight; (2) with addition of TiO_2 NPs but not exposed to simulated sunlight, (3) with 0.1mg/mL TiO_2 and exposed to simulated sunlight for 30 min and (4) for 60 min. ESR spectra were recorded at 5 min after mixing the solutions. Means sharing the same superscript are not significantly different from each other ($P<0.05$).

Fig. 4-5 shows the quantitative determination of hydroxyl radical quenched by those antioxidants with or without being exposed to TiO_2 and sunlight. Exposure to sunlight and TiO_2 NPs significantly reduced the hydroxyl radical scavenging ability of those antioxidants, including EC, ECG, RV, AA, GSH and Cyst, with GSH being the most resistant to such treatment. Interestingly, increased hydroxyl radical scavenging ability was observed for TCP that has been mixed with TiO_2 NPs solution and irradiated by sunlight. The hydroxyl radical scavenging capacity of TCP was 40 ±3%, 37 ±2%, 63 ±6% and 50 ±3% for group (a) – (d).

4.4 Discussion

4.4.1 Initial radical scavenging ability of antioxidants

The intrinsic properties, in particular, the chemical characteristics, are one of the determination factors of the oxidant scavenging capacity of antioxidants (Chang et al., 2007). This study found that before any treatment, different radical scavenging behaviors were observed for the selected antioxidants. The DPPH• scavenging capacity of those antioxidants at the same concentration (1mM) were found to follow the sequence RV ≈ TCP ≈ EC > AA ≈ ECG > Cyst > GSH (Fig. 4-3). The antioxidative action of these

antioxidants quenching the generation of superoxide radicals was found to follow the activity sequence EC ≈ ECG ≥ TCP ≈ AA > RV > Cyst> GSH (Fig. 4-4). Those antioxidants also scavenge hydroxyl radical generated by Fenton reaction, following the activity sequence Cyst ≥ GSH > RV > EC ≥ ECG > AA > TCP (Fig. 4-5).

As noted before, the mechanism of radical scavenging and antioxidant defense is very complicated and yet to be established (Lacopini et al., 2008). In general it seems to be clear that in addition to the structure of the radical scavenger, intrinsic properties of the free radical and the stability of the reaction products are also very important in the scavenging mechanism (Sadeghipour et al., 2005). The phenolic compounds that were used in this study(EC, ECG and RV) all showed strong radical quenching ability (Fig. 3-5). The aromatic OH groups are the reactive centers, primarily 3',4'-dihydroxy catechol group. For flavonoids EC and ECG, the *ortho*-dihydroxy group in the B-ring (Fig. 4-1) has a decisive effect on the antioxidant activity. In addition, the presence of a 2,3- double bond in the C ring, in conjunction with 4-oxo group can enhance antioxidant potential by electron donating effects. The 3- and 5- OH in the A rings also contributes to an increased antioxidant capacity (Chang et al., 2007; Lopez et al., 2003).

GSH and Cyst are thiol containing antioxidants that are important substrate for enzymatic antioxidant functions and capable of nonenzymatic radical scavenging. Thiols react mainly by hydrogen transfer, yielding sulfur centered radicals. The antioxidant function can also proceed by reacting with hydroxyl radical to yield carbon centered radicals (Galano & Raul, 2011). From the results shown in Fig. 4-3 to 4-5, GSH and Cyst showed high inhibition/scavenging effects on hydroxyl radicals compared to their effects on DPPH and superoxide radicals. The classic Fenton reaction was used as a resource of

hydroxyl radical in this study. It is possible that in a Fenton system containing Fe^{2+}, thiol antioxidants (GSH and Cyst) also act as metal chelators as well as radical quenchers (Deneke 2000).

As one of the strongest reductants and radical scavengers, AA reduces oxygen, nitrogen, carbon and sulfur centered radicals and acts as a primary defense against radicals in aqueous solutions (Niki, 1991). AA has two protons available per molecule for antioxidative donation while the number has been determined to be 3 protons for EC (Yilmaz & Toledo 2004), which is likely to be the reason that the radical quenching capacity of AA is smaller than EC for DPPH, hydroxyl and superoxide radicals, as shown in Fig. 4-3 to 4-5.

4.4.2 Intrinsic characteristics of free radicals

Reaction kinetics and mechanisms of radical scavenging reaction not only depends on the antioxidant capacity of the antioxidants, but also the intrinsic properties of each radical. In this study it was observed that for superoxide radicals, the scavenging capacity of the tested antioxidants was generally of smaller magnitude than those of DPPH and hydroxyl radicals (Fig. 4-3 to 4-5). A possible explanation for this observation is that in an XAN/XOD system, $O_2^{-\bullet}$ can be continuously generated in the system thus equilibrium state is hard to obtain (Frankel and Meyer, 2000). Most antioxidants react very rapidly with DPPH radical and the number of DPPH• molecules that can be scavenged is correlated with the number of available hydroxyl group in those antioxidants (Brand et al., 1994). Previous studies reported that flavonoids such as EC and ECG have high scavenging ability against DPPH• compared to RV (Lee et al., 2004). The superoxide

radical scavenging activity was found to be RV > EC (Yilmaz & Toledo, 2004). However, Fig. 4-3 shows that RV exhibited excellent DPPH• scavenging activity, which may due to the solvents effect. As both RV and DPPH• have high solubility in organic solvents such as methanol or acetonitrile.

Superoxide radicals are a common free radical species found in biological substrates and used in antioxidants assays. These radicals are slightly less reactive than ·OH and possess an extended half-life (~ 10^{-5}S) compared to ·OH (~10^{-9} S). In this study, superoxide radicals were generated using a XAN/XOD system in which the activity of the XOD enzyme strongly affects superoxide radical concentration. One possible defect of this method is that the antioxidants may suppress the generation of $O_2^{-\bullet}$ by hindering XOD activity rather than directly interacts with radicals. Based on ESR measurement, Unno et al. (2000) suggested that a likely action of certain antioxidants is to scavenge $O_2^{-\bullet}$ without inhibition with the function of XOD. Moreover, to rule out the possible interference, we used excessive amounts of XOD in this study.

4.4.3 Effect of sunlight and TiO_2 NPs

Fig. 4-3 to 4-5 shows that with the presence of TiO_2 NPs, sunlight irradiation resulted in significant loss of DPPH• scavenging ability of EC, ECG, TCP, AA and Cyst, but did not alter the scavenging capacity of RV and GSH. Under the same treatment, significant loss of $O_2^{-\bullet}$ scavenging ability was observed for EC, ECG, TCP, AA, but not for GSH. The $O_2^{-\bullet}$ scavenging effect was promoted when RV had been irradiated by sunlight with TiO_2. We also observed significant loss of ·OH scavenging ability for EC, ECG, RV, AA and Cyst. However an increasing in ·OH scavenging capacity of TCP was observed. These

results seem to be random and irrelevant at first glance, but here we made the first effort to explain them from the following aspects.

4.4.3.1 General destructive effects proceed via degradation

It has been well recognized that semiconductors, such as TiO_2, exhibit photoactivity and promote oxidative ROS as well as hole/electron pairs in aqueous solution. Those oxidative species can result in oxidative degradation of a wide range of compounds. Therefore TiO_2 is widely used as a photocatalyst. The results in this study indicate that in general when TiO_2 is present in the solution, even at low concentrations, simulated sunlight had negative effects on antioxidant capacity of antioxidants, most probably by their oxidative destruction. In our study this case was found to be true with EC, ECG, AA and Cyst, regardless of the free radical species.

4.4.3.2 Surface interaction with TiO_2 NPs

The free radical scavenging ability of GSH is found to be barely influenced when treated with TiO_2 exposure and light irradiation. However, a different result was observed for another thiol-containing antioxidant, Cyst—the constituent amino acid of GSH. This interesting observation agrees with a previous study reported by Nosaka et al. (2012), in which the authors detected that TiO_2, under light irradiation for 120 min resulted in slight decomposition of GSH, while a much higher decomposition rate was found for Cyst. Adsorption of antioxidants on the TiO_2 surface not only contributes to the decomposition of antioxidants, but also directly hinders the radical scavenging capacity by reducing the functional group. For example, S-H groups of Cyst bind with the active OH site on TiO_2 surface, leading to S-S bond which can no longer donate H. In contrast, the

decomposition of GSH resulted from the adsorption of TiO_2 surface was less likely compared to Cyst. The adsorption sites of GSH could be the carboxyl group or amino group rather than SH group, leading to self-defensive ability of GSH to photoexited TiO_2 (Nosaka et al., 2012).

4.4.3.3 Reaction media

Besides GSH, RV and TCP both responded differently to TiO_2 and sunlight treatment compared with EC, ECG, AA and Cyst. One possible reason for the difference could be the reaction solvent. It is common knowledge that solvent composition is an important factor in light-triggered decomposition of antioxidants. Sabliov et al. (2008) found that TCP in free form did not degrade when exposed to UV light, but the samples in organic solvent degraded significantly as a matter of time. The solution of RV and TCP used in this study contained 10% $CHCN_3$. The DPPH• scavenging ability of RV remained after exposure to sunlight with TiO_2 (Fig. 4-3), and the $O_2^{-\bullet}$ scavenging ability indeed increased (Fig. 4-4). An increase of ·OH scavenging capacity was observed for TCP (Fig. 4-5) after being irradiated with simulated sunlight with TiO_2. RV and TCP are hydrophobic dietary antioxidants. The additional organic solvent could result a higher affinity between DPPH• (10% methanol) and RV (10% $CHCN_3$), which may explain why RV showed strong DPPH• scavenging capacity, even after exposure to sunlight.

4.5 Conclusion

TiO_2 nanomaterials are one of the most extensively studied materials in the field of nanotechnology. Upon light irradiation, TiO_2 NPs generate elevated level of reactive oxygen species, which has been associated with oxidative stress and many diseases.

Antioxidants can scavenge reactive free radicals in chemical and biological systems, protecting cells from oxidative damage. As a result, they have been used as dietary supplements. In the current study, we selected seven common antioxidants that are widely used in food and skin care products to study the effect of sunlight and TiO_2 exposure on their radical scavenging abilities. The radical scavenging capacity of most antioxidants was compromised when treated with TiO_2 NPs and exposed to simulated sunlight, including epicatechin, epicatechin gallate, ascorbic acid, cysteine, α-tocopherol, glutathione and resveratrol. GSH was found to be most resistant to such treatment and showed preserved radical scavenging ability after being treated with TiO_2 NPs with sunlight irradiation. Interestingly, the radical scavenging ability of α-tocopherol towards hydroxyl radical and resveratrol towards superoxide radical increased after being mixed with TiO_2 NPs then simulated by sunlight irradiation. Those results suggest that exposure to simulated sunlight with the presence of TiO_2 NPs alters the free radical scavenging abilities of antioxidants. The effects vary, largely depending on the chemical structure of antioxidants as well as the targeted radical.

Chapter 5: FD&C Yellow No. 5 (Tartrazine) Degradation via Reactive Oxygen Species Triggered by TiO_2 and Au/TiO_2 Nanoparticles Exposed to Simulated Sunlight

Partially adapted from Li, M.; He, W; Wu, H; Liu, Y; Wamer, W; Lo, Y. M.; Yin, J-J. FD&C Yellow No. 5 (Tartrazine) Degradation via Reactive Oxygen Species Triggered by TiO_2 and Au/TiO_2 Nanoparticles Exposed to Simulated Sunlight**.** *Journal of Agricultural and Food Chemistry,* 2014 (accepted by journal as of Nov. 13th, 2014)

5.1 Introduction

Titanium dioxide (TiO_2) has been used as ingredients in a wide range of consumer products. Important examples include its use as a UV protectant in sunscreens, a pigment in paints, as well as coloring and anti-caking agents in drugs and food products (Carlotti et al., 2009). Additionally, TiO_2, particularly in its anatase form, is an efficient photocatalyst. For this reason, TiO_2 has also been extensively used as photocatalyst for wastewater treatment to detoxify biocides or other hazardous pollutants (Hamal et al., 2010; Ochiai et al., 2013). To date, in the food industry TiO_2 is primarily found in soft drinks, yogurts, ice cream, chips, pickles, honey, mustard, gum, puddings and gelatins, confectionary products, and baked goods (Gomez et al., 2012). While use of TiO_2 in food is generally considered as safe, in the US, there is a 1% by weight maximum allowance in food (FDA, 21CFR73.575), unlike Japan where it is permitted without limitations, except in specific types of food (Japan, 2000). On the other hand, tighter controls over the use of TiO_2 are seen in different parts of the world. The European Union authorizes its use at 100 mg/L (individually or in combination with other dyes) in non–alcoholic flavored drinks, 0.015% in desserts including flavored milk products, and

0.02 % in candied fruits and vegetables (EU, 1994). In India the use of TiO_2 is restricted to chewing gum and bubble gum at no more than 1% and to powdered concentrate mixes for fruit beverage drinks not to exceed 0.01% by weight (India, 2004a; b).

Accompanying the advancements of nanotechnology was the increased chemical and biological reactivity of food ingredients due mainly to the drastic reduction in particle size and increase in surface area. Recent studies revealed that the size of most TiO_2 used in food falls into nano-range (Yang et al., 2014; Weir et al., 2012; Chen et al., 2013). When irradiated, TiO_2 nanoparticles (NPs) absorb photon energy equal to or higher than its band gap (3.0 eV for the rutile and 3.2 eV for the anatase phase), exciting electrons in the valence band to the conduction band, resulting in conduction band electrons, and leaving valence band holes that can extract electrons from water or hydroxyl ions while generating hydroxyl radicals (•OH) (Mao&Chen, 2007; Yin et al., 2012). This process also involves formation of other reactive oxygen species (ROS), including superoxide radicals ($O_2^{-\bullet}$) and singlet oxygen ($^1O_2$) (Daimon & Nosaka, 2007), as well as some intermediate species such as H_2O_2 or O_2 (Chen & Mao, 2007). Taking advantage of its light-tunable ROS promotion ability, TiO_2 NPs have been used in food package materials as an anti-microbial agent (Yu et al., 2013; Wu et al., 2010) as well as in intelligent ink for oxygen detection (Mills, 2005).

However, ROS generated by photoexcited TiO_2 NPs may lead to oxidative damage in biological systems (Wamer et al., 1997; Liu et al., 2010). Of particular interest are food matrices because they are complicated and contain many reactive compounds. ROS have been observed to oxidize sensitive food colors, leading to discoloration of food products (Chu et al., 2009). To date, synthetic azo dyes, e.g. FD&C Yellow No. 5, FD&C Red No.

40 (allura red) and FD&C Yellow No. 6 (sunset yellow), are still widely used in the food, drug, and cosmetic industry over natural dyes because of their cost advantage and high stability to light, oxygen, and pH changes (Gomez et al., 2012). However, the potential hazard of FD&C Yellow No.5 remains controversial. It has been associated with possible toxicity that might result in allergic and intolerance reactions, especially among asthmatic patients and those with aspirin intolerance (Alvarez Cuesta et al., 1981). Nevertheless, recent oral administration studies proved limited reproducibility of tartrazine-induced angioedema (Nettis et al., 2003) or lack of genotoxicity lesions (Poul et al., 2009). Therefore, the present study aimed at using FD&C Yellow No. 5 as a model of azo dyes to evaluate its degradation in the presence of TiO_2 NPs, which were photoexcited by simulated sunlight. During this process, ROS generation was identified and the interaction between different ROS species and this azo dye was monitored at different pH.

5.2 Materials and Methods

5.2.1 Materials

The sample of FD&C Yellow No. 5 (Y5) used in this study originated from a batch submitted to the FDA for certification. The purified main component of FD&C Yellow No. 5 (MY5) was separated by countercurrent chromatography from a portion of FD&C Yellow No. 5 and was generously provided by Dr. Adrian Weisz in FDA (Weisz et al., 2014). Methanol (Fisher Scientific, Fair Lawn, NJ, USA), ammonium acetate (NH_4OAc, Fisher), and water were of chromatography grade. The mixed-phase titanium dioxide Deggussa Aeroxide P25 (75% anatase and 25% rutile phase, surface area 50±15 m^2/g)

was purchased from Degussa Corporation (Parsippany, NJ). The spin-trap, 5-tert-butoxycarbonyl 5-methyl-1-pyrroline N-oxide (BMPO), was purchased from Applied Bioanalytical Labs (Sarasota, FL). 2,2,6,6-Tetramethyl-4-piperidone (TEMP) was purchased from Wako Pure Chemical Industry, Ltd. Japan. 2,2,6,6 - Tetramethylpiperidine-1-oxyl (TEMPO) was purchased from Alexis, Enzo Life Sciences, Inc. (NY, USA). ^{15}N-labeled 4-oxo-2,2,6,6-tetramethylpiperidine-d16-1-oxyl (^{15}N-PDT) was purchased from Cambridge Isotope Labs (Andover, MA). Superoxide dismutase (SOD) and standard buffer solutions were purchased from Sigma Chemical Co. (St. Louis, MO). Before use, each buffer stock solution (pH 3.9 HAc-NaAc, pH 5.0 PBS, pH 7.4 PBS, all at 0.1 M) was treated with Chelex100 molecular biology grade resin from Bio-Rad Laboratories (Hercules, CA) to remove trace metal ions. Distilled deionized water (18.2 MΩ.cm) from a Milli-Q water purification system was used in all experiments.

5.2.2 Preparation of Au/TiO_2 hybrid nanostructures

Au/TiO_2 hybrid nanostructures were prepared according to a previously reported photo-reduction method (Tanaka et al., 2012) with modifications according to He et al. (2013). To obtain a Au/TiO_2 sample with a Au: TiO_2 ratio = 1:100 (by weight), 10 mL of 2.0 mg/mL TiO_2 suspension in methanol (50% by volume) was mixed with 0.1 ml aqueous solution of $HAuCl_4$ (2 mg/mL Au) in a 50 mL quartz Erlenmeyer flask and sealed. The above solution was sonicated for 5 min, then irradiated for 30 min under simulated sunlight with magnetic stirring in a ice water bath. The light source was an Oriel Xenon Arc Lamp Solar Simulator. A clearly evident color change from white to greyish pink was observed, indicating the formation of TiO_2/Au hybrid nanostructures. After

centrifugation, UV spectral analysis of the supernantant after each photodeposition revealed that the Au had been almost completely (>99%) deposited as Au on the TiO_2 particles.The precipitate was collected, washed three times with double distilled water, and then dried at 45°C overnight in oven and used for further experiments.

5.2.3 Characterization of nanomaterials

UV-Vis absorption spectra were obtained using a Varian Cary 300 spectrophotometer. Transmission electron microscopy (TEM) and high resolution TEM (HRTEM) images were captured on a JEM 2100 FEG (JEOL) transmission electron microscope (accelerating voltage of 200 kV) located at the NanoCenter, University of Maryland, College Park, MD. Energy-dispersive X-ray analysis (EDX) was conducted using the same microscope. The samples for TEM analysis were prepared by adding drops of the dispersed colloidal solutions onto standard holey carbon-coated copper grids, which were then air dried at ambient temperature.

5.2.4 Dye degradation

For examining the degradation of the food dye, 10 mL aqueous solution containing 25 mg/L MY5 or Y5 and selected concentrations of TiO_2 or Au/TiO_2 NPs were continuously stirred in the dark for 30 min to establish an adsorption-desorption equilibrium between the NPs and dyes. The above suspension was transferred to a 50 mL quartz Erlenmeyer flask, sealed and irradiated using a light source to deliver simulated sunlight. The light resource consisted of a Universal Arc Lamp Power Supply (69920 Universal Supply, Newport, Irvine, CA) using xenon lamps (880 W) and an Oriel® Xenon Arc Lamp Solar Simulator. During irradiation, the suspension was continuously stirred and kept in ice

water bath. The degradation process was monitored using a Varian Cary 300 spectrophotometer. Before UV-Vis analysis, the reaction mixture was centrifuged to remove the TiO_2 or Au/TiO_2 particles. The photocatalytic degradation of MY5 was observed to follow pseudo-first-order kinetics. When the dye concentration was in the millimolar range, the apparent first-order rate constant, k_{app} was determined from the slope of ln (C/C_0) vs irradiation time according to the following relation:

$$-ln\frac{C}{C_0} = k_{app}t \quad (1)$$

Where t is the irradiation time, C_0 is the initial concentration of dye, and C is the concentration of dye (mg/L) at time t (Konstantinou & Albanis, 2004). The concentration was determined by spectrophotometry. The UV-Vis spectrum of MY5 consists of two characteristic peaks at 425 nm and 258 nm. The λ_{max} of the dye (425 nm) was chosen for quantitative degradation studies.

5.2.5 Electron Spin Resonance

ESR spin-trap spectroscopy was employed to detect the generation of reactive oxygen species (ROS) and occurrence of electron transfer during simulated sunlight irradiation of samples. The spin trap, BMPO, was used to detect the generation of superoxide radicals ($O_2^{-\bullet}$) and/or hydroxyl radicals (•OH). TEMP was used to investigate the generation of singlet oxygen ($^1O_2$). TEMPO, a stable radical that exhibits an ESR signal have three identical peaks, was used as spin probe to study the electrons generated in the TiO_2 aqueous solution. Oxygen consumption during dye degradation photocatalyzed by TiO_2 NPs was monitored by ESR oximetry. A water soluble spin label, ^{15}N-PDT, was used to detect the oxygen content in sample solutions. The shape of ^{15}N-PDT ESR spectrum is

dependent on the amount of O_2 interacting with it, where higher peak-to-peak amplitude (A) and narrower peak-to-peak line width (W) are found when the levels of O_2 in solution are reduced (Yin et al., 2012). O_2 concentration was calculated by a calibration standard curve described by:

$$[O_2] = 419.72 * W - 44.12 \quad (2)$$

where $[O_2]$ is the concentration in solution (μM). The consumption of oxygen was expressed as $[O_{2\text{-time}}]/[O_{2\text{-initial}}]$.

Fifty microliter aliquots of control or sample solutions were put in glass capillary tubes with internal diameters of 1 mm and sealed using Critoseal™ capillary tube sealant, then placed into the microwave cavity of a Bruker EMX ESR Spectrometer (Billerica, MA) for obtaining ESR spectra. All ESR measurements were carried out in *situ* using the following settings for detection of the spin adducts: 10 mW microwave power for detection of spin adducts using spin traps, and 1 mW microwave power for ESR oximetry using ^{15}N-PDT, 100 G scan range and 1 G field modulation. Photoirradiation was accomplished by a lighting system consisting of a 450 W Xenon lamp equipped with a Schoeffel xenon arc solar simulator to generate simulated sunlight. ESR spectra were collected during irradiation at different time intervals. All measurements were performed in replicate at ambient temperature. Control groups, either without catalysts or without irradiation, were also recorded for comparison. The final concentration of each component is described in each figure caption.

5.2.6 Analytical HPLC

HPLC analyses were performed with a Waters Alliance 2690 Separation Module (Waters, Milford, MA, USA). The eluents were 0.2 M aqueous NH_4OAc and methanol. The column (Xterra C18, 5 μm, 250 mm × 4.60 mm i.d., Waters, Waltham, MA, USA) was eluted by using consecutive linear gradients of 0–10% methanol in 5 min, 10–25% methanol in 10 min, and 25–40% methanol in 20 min, followed by 100% methanol for 6 min. The effluent was monitored with a Waters 996 photodiode array detector set at 254 nm. Other conditions included: flow-rate, 1 ml/min; column temperature, 25±5°C; injection volume, 20 μL. The sample analyzed consisted of an aliquot (~1.5 ml) from the aqueous dye solution that was irradiated in the presence of TiO_2.

5.2.7 Liquid chromatography–mass spectrometry

The high-resolution mass spectra of the components found in the irradiated dye solutions were acquired using an Agilent 6520 Q-TOF LC/MS system (Agilent Technologies, Santa Clara, CA, USA) equipped with Agilent MassHunter Workstation software for data acquisition and data analysis. The separated components were analyzed in the positive electrospray ionization (ESI) mode.

5.3 Results and discussion

5.3.1 Characterization of TiO_2 nanoparticles and Au/ TiO_2 hybrid nanostructures

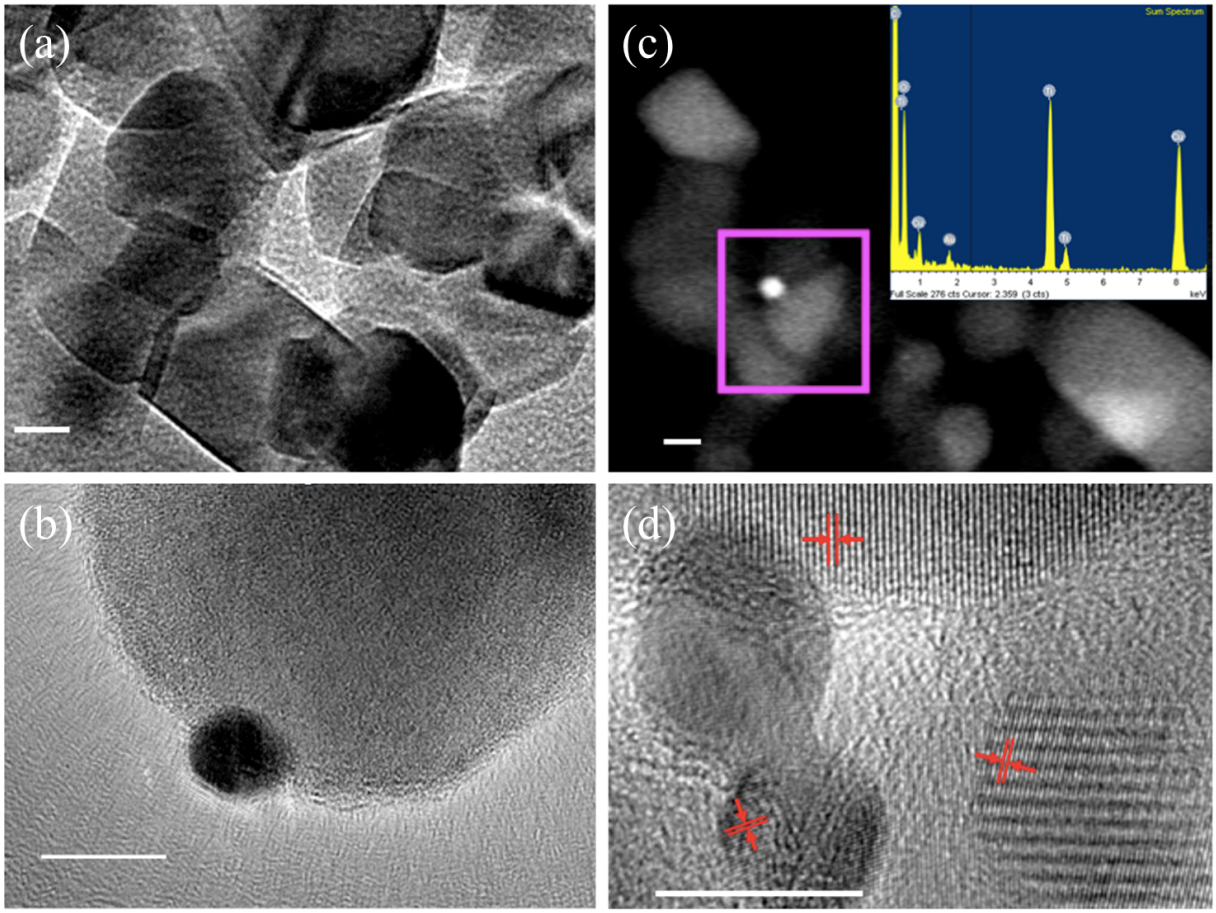

Figure 5-1 TEM images of TiO_2 NPs (a) and (b) Au/ TiO_2 hybrid nanostructures; (c)dark field STEM of Au/ TiO_2 hybrid nanostructures, insert showing EDS analysis; and (d)HRTEM of Au/ TiO_2 ($Au:TiO_2$ ratio = 1:100 by weight) hybrid nanostructures formation after photodeposition. Scale bars are all 10 nm.

The morphology of TiO_2 NPs and Au/ TiO_2 hybrid nanostructure was characterized by transmission electron microscopy (TEM). Fig. 5-1a shows the original TiO_2 P25 agglomerates with the size ranging from 22 to 48 nm. The high-resolution TEM (HRTEM) image (Fig. 5-1c) shows the Au NPs (dark dots) located on the surface of the individual TiO_2 NPs. The size of the photo-deposited Au NPs was estimated to be 4 to10 nm. After doping Au on to TiO_2 surface, the surface characteristics and size of the TiO_2 NPs remained unchanged. Electron dispersive spectrum (EDS) analysis was performed to further confirm the formation of Au/ TiO_2 nanostructure (Fig. 5-1b). The EDS spectrum

in Fig. 5-1c shows a strong signal for Ti and a weak signal for Au. The mass ratio of Au/ TiO_2 for the selected area was estimated to be approximately 5% based on this spectrum. Elemental copper and carbon were also detected by EDS, which was associated with the supporting carbon coated copper grids. The HRTEM image taken from the interfacial region of Au and TiO_2 shows the lattice image with a lattice spacing of 0.353 nm that corresponds to the {001} facets of anatase phase. Lattice fringes with interplanar distance of 0.202 nm was observed on the dark dots in Fig. 5-1d, which is similar to the planar distance for Au {200} (d = 0.204 nm).

5.3.2 Degradation of FD&C Yellow 5

5.3.2.1 Effect of initial TiO_2 concentration

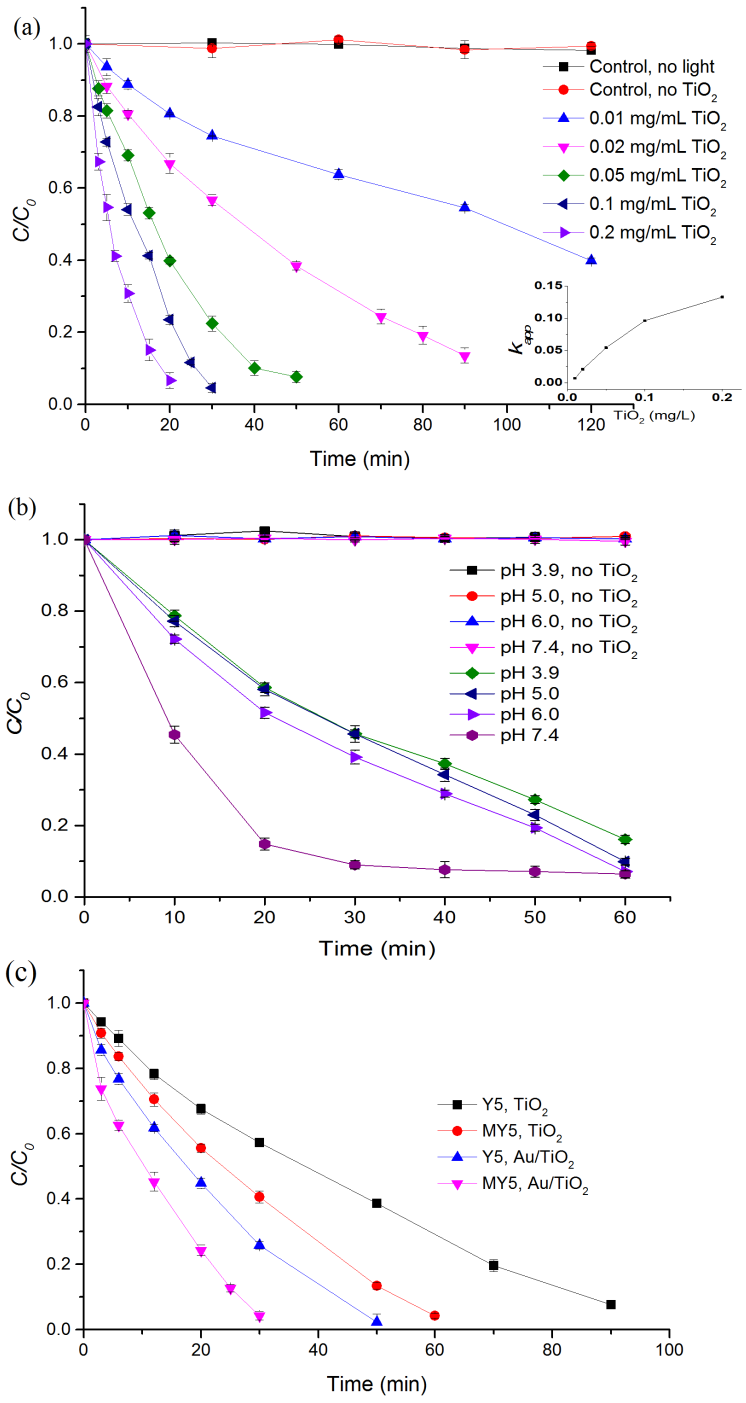

Figure 5-2 Decomposition of purified main component of FD&C Yellow No. 5 (MY5) under simulated sunlight. Y axis (C/C_0) shows the concentration of remaining dye at irradiation time divided by the initial dye concentration. Reactions were carried out in (a) water solutions of MY5 and 0 (control), 0.01, 0.02, 0.05, 0.1, and 0.2 mg/mL TiO_2 NPs irradiated by simulated sunlight for different time intervals or without sunlight exposure (control); (b) 10 mM PBS buffer (pH 5.0, 6.0 and 7.4) or 10 mM acetic acid buffer (pH 3.9) solutions containing MY5 and 0.1 mg/mL TiO_2 NPs; (c) water solutions of MY5 or batch certified

FD&C Yellow No. 5 (Y5) containing 0.1 mg/mL TiO_2 NPs or Au/TiO_2 hybrid nanostructures. The initial dye concentration in all samples was fixed at 25 mg/mL.

The degradation of FD&C Yellow 5 (Y5) and the purified main component of Y5 (MY5, also referred to as tartrazine) in the presence of nano TiO_2 was carried out under simulated sunlight. Fig. 5-2a illustrates the effect of the initial TiO_2 NPs concentration on degradation kinetics. The initial concentration of MY5 was fixed at 25 mg/L, while the concentration of TiO_2 NPs was adjusted to 0.01, 0.02, 0.05, 0.1 and 0.2 mg/mL. Fig. 5-2a, clearly demonstrates that MY5 remains unchanged after 120 min for the control group which contained no TiO_2 NPs but was exposed to simulated sunlight. Dos Santos et al (2014) have reported a significant reduction of tartrazine in aqueous solution with 15 min UV irradiation. The difference between our observation and the results obtained by those investigators may be attributed to the different light sources and intensities used. Fig. 5-2a shows that an increase in the concentration of TiO_2 results a higher rate of degradation rate for MY5. At TiO_2 NPs concentration of 0.1 mg/mL, the dye was not spectrophotometrically detectable after 30 min exposure to simulated sunlight, which was also confirmed using HPLC (Fig. S1). The decrease in dye concentration was plotted as ln (C/C_0) versus time and fitted into a first-order reaction model as described in materials and methods. The insert of Fig. 5-1a shows the calculated reaction constant, k_{app}, at different concentrations of TiO_2. The highest rate constant (k_{app} = 0.133 min^{-1}) was observed at 0.2 mg/mL TiO_2 NPs.

5.3.2.2 Effect of pH

The pH of the reaction mixture plays multiple roles in dye degradation process by affecting the ionization state of the TiO_2 surface, hydroxyl radical generation in the

solution (Konstantinou & Albanis, 2004), as well as the structure of tartrazine (Weisz et al., 2014). In this study we investigated pH 3.9, 5.0, 6.0 and 7.4 to mimic the pH range of particular food products. Fig. 5-2b shows that under slightly alkaline condition (pH = 7.4) the degradation rate was significantly promoted (k_{app} = 0.084 min^{-1}), whereas the rate constant k_{app} were calculated to be 0.028, 0.035 and 0.039 min^{-1} for pH 3.9, 5.0, and 6.0, respectively. Under acidic conditions (pH < 6.8), the TiO_2 surface is positively charged whereas it is negatively charged for pH > 6.8 (Poulios et al., 1999). When TiO_2 is negatively charged, the hydroxyl radical and superoxide radical generated on TiO_2 surface more readily diffuse into solution and are available for chemical reactions. However, it has been reported that the effect of pH on TiO_2 is not as significant as it is on the structure of azo dyes (Zhan et al, 1998). In acidic media (pH < 6), a strong adsorption of the dye on the TiO_2 particle has been observed, resulting from the significantly high electrostatic attraction force between the positively charged TiO_2 with the anionic dye molecule, whereas in alkaline condition, OH^- ions compete effectively with dye ions, causing a decrease in adsorption and accelerating the degradation process (Banerjee & Chattopadhyaya, 2013).

5.3.2.3 Effect of dye composition

FD&C Yellow No. 5 (Y5) is batch-certified by the U.S. Food and Drug Administration (FDA) to ensure compliance with specifications in the Code of Federal Regulations (CFR) (FDA, 2014). Among the specifications is a limit of 1% for each of two polysulfonated subsidiary colors: the tetrasodium salt of 4-((4′,5-disulfo(1,1′-biphenyl)-2-yl)hydrazono)-4,5-dihydro-5-oxo-1-(4-sulfophenyl)-1H-pyrazole-3-carboxylic acid; and the trisodium salt of 4,4′-(4,5-dihydro-5-oxo-4-((4-sulfophenyl)hydrazono)-1H-pyrazol-

1,3-diyl)bis(benzenesulfonic acid), which has been assigned the abbreviations Pk5 and Pk7 by Weisz et al., 2014. To our best knowledge, most of the Y5 samples in previously published studies were obtained from commercially available tartrazine samples which contain around 85% MY5. It is noteworthy that the purity and composition of those samples may not be similar and thus may lead to misunderstanding and inconsistency among studies. Therefore, we studied the batch-certified dye for food, drug and cosmetic

use, as well as its purified main component (MY5, ~99% purity).

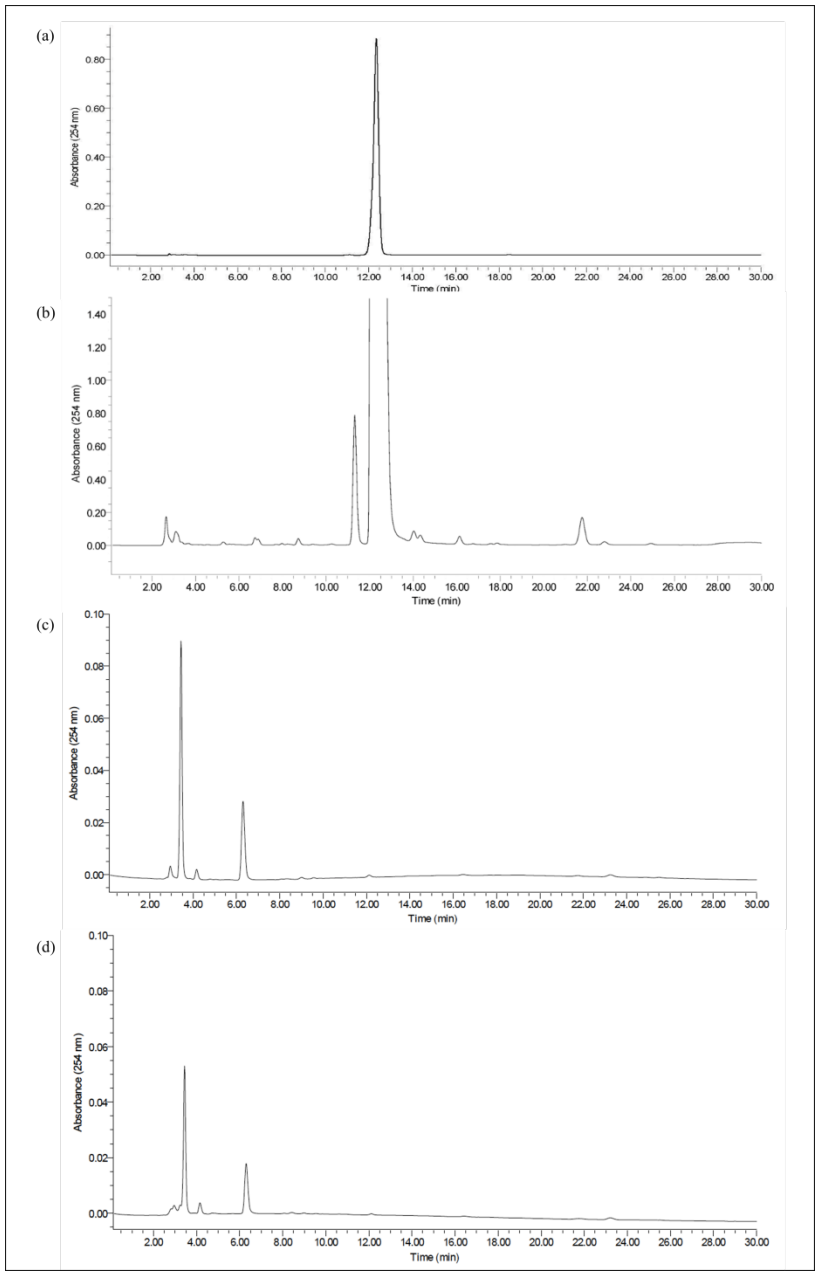

Figure 5-3 HPLC chromatograms of (a) purified main component of FD&C Yellow No. 5 (MY5; aka. tartrazine); (b) batch certified FD&C Yellow No.5 (Y5); degradation products of (c) MY5 and (d) Y5 resulted by 30 min irradiation of simulated sunlight. Sample solutions in (c) & (d) contained 0.1 mg/mL TiO_2 NPs. The effluent was monitored at wavelength 254 nm.

The HPLC chromatograms of Y5 and MY5 used in this study were shown in Fig. 5-3 a&b. Fig. 5-3c&d shows the decomposition of solutions containing those samples, respectively. Under the same treatment conditions, the FDA certified dye showed lower degradation rate compared to the purified main component according to data obtained by spectrophotometer analysis. However, it is too early to conclude that Y5 has greater stability in the presence of photoexcited TiO_2. Pk5 and Pk7 both have higher molecular weight than MY5 and moreover, have different light absorption characteristics.

5.3.2.4 Effect of doping Au onto TiO_2 surface

Nobel metals have been widely used to enhance the photoactivity of TiO_2. Au nanoparticles deposited on TiO_2 act as electron traps, enhancing the electron–hole separation and the subsequent transfer of the trapped electron to the adsorbed O_2 acting as an electron acceptor. Therefore, to investigate the relationship between dye degradation and electron/hole pair as well as ROS generation, we synthesized Au/TiO_2 hybrid nanostructure by depositing Au onto the surface of TiO_2. Fig. 5-2c shows that, for both MY5 and Y5, Au/TiO_2 exhibited enhanced photoactivity and accelerated color degradation. HPLC analysis showed that the decomposition of MY5 resulted by TiO_2 and Au/TiO_2 NPs yielded the same degradation products (data not shown here).

5.3.3 TiO_2 generated electrons and ROS

5.3.3.1 Detection of electron reactivity during photoexcitation of TiO_2 NPs

Electron spin resonance was employed to investigate the generation of reactive oxygen species (ROS) and occurrence of electron transfer during photoexcitation of TiO_2 in aqueous solution. The reactive electrons generated in 0.1 mg/mL TiO_2 NPs were detected

using a stable spin probe, 2,2,6,6-tetramethylpiperidine-1-oxyl (TEMPO). TEMPO is a stable radical that has been widely used as a spin label in ESR spectroscopy, exhibiting a triplet ESR spectrum, whereas its reduced form, hydroxyl amine (TEMPOH), is ESR silent (Lavi et al., 2004). As shown in Fig. 5-4a, the triplet-peak ESR signal of TEMPO remained unchanged for the control groups, either without TiO_2 NPs or without simulated sunlight irradiation. However, with the addition of TiO_2 NPs (0.1 mg/mL), the signal intensity significantly reduced after 3 min irradiation with simulated sunlight. Further flattening of ESR spectrum was observed for samples containing the same amount of Au/ TiO_2 NPs, indicating a higher fraction of TEMPO being reduced to TEMPOH. Since our results indicated that TEMPO does not react with other species in the solution, such as hydroxyl radical or superoxide radical generated by H_2O_2 (See Figure A1 in Appendix), the reduction of TEMPO necessarily resulted from the electrons generated during photoexcitation of TiO_2 NPs.

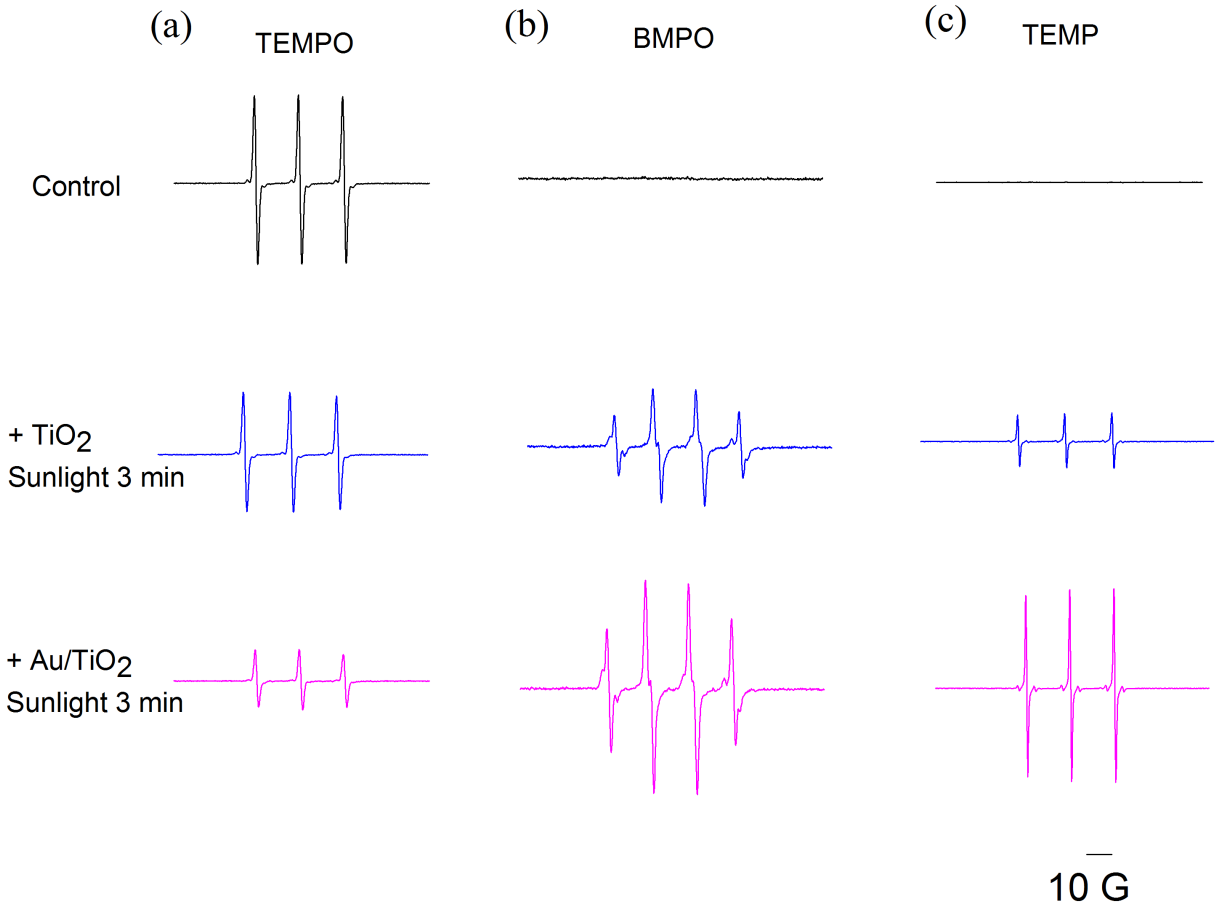

Figure 5-4 Detection of photogenerated electrons and ROS in solutions containing 0.1 mg/ml TiO_2 NPs or Au/TiO_2 hybrid nanostructures. ESR spectra obtained from samples containing different spin probes: (a) 0.02 mM TEMPO; (b) 25 mM BMPO; (c); 2 mM TEMP and. Control group represents samples without nanoparticles or no exposure to simulated sunlight. All the spectra were recorded after 3 min of irradiation with simulated sunlight.

5.3.3.2 Generation of hydroxyl and superoxide radicals

The generation of hydroxyl radical by photoexcited TiO_2 NPs in aqueous solution was confirmed using the spin trap BMPO. Being ESR silent itself, BMPO can trap hydroxyl radical or superoxide radical and become ESR detectable. The spin adduct BMPO/•OH exhibits a 1:2:2:1 peak ESR signal, with hyperfine coupling constant a^N = 13.5 G, a^H_β =

15.3 G and a^{H}_{γ} = 0.62 G, while the spin adduct of BMPO and superoxide radical (BMPO/$O2^{-\bullet}$) has a typical 4 line ESR spectrum with hyperfine splitting structure (a^{N} = 13.4 G, a^{H}_{β} = 12.1 G) (Zhao et al., 2001). Fig. 5-4b shows an ESR spectrum identical to BMPO/•OH spin adduct signal for TiO_2 exposed to simulated sunlight. A similar ESR pattern with higher intensity was observed for Au/ TiO_2 NPs under the same experimental conditions. Previous studies have reported difficulty when using BMPO as a spin trap for a system containing both •OH and $O_2^{-\bullet}$ due to possible overlap of BMPO/•OH and BMPO/ $O_2^{-\bullet}$ signals (Yin et al., 2012). For irradiated TiO_2 solutions, the formation of •OH has been widely recognized while several studies have reported observation of $O_2^{-\bullet}$ detected by ESR spectroscopy (Li et al., 2014). To determine whether superoxide radical is involved in this process, superoxide dismutase (SOD) was employed to scavenge superoxide radicals in order to eliminate any BMPO/ $O_2^{-\bullet}$ signal (See Figure A2 in Appendix). With the addition of SOD (0.2 U/ml) to the above TiO_2 NPs solution, the 1:2:2:1 peak ESR signal remained the same pattern that is identical to BMPO/•OH spin adduct. However, the intensity of the above signal was reduced to half. Since SOD does not scavenge •OH, we believe that the reduction of this ESR signal implies that O_2^- , in addition to •OH, is generated in photoexcited TiO_2 NPs solutions.

5.3.3.3 Generation of singlet oxygen

In addition to hydroxyl and superoxide radicals, singlet oxygen is another important ROS that has been implicated in the degradation of azo food dyes (Rembold & Kramer, 1978). We used the spin probe TEMP to study singlet oxygen ($^1O_2$) generation during photoexcitation of TiO_2 NPs. TEMP is ESR silent. When it reacts with singlet oxygen, the reaction product, a nitroxide radical, 4-oxo-2,2,6,6-tetramethylpiperidine-N-oxyl

(TEMPONE), is formed and shows a 1:1:1 peak ESR spectrum (Lion et al., 1976). No ESR signal was observed for control groups containing the spin probe and TiO_2 NPs without exposure to simulated sunlight or when TEMP alone was irradiated. ESR spectra having three lines with equal intensities (a^N=16.0 G), typical of nitroxide radicals, was found for irradiated solutions containing TEMP and TiO_2 (Fig. 5-4c) The hyperfine splitting constant and g factor of the observed signal were identical to those of commercial TEMPONE, indicating the generation of singlet oxygen during irradiation. Similar spectrum with higher intensity was observed for Au/ TiO_2. Previous studies found evidence that singlet oxygen was formed through the following pathway (Daimon et al., 2008):

$$O_2^{-\bullet} + h^+_{vb} \rightarrow {}^1O_2 \quad (3)$$

To test this theory SOD (0.2 U/mL) was added to the above mixture. This resulted in a reduction of this triplet ESR signal (See Figure A2 in Appendix). TEMPO signal significantly reduced upon the addition of SOD. Again, due to the fact that SOD is a specific enzyme that catalyzes the dismutation of superoxide ($O_2^{-\bullet}$), this result confirms that, during photoexcitation of TiO_2 NPs aqueous solution, superoxide radicals play a role in the formation of singlet oxygen.

5.3.4 Interaction between ROS and FD&C Yellow 5

5.3.4.1 Hydroxyl radical consumption

A time and pH dependence study was carried out to further investigate the role of hydroxyl radical in the decomposition of food dye (Fig. 5-5a). Insert of Fig 4a depicts the ESR spectrum of a typical BMPO/$^{\bullet}$OH spin adduct that was observed for all sample

solutions. The time dependence of the ESR signal intensity was obtained by measuring the peak to peak height of the second line of this ESR spectrum. Fig. 5-5a shows the time dependent ESR signal intensity obtained for photoexcited TiO_2 NPs solutions with or without MY5 at pH 5.0 or 7.4. For solutions containing only TiO_2 NPs, the signal intensities of BMPO/•OH adduct tested at pH 5.0 were significantly lower than samples tested at pH 7.4. This is most likely due to the lower availability of hydroxyl anions in acidic media. At pH 7.4, TiO_2 solutions with MY5 shows significantly lowered ESR intensity compared with TiO_2 NPs only, indicating that under the simulated sunlight irradiation, hydroxyl radicals generated on photoexcited TiO_2 NPs were consumed by the azo dye MY5, which results in decomposition. Interestingly, at pH 5.0, the addition of MY5 did not result in a significant change in ESR intensity for •OH spin adduct, implying that no or little •OH was used for dye degradation. The results from this ESR time and pH dependent study agrees with our previous observations shown in Fig. 5-2b, where lower reaction rate constant was found for acidic solution. This phenomenon might be explained by the previously reported theory that in acidic conditions, a strong adsorption of the dye on the TiO_2 particle has been observed as a result from the significantly high electrostatic attraction force between the positively charged TiO_2 with the anionic dye molecule.

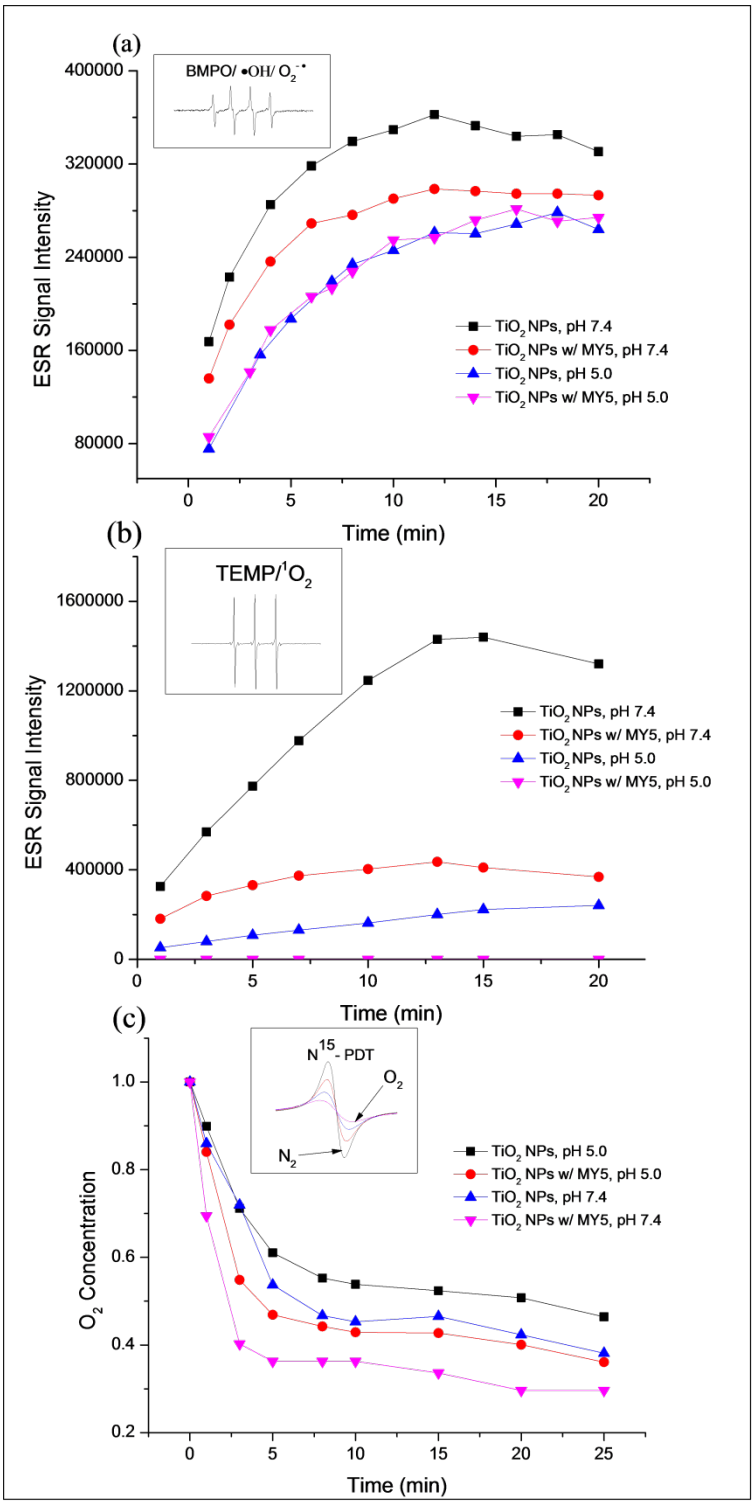

Figure 5-5 ROS and O_2 consumption during decomposition of dye upon simulated sunlight irradiation. Reactions were conducted in 10 mM buffered solutions with pH 5.0 or pH 7.4 containing different spin probes: (a) 25 mM BMPO; (b) 5 mM TEMP; (c) 0.2 mM ^{15}N-PDT. Sample solutions contained 0.1 mg/mL TiO_2 or Au/TiO_2 NPs with (or without) 25 mg/mL

MY5. Insert pictures present the ESR spectra of the detected species using corresponding spin probes. The time dependence of the ESR signal intensity was obtained by (a) measuring the peak to peak height of the second line of the ESR spectrum of the BMPO/•OH; (b) peak to peak height of the first line of the ESR spectrum of TEMP/$^1O_2$ adduct. O_2 concentration (c) was calculated based on the peak-to-peak line width of spin probe ^{15}N-PDT.

5.3.4.2 Singlet oxygen consumption

Fig. 5-5b shows the time dependence of ESR signal for the formation of TEMPONE from TEMP due to the generation of $^1O_2$. The insert in Fig. 5-5b shows the ESR spectrum of TEMPONE observed in all samples. ESR intensity detected at pH 7.4 was significantly higher compared to pH 5. This observation agrees with a previous study by Daimon et al. (2008), in which the generation of $^1O_2$ was suppressed when pH < 5 and reaches its maximum between pH 6 to pH 11. The decrease in $^1O_2$ at pH 5 compared to pH 7.4 is attributable to the suppression of $O_2^{-\bullet}$ at the TiO_2 surface, taking consideration that the $^1O_2$ originated from the oxidation of $O_2^{-\bullet}$ by the valence band holes h^+ (Equation 1). Unlike hydroxyl radical, the consumption of $^1O_2$ by the azo dye MY5 was found for both acidic and alkaline conditions. At pH 5, the ESR signal for $^1O_2$ was largely reduced when MY5 was added into the reaction mixture thus we did not observe any ESR signal for $^1O_2$. However, when BMPO is used in the above solution, a 6 peak ESR signal indicating the formation of carbon center radical was recorded by ESR spectroscopy (data not shown)(Yin et al., 2012), confirming the oxidation of dye MY5. The decrease in $^1O_2$ may take place by two mechanisms: one is by direct reaction with the food dye, the other is due to the decrease of available $O_2^{-\bullet}$ that has been consumed by dye oxidation.

5.3.4.3 Oxygen consumption

It has been well established that the $O_2^{-\bullet}$ in aqueous solutions containing TiO_2 NPs is produced from the reduction of oxygen by conduction band electrons (e^-_{cb}):

$$O_2 + e^-_{cb} \rightarrow O_2^{-\bullet} \quad (4)$$

Even though $O_2^{-\bullet}$ was indirectly detected by adding SOD to the solution containing both TiO_2 NPs and BMPO spin trap as discussed above, it was unclear how $O_2^{-\bullet}$ was involved in the decomposition process of MY5. Since difficulties arise when detecting $O_2^{-\bullet}$ by ESR due to the overlap of BMPO/ $O_2^{-\bullet}$ and BMPO/•OH spin adducts, a time and pH dependent study was conducted for O_2 consumption using ESR oximetry. The insert for Fig 4c shows the ESR spectrum of a commonly used water-soluble spin label ^{15}N-PDT. Fig 4c shows that for photoexcited solutions containing TiO_2 NPs, azo dye MY5 leads to higher O_2 consumption in both acidic (pH 5) and alkaline (pH 7.4) media. For solutions only containing TiO_2 NPs, O_2 was consumed at higher rate at pH 7.4 compared with pH 5. In the case that dissolved O_2 in solution does not directly cause dye decomposition (control group in Fig. 5-2 a&b), our finding suggests that the effect of pH primarily affects the initial rate of $O_2^{-\bullet}$ generation, other than the interaction between the azo dye and $O_2^{-\bullet}$.

5.3.5 Degradation products

In order to determine the main products generated during the degradation process, LCMS analysis was conducted using electrospray ionization (ESI) in positive mode. The high-resolution measurements of the quasi-molecular ions $(M+H)^+$ of the decomposition products was performed for 25 mg/L MY5 solution containing 0.1 mg/mL TiO_2 NPs after being exposed to simulated sunlight for 30 min. Fig. 5-6a shows the retention time for detected compounds after HPLC elution. Two major peaks were found at elution time t_r =

3.3 min and t_r = 6.0 min. The corresponding molecular mass of each of the characterized products in addition to the mass fragments obtained during the measurement is shown in Fig. 5-6b&c. The result indicates the formation of Product I (m/z=284.24), resulted by the destruction of the C–N (=) bond bound during MY5 degradation. The fragment ion at m/z = 111.04 could be a protonated dihydroxyphenyl group ($C_6H_7O_2$) for which the calculated mass of 111.0446 matches well with the obtained mass of 111.0442. Similar fragmentation behavior was reported by Meetani et al. (2011). The fragment with m/z = 59.06 could also result from the reduction of the dye molecules occurring during the ionization process. Furthermore, the spectrum reported for Product II (m/z = 174) matches the calculated molecular weight sulfalinic acid. At the same retention time, fragment m/z = 191 was detected and could be assigned to its hydrate. Our result confirms that the decomposition was due to the destruction of chromosphere azo –N=N– group, which has a maximum absorbance at a wavelength of 427 nm (Ghezzar et al., 2013). Zhan et al. (1998) also reported that the azo bond was attacked during TiO_2 NPs catalyzed degradation of MY5. In this study we also detected the degradation products of MY5 catalyzed by Au/TiO_2 NPs. Similar results were found for both nanoparticles, indicating that doping Au on to TiO_2 surface enhances the photoreactivity, but does not change the reaction pathways of azo dye destruction during simulated sunlight irradiation.

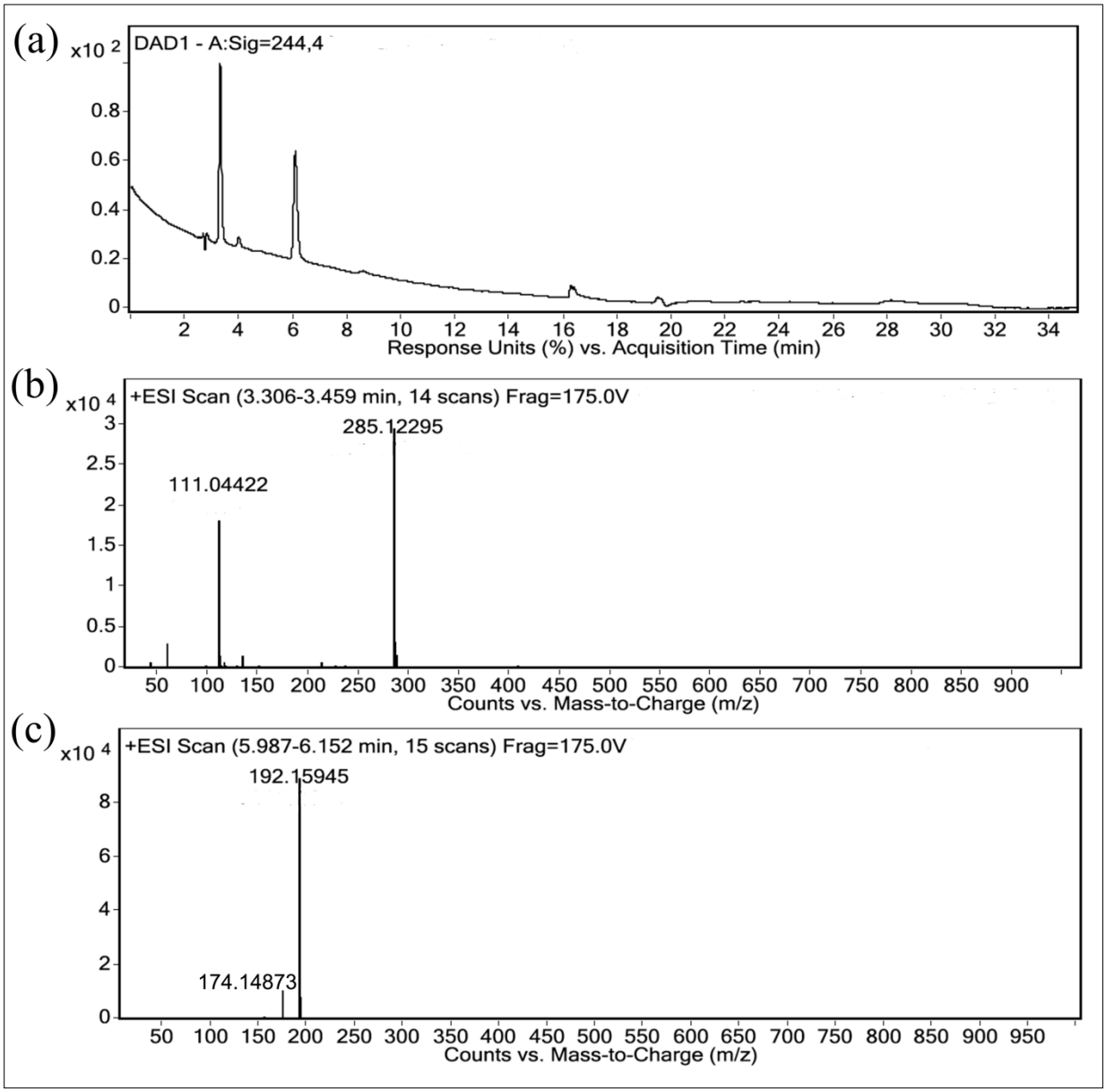

Figure 5-6 LC–ESI (+)–MS chromatograms obtained for sample mixture of TiO_2 NPs (0.1 mg/mL) and purified main component of FD&C Yellow No. 5 (MY5, 25 mg/mL) solutions after 30 min exposure to simulated sunlight.

5.4 Conclusion

Nanosized TiO_2 particles have been found in a broad range of consumer products, in particular, foods and cosmetics. Our results confirmed that when exposed to sunlight, TiO_2 NPs at low concentration can trigger decomposition of the azo dye, FD&C Yellow

No.5, which has been widely used in food, drug and cosmetic products. ESR spin trap technique was first used to direct observe the time- and pH-dependent color degradation that proceeds via reaction with ROS generated on photoexited TiO_2 surface. LC/MS results confirmed that the azo bond is the main targeted group during decomposition. At pH 7.4, a significant reduction in both hydroxyl radical and singlet oxygen were observed after adding dye into the solution, while it was indicated that singlet oxygen became the main reaction species at pH 5.0. Using the widely used and relatively stable synthetic color FD&C Yellow No. 5 as an example, our study characterized the decomposition procedure and directly monitored the involving of ROS, of which the significance is found in both food materials as well as in physiological entities since it leads to oxidative stress and damage. The findings in this study may provide important insight when designing new applications or evaluating the safety of nano TiO_2 in food and cosmetics, as the interaction between nanomaterials and other ingredients should also been investigated in addition to study the nanomaterials as an independent components.

Chapter 6: Phase-dependent ROS promoting ability of TiO_2 NPs and degradation of food dye chlorophyllin copper sodium salt, tartrazine, sunset yellow, and allura red

6.1 Introduction

Titanium dioxide (TiO_2) is primarily used to provide whiteness in a wide range of commercial products including food, cosmetic, pharmaceutical and personal care products (Marmion, 1991). Moreover, it has been widely used in sunscreens because it effectively attenuates UV-B radiation and protects skin damage from sunlight irradiation (Popov et al., 2005). As a metal oxide semiconductor, it also has been extensively used in environmental science for pollutant treatment because of its well-recognized photocatalytic property (Park et al., 2007). The use of TiO_2 in sunscreens can be as high as 10% by weight (Weir et al., 2012), while in food products it is limited not to exceed 1% by weight in the US (FDA, 2014).

The total production of TiO_2 as a pigment has been estimated to be approximately 2 million tons per year in the US by 2016, with a nano-TiO_2 portion around 20% (Robichaud et al., 2009). Many applications of TiO_2 would benefit from smaller particle sizes. The nanosized TiO_2 is advantageous because it retains UV filtration and absorption properties while eliminating the white chalky appearance (Mu & Sprando, 2010). When discussing the safety of TiO_2 NPs, one may argue that the use of TiO_2 NPs as a pigment is not feasible, since the nanosized TiO_2 is normally assumed to present less whiteness and thus may render it unfavorable compared to the traditional microsized TiO_2 (Robichaud et al., 2009). However, with the development of synthetic methods, the loss

in whiteness can be avoided by particle size control that allows higher contrast ratio and hardness (Zhang et al., 2007).

Moreover, large amounts of TiO2 NPs have been detected in commercial food products as well as in commercial food-grade TiO2 powders that have been labeled as E 171. A systematic study with a focus on the size distribution of TiO_2 in food and personal care products round approximately 36% of the particles (by total particle counts) in food-grade TiO_2 (E171) were found to be less than 100 nm (Weirs et al., 2012). Yang et al (2014) investigated 5 food-grade TiO_2 (E171) samples and found that nanosized materials were present in all of the food-grade TiO_2 samples, with different portions ranging from 19% to 35% by number. Their results also indicated that samples obtained from different vendors can have distinguishable properties in particle size and phase composition. Chen et al. (2013) characterized the TiO_2 in chewing gum and discovered that over 93% of TiO_2 particles in gum were in the nano range. Crystalline phase is another important characteristic that determines the physicochemical property of TiO_2. Both anatase and rutile phase were found in food-grade TiO_2 samples, and the composition of each phase was found to vary from sample to sample.

Nanosized TiO_2 shows improved photoactivity therefore being extensively applied as catalysts in advanced oxidation processes for the degradation of industrial waste and detoxification of pesticide residues. However, this photocatalytic degradation behavior is unwanted when using TiO_2 as an ingredient in food or cosmetic products, since it may damage light sensitive compounds such as food colors or antioxidants. Our previous study suggested that when exposed to simulated sunlight, nanosized TiO_2 results degradation of food color tartrazine and leads to loss of radical quenching ability of

various antioxidants. Chen et al. (2013) demonstrated that commercial food-grade TiO_2 samples exhibited photocatalytic activity. The degradation proceeded via oxidative decomposition that is associated with reactive oxygen species (ROS) generated by photoactivated TiO_2 nanoparticles (NPs). In this study, food-grade TiO_2 samples were compared with anatase, rutile TiO_2, as well as the widely studied mixed phase TiO_2, P25 to determine its ROS promoting ability. The possible degradation of food colors resulted by food-grade TiO_2 were investigated on four selected food colors, including one semi-natural dye chlorophyllin copper sodium salt (E141) and three widely used synthetic food dyes, namely tartrazine (E102), sunset yellow (E110) and allura red (E129) (structures shown in Fig. 6-1). Since food materials are complicated matrix of various active ingredients, antioxidant may protect the color from being damaged by light irradiated TiO_2. Therefore, we employed ascorbic acid to study its influence on the degradation of chlorophyllin copper sodium salt in solution containing food-grade TiO_2.

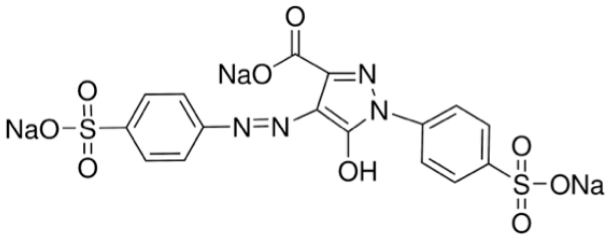

Tartrazine (TZ)

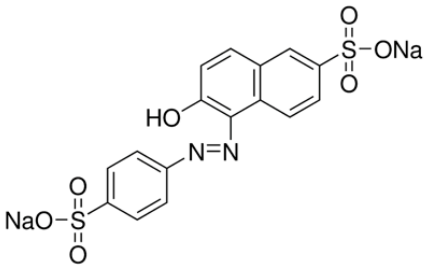

Sunset Yellow (SY)

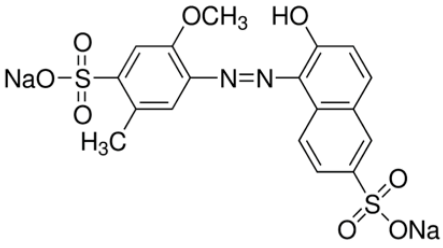

Allura Red (AR)

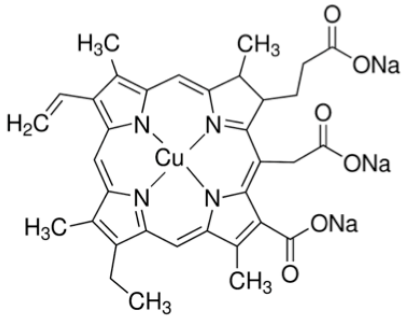

chlorophyllin copper sodium salt (CCS)

Figure 6-1 Structures of the synthetic azo dye tartrazine, sunset yellow allura red and the semi-synthetic dye chlorophyllin copper sodium salt.

6.2 Materials and Methods

6.2.1 Materials

Four TiO_2 samples were obtained from different vendors. The food ingredient TiO_2 powder (FG) that has been market as white pigment was obtained from a US vendor on market (catalog #0514068011). Anatase TiO_2 powder (AN, 325 mesh anatase, catalog #248576) was purchased from Sigma Chemical Co. (St. Louis, MO). TiO_2 P25 powder (P25, 31 nm anatase/rutile, catalog Aeroxide® TiO_2 P25) was purchased from Degussa (Alpharetta, GA). Rutile TiO_2 water dispersion (RU, 20% wt., catalog #7732-18-5) was purchased from US Research Nanomaterials, Inc (Huston, TX). Spin trap 5-

tertbutoxycarbonyl 5-methyl-1-pyrroline N-oxide (BMPO) was purchased from Bioanalytical Labs (Sarasota, FL). The spin probe 2,2,6,6-Tetramethyl-4-piperidone (TEMP) was purchased from Wako Pure Chemical Industry, Ltd. Japan. Stable free radical 1,1-diphenyl-2-picryl-hydrazyl (DPPH•), Allura Red AC (AR, dye content 80%), Sunset Yellow FCF (SY, dye content 90%), and tartrazine (TZ, dye content >85%), L-ascorbic acid (AA), and the chlorophyllin sodium copper salt (CCS) were all purchased from Sigma-Aldrich (Saint Louis, MO). Distilled deionized water (18.2 MΩ.cm) from a Milli-Q water purification system was used in all experiments. The copper grids coated with carbon film for TEM sampling were purchase from SPI supplies (West Chester, PA).

6.2.2 Transmission electron microscopy

Transmission electron microscopy (TEM) and high resolution TEM (HRTEM) images were obtained by a JEM 2100 LaB6 (JEOL) transmission electron microscope operated at 200 kV, coupled to an energy dispersive X-ray analysis system (EDX). The experiment was conducted at the NanoCenter, University of Maryland, College Park, MD. For TEM analysis, 0.01 mg/mL aqueous suspension of each TiO_2 samples was treated with ultrasonication in a water bath for 5 min at ambient temperature. Five milliliter of the above dispersion was dropped to standard holey carbon-coated copper grids, which were then air dried at ambient temperature before subsequent electron microscopy work.

6.2.3 X-ray diffraction

The X-ray diffraction (XRD) pattern was determined to analyze the crystal structure of FG TiO_2. The experiments were performed using a Bruker D8-Advance Diffractometer

(Bruker AXS, Inc., Madison, WI) with Cu Kα radiation and an aluminum holder. Each sample was scanned at 2θ degree from 20° to 60° to detect characteristic TiO_2 peaks. Semi-quantitative analysis of the crystalline phases (e.g., the ratio of anatase to rutile) was calculated for appropriate samples using PANalytical HighScore Plus software (based on the Rietveld method).

6.2.4 ESR spectroscopy

All ESR measurements were carried out using a Bruker EMX ESR spectrometer (Billerica, MA) at ambient temperature (23˚C). All samples were put in 50 μL capillary tubes and sealed with Critoseal™ capillary tube sealant before being placed in the ESR cavity. All ESR measurements were carried out using the following settings for detection of the spin adducts: 20 mW microwave power, 100 G scan range and 1 G field modulation. A solar simulator consisting of a 450 W Xenon lamp filtered to provide simulated sunlight was used as the light resource in ESR studies. The spin trap BMPO was used to verify the formation of superoxide ($O_2^{-\bullet}$) and/or hydroxyl radicals (•OH) during exposure of each TiO_2 samples to simulated sunlight. The spin probe TEMP was used to detect the formation of singlet oxygen ($^1O_2$) in sunlight irradiated TiO_2 solutions. The amount of radicals generated in TiO_2 solution upon light irradiation was quantitatively measured by the ESR spectroscopy. ESR spectra were recorded from the sample mixture, containing BMPO or TEMP spin probes and TiO_2 aqueous solutions. For samples containing BMPO or TEMP, spectra were recorded after 3 min of simulated sunlight irradiation. The stable free radical DPPH (DPPH•) was used to demonstrate the radical scavenging ability of the semi-nature color CCS and AA. ESR spectra were measured after 2 min of mixing for samples containing DPPH•. Control samples, either

without TiO_2 or without simulated sunlight irradiation were also recorded for comparison. The final concentration of each component is described in each figure caption.

6.2.5 Color degradation

Stock solutions of AR, TZ, SY and CCS were prepared at 2500 mg/L, stored in refrigerator and sheltered from light. The stock solutions were used within one week. To exam the photocatalytic degradation of color, 0.2 mg/mL TiO_2 (FG or RU) were mixed with 25 mg/L AR, TZ SY, or CCS. 10 mL of each mixture were transferred to a 50 mL quartz Erlenmeyer flask and sealed. Ascorbic acid was added to CCS solutions containing FG TiO_2 sample to study its effect on color degradation. The mixed suspensions were stirred in the darkness for 30 min to allow equilibrium and irradiated using a light source consisting of a Universal Arc Lamp Power Supply (69920 Universal Supply, Newport, Irvine, CA) using xenon lamps (880 W) and an Oriel® Xenon Arc Lamp Solar Simulator. During irradiation, the Erlenmeyer flasks were kept in an ice tray to prevent thermal degradation of food colors. The degradation process was monitored using a Varian Cary 300 spectrophotometer. Before UV-Vis analysis, the reaction mixture was centrifuged to remove the TiO_2 particles. The maximum absorbance λ_{max} of TZ at wavelength 425 nm, AR at 504 nm, SY at 482 nm were studied for color degradation. The quantitative degradation study of CCS was assayed as a loss of absorbance at 627 nm, corresponding to both the observed and published red absorption maximum of CCS (Chernomorsky et al., 1997; Ferruzzi & Schwartz, 2005). Solutions were diluted with water (V:V = 1:1) before measurement. The results presented were the mean values with a total error of less than 5%.

6.3 Discussion

6.3.1 Size distribution and surface morphology

The surface morphology and number-based particle size distribution of TiO_2 samples were studied by transmission scanning microscopy. Fig. 6-2 a-d shows the TEM pictures of sample RU, AN, FG, P25, respectively, while Fig. 6-2 A-D represents the corresponding HRTEM pictures of these samples. Particle size is recorded as the maximum diameter of the particle and derived from TEM images. 30 particles were counted for each sample and data is shown as average ± standard deviation. The primary particle size of RU, AN, FG, P25 TiO_2 samples were found to be 52±23, 51±17, 20±15, 22±11 nm. The sizes of RU, AN and P25 are roughly consistent with the sizes claimed by the vendors. Nearly all of the particles in FG TiO_2 fell into nano-size which defines a dimension < 100nm in diameter. The TEM images shows that aggregates or big clusters are formed for all samples, while the biggest aggregates were observed especially for the smallest P25 sample. Sample FG and AN TiO_2 formed comparatively smaller aggregates with a diameter approximately at 150-200 nm. This observation agrees with the previous report in which the P25 TiO_2 aggregated more rapidly and into larger aggregates than food-grade TiO_2 (Weirs et al., 2012).

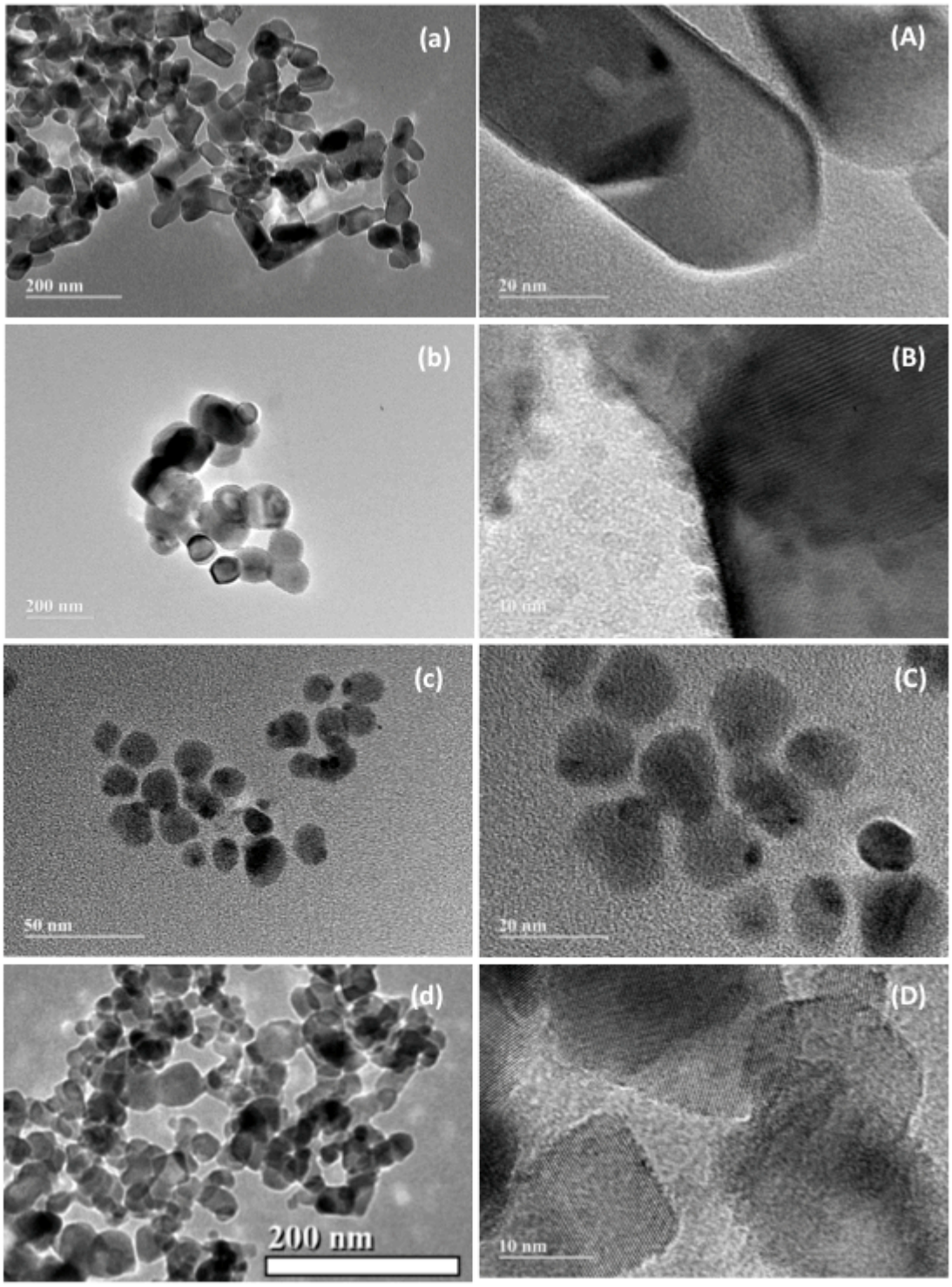

Figure 6-2 TEM (left panel) and HRTEM (right panel) images of (a) rutile (RU); (b) anatase (AN); (c) food-grade (FG) and (d) Degussa P25 (P25) TiO_2samples. Samples were prepared by dropping 0.01 mg/mL aqueous suspension of TiO_2 on to carbon coated copper grip.

The RU TiO_2 sample appears as nano-rods whereas the other samples took the form of more spherical-like structures. HRTEM images were captured to study the surface characteristics of each sample, and the lattice distance was investigated by the built-in function in TEM software. Fig. 6-2B shows that for AN, the anatase {101} facets (lattice fringes with spacing of 0.35 nm) were observed as the dominant facets. A clear lattice structure with lattice distance of 0.33nm, characteristic of the most stable rutile {110} facet (Yan et al., 2013) was observed for RU TiO_2 (Fig. 6-1A). It is interesting that small dots (< 3nm) were found on the AN TiO_2 surface. EDX analysis results (See Fig. B1 in Appendix) indicated that they were most likely to be TiO_2 small dots since no other elements or impurities were detected. Fig. 6-1D reveals the polycrystalline nature of the anatase and rutile phases for the P25 TiO_2 powders. By measuring the lattice fringes, the interplanar distances , 0.35 and 0.33 nm, were both observed, corresponding to the {101}planes of anatase and the {110} planes of rutile, respectively (Wang et al., 2011). The crystalline structure observed on FG TiO_2 was less obvious compared with other samples (Fig. 6-2C), indicating that only a few portions of FG TiO_2 exhibit clear crystalline structure. This may be the result of the techniques and methods used when TiO_2 was produced, for example, the calcination temperature (Chen et al., 2002).

6.3.2 Crystalline phase

HRTEM results suggested that the phase composition of the RU, AN and P25 samples were consistent with the descriptions provided by the vendors. It was difficult to determine whether anatase, rutile or brookite TiO_2 is the primary phase in food-grade

TiO_2. X-ray diffraction analysis (XRD) was performed to determine the phase composition of FG TiO_2. XRD patterns exhibiting strong diffraction peaks at 27°, 36° and 55° indicate that TiO_2 was in the rutile phase. On the other hand, XRD patterns exhibiting strong diffraction peaks at 25° and 48° indicate TiO_2 in the anatase phase (Thamaphat et al., 2008). Fig. 6-3 shows the XRD pattern of the FG TiO_2. The black line represents the sample (FG) while the red line represents the standard pattern of anatase TiO_2. The peaks in black line matches well with it in the red line, indicating that the food-grade TiO_2 sample we obtained were all anatase TiO_2. The main peak at 2θ degree equal to 25.27° is the anatase {101} reflection. Yang et al. (2014) screened five food-grade TiO_2 samples from different vendors and also found that four of them contain only anatase phase, while only one was a mixture of both anatase and rutile TiO_2.

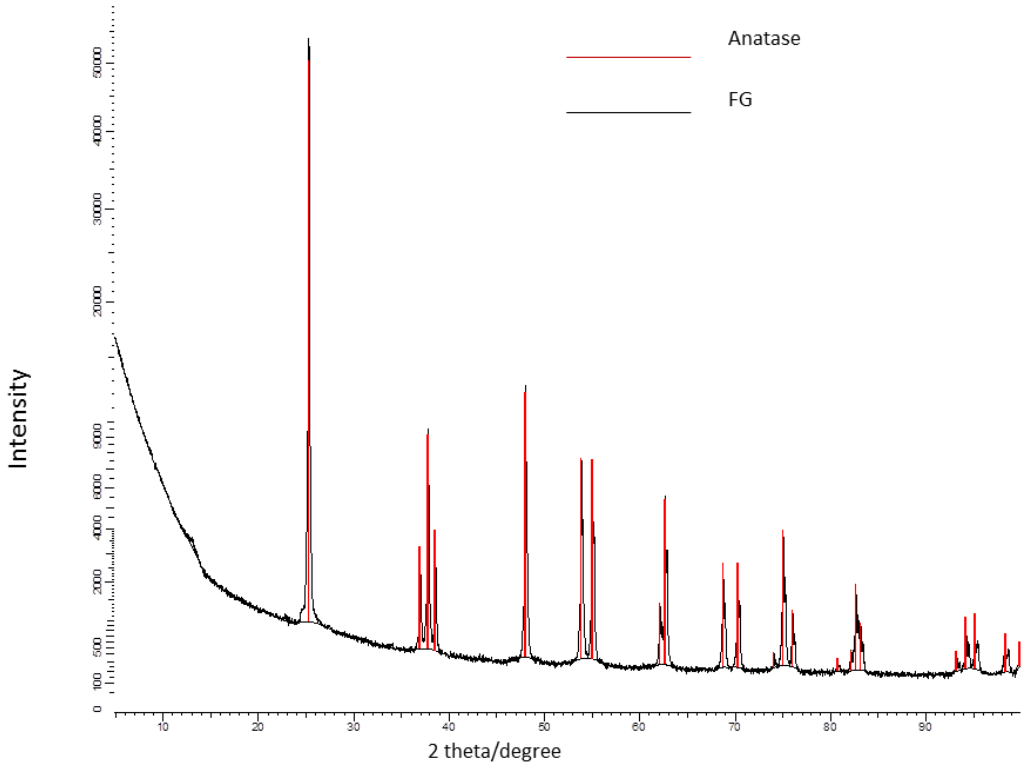

Figure 6-3 XRD pattern of food-grade (FG) TiO_2sample (black line). Red line represents the XRD pattern of standard anatase TiO_2 samples as a reference.

6.3.3 Promotion of reactive oxygen species (ROS)

TiO_2 triggers the generation of reactive oxygen species (ROS) when irradiated with ultra-visible (Miller et al., 2012), visible (Lipovsky et al., 2013) and simulated sunlight (Mansfield et al., 2014). The main ROS species generated in light irradiated TiO_2 aqueous dispersion includes hydroxyl radical (•OH), superoxide radical ($O^{2-\bullet}$) and singlet oxygen ($^1O_2$). The magnitude of ROS promotion largely depends on the particle size, surface morphology, crystalline phase and the concentration of TiO_2. It has been previously reported that when the concentration and particle size are at comparable levels, ROS promotion ability of TiO_2 follow the sequence P25 > anatase > rutile.

Here we compared the ROS promotion ability of FG TiO_2 with RU, AN and P25 by electron spin resonance (ESR) spectroscopy. ROS are highly reactive species that are difficult to detect, therefore the spin trap 5-tertbutoxycarbonyl 5-methyl-1-pyrroline N-oxide (BMPO) was employed to trap the short-lived ROS such as •OH and $O^{2-\bullet}$, forming stable radicals that allow reliable measurement of ROS. The left panel of Fig. 6-4 shows ESR spectrum presenting a 1:2:2:1 peak pattern, which is the characteristic spectra of the BMPO/•OH signal. Our results confirm the observation in previous studies that P25 shows the highest ROS generating ability, followed by anatase sample The rutile sample exhibits little radical signal. Food grade samples promoted nearly same amount of •OH compared to the anatase TiO_2 sample AN. This observation agrees with the XRD crystallography which indicate that FG TiO_2 contains >99% anatase phase.

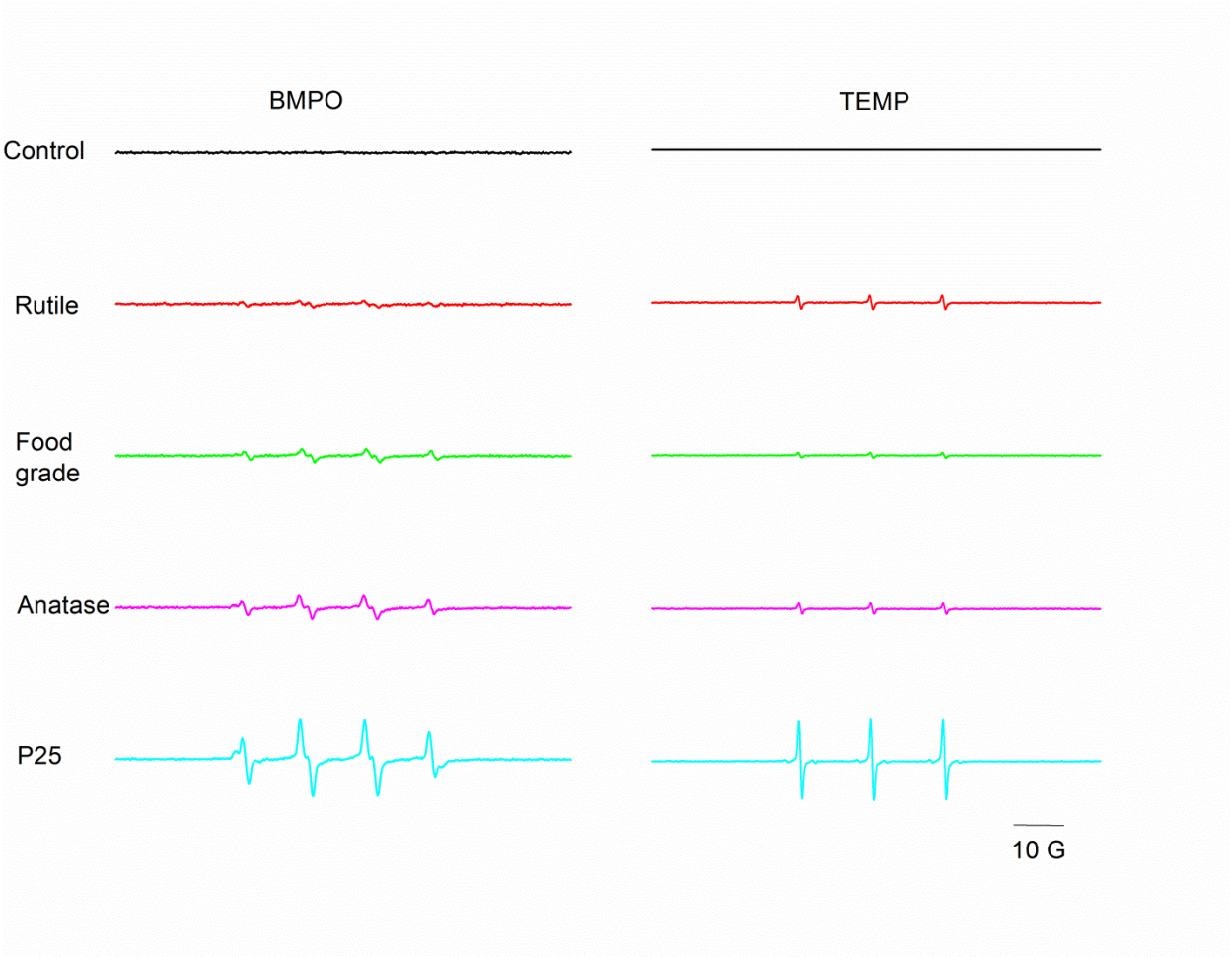

Figure 6-4 ESR detection of ROS in solutions containing 0.1 mg/ml TiO_2 samples. ESR spectra obtained from samples containing spin probe 25 mM BMPO or 2 mM TEMP and. Control group represents samples without nanoparticles or no exposure to simulated sunlight. All the spectra were recorded after 3 min of irradiation with simulated sunlight.

Singlet oxygen generation was studied using spin probe 2,2,6,6-Tetramethyl-4-piperidone (TEMP). The spin-trapping was accomplished by utilizing the oxidation of 2, 2, 6, 6-tetramethyl-4-piperidone (TMPD) by $^1O_2$ which yields paramagnetic 2, 2, 6, 6-tetramethyl-4-piperidone-1-oxyl (TEMPONE) (Yadav & Pospíšil et al., 2012). Previous study in our lab proved that this oxidative reaction is exclusively promoted by $^1O_2$. The control group in the right panel of Fig.4 contains only TEMP and it was ESR silent upon

simulated sunlight irradiation. Three-peak ESR spectra were recorded for all TiO_2 samples, indicating the formation of the radical 4-oxo-2,2,6,6,-tetramethyl-1-piperidinyloxyl (TEMPONE). The $^1O_2$ promotion of each TiO_2 sample followed the same sequence with •OH promotion, i.e. P25> AN ≈ FG > RU. The ROS promotion ability of food TiO_2 NPs under dark has also being reported, as they induced a slight increase of ROS in cells, but no obvious cell viability and membrane damage (Chen et al., 2012).

6.3.4 Food color degradation resulted by food-grade TiO_2

The highly active ROS triggered by light irradiated TiO_2 in aqueous solution can attack other chemical compounds in the system and thus lead to oxidative destruction. Our ESR study suggested that upon simulated sunlight irradiation, food-grade TiO_2 samples generated high amounts of •OH and $^1O_2$, which are the main species that cause the loss of food colors (Salem et al., 2009). RU TiO_2 resulted less amount of ROS generation. Therefore, we studied TiO_2s sample RU and FG to investigate whether they lead to food color degradation upon simulated sunlight irradiation.

6.3.4.1 Tartrazine, sunset yellow, allura red

Tartrazine (TZ), sunset yellow (SY) and allura red (AR) are three of the seven synthetic dyes permitted by FDA as food colorants (Vachirapatama et al., 2008). These synthetic azo dyes have broad industrial application due to their low cost and relative stability compared to natural colorants. In our study solutions containing 25 mg/L food synthetic dye, including TZ, SY or AR were each mixed with 0.2 mg/mL TiO_2 and irradiated by simulated sunlight. The concentration of the color was monitored by UV-Vis spectroscopy and the result is shown in Fig.5. The maximum absorbance λ_{max} were

observed for TZ at wavelength 425 nm, AR at 504 nm, SY at 482 nm. The control group contained food dye without TiO_2 and were also exposed to simulated sunlight irradiation. As expected, the azo dyes showed fairly good stability to sunlight irradiation. The UV spectra of samples in the control group did not change compared to the untreated group (labeled as "blank").

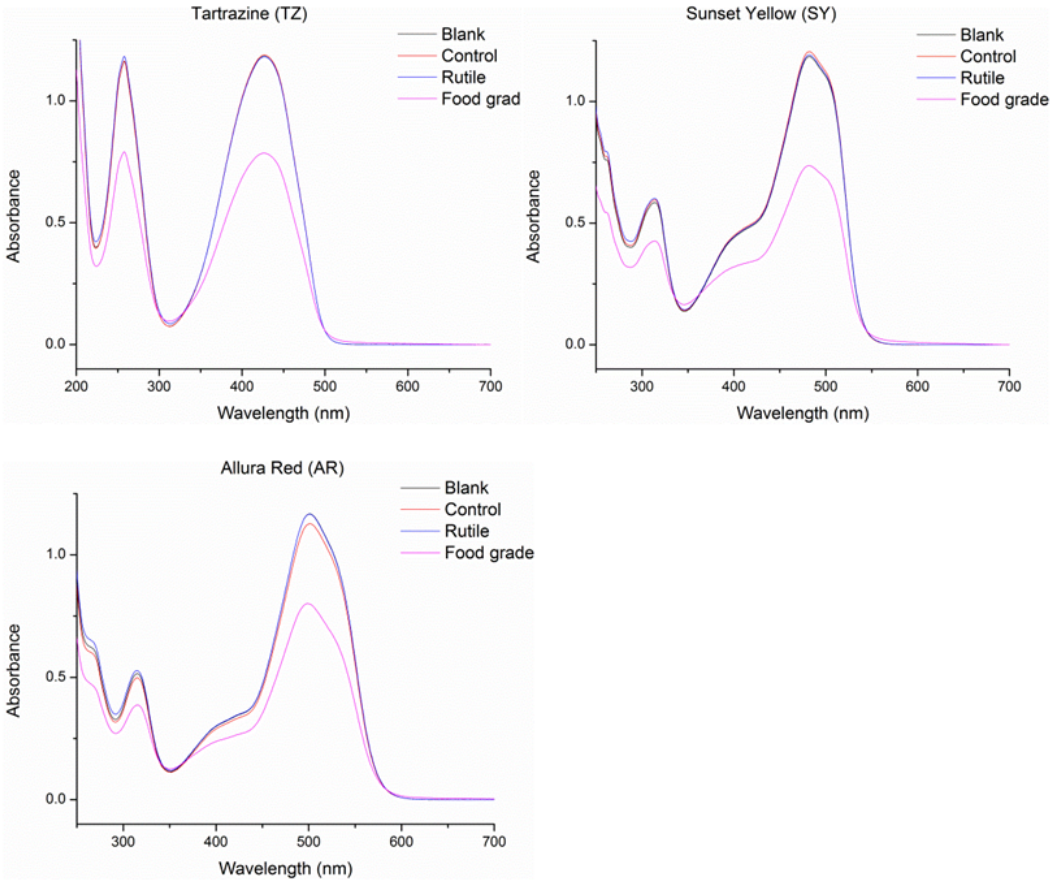

Figure 6-5 UV-Vis spectra of tartrazine, sunset yellow and allura red upon 2hr simulated sunlight irradiation. The initial concentration of dye was fixed at 25 mg/L. Groups marked as "blank" were not exposed to light irradiation. Reaction mixtures contained 0.2 mg/mL rutile or food-grade TiO_2, or no TiO_2 (for control group).

Data in Fig. 6-5 shows that the addition of Rutile TiO_2 did not result in noticeable decomposition of azo dye in the observed time period (2hr). However, when adding the

same amount of food-grade TiO_2 into the dye solution, a significant degradation of dye was detected for all three color samples. The food-grade TiO_2 caused 33%, 42%, 29% reduction of TZ, SY and AR respectively. The photocatalytic activity of semiconductors has been associated with its ROS generating ability (He et al., 2014). The difference in particle size is one possible reason that a significantly higher photocatalytic activity of FG sample (20±15) compared to RU (52±23). Smaller particles with higher surface to volume ratio generally exhibit improved chemical activity. Also, the FG sample was characterized as anatase TiO_2, which has a higher Fermi level over the rutile by 0.1 eV (Kogo et al., 2012). This leads to a lower O_2 affinity and an increased hydroxyl radical generation on the surface, whereas the hydroxyl radicals lead to the oxidation of dye molecules (Mohamed et al., 2009).

6.3.4.2 Chlorophyllin

Chlorophyllin copper sodium salt (CCS), the semi-synthetic water soluble bright green colorant has been used as food colorant as well as dietary supplement for its DNA-protective and antioxidant properties. Derived from natural chlorophyll, CCS is not heat stable compared to some synthetic dyes (Ferruzi et al., 2005). In this study, in addition to the synthetic azo dyes, CCS was also studied for possible degradation resulting from sunlight irradiated TiO_2 NPs. Fig. 6-6 represents the UV-Vis spectrum of CCS after irradiated by simulated sunlight for 0, 6, 12, 20, 40 and 60 min. As expected, CCS is more vulnerable to simulated sunlight irradiation compared with the synthetic azo dyes TZ, SY and AR. The control group (Fig. 6-6a) without TiO_2 added to the solution showed significant loss of color upon light irradiation. However, an unexpected result was observed when adding the FG TiO_2 into the reaction solution (Fig. 6-6b). The additional

TiO_2 did not accelerate the light induced degradation as expected (36±7% degradation, compared with control group 44±6%). This result showed that different from the azo dyes, CCS showed high tolerance towards the photocatalytic activity of TiO_2 NPs, even though it is very sensitive to light. To our best knowledge, only a few studies were reported on the interaction between photocatalyst TiO_2 and CCS, it is hard to make an explanation for the observed phenomenon. However, the mechanism is possibly involved with the intrinsic property of CCS as its natural derivation, chlorophyll, exhibits high photosensitization activity (Neverov et al., 2011). Photosensitized oxidation proceeds by a different pathway compared to photocatalyzed degradation, as the electrons (e^-) originate from the photosensitized dye molecules rather than TiO_2 (Konstantinou & Albanis, 2014).

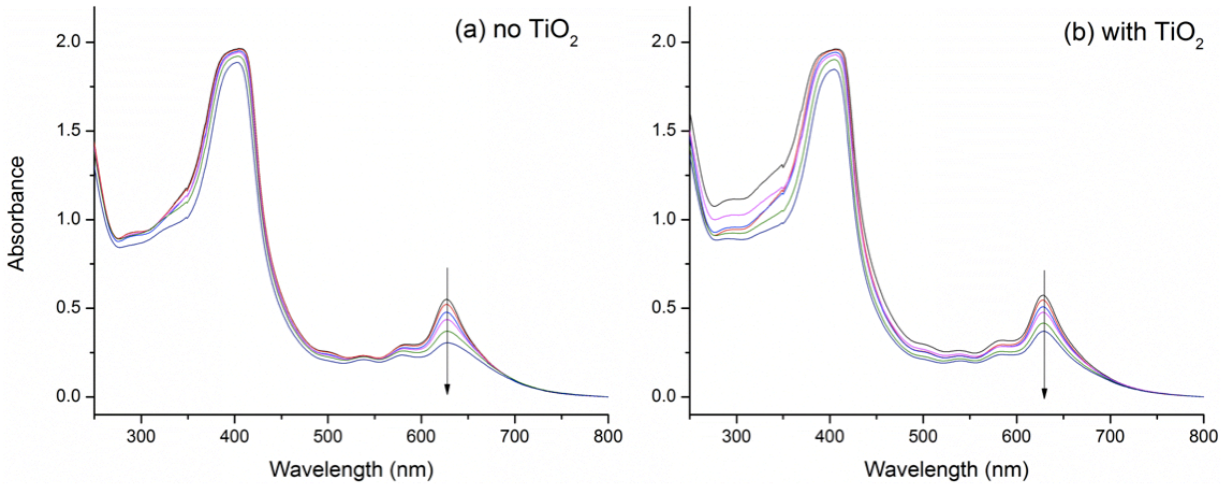

Figure 6-6 UV-Vis spectra of chlorophyllin copper sodium salt solution upon 2hr simulated sunlight irradiation. The initial concentration of dye was fixed at 50 mg/L. Control (a) contained no TiO_2 while sample solution (b) contained 0.2 mg/mL food-grade TiO_2 samples.

6.3.5 Effect of ascorbic acid

Radical scavengers are able to quench hydroxyl radicals formed on photoactivated TiO_2 surfaces that lower the degradation rates (Sakai et al., 1998). In food systems, the most common radical scavenger is ascorbic acid. As an excellent antioxidant, ascorbic acid is added to during processing or before packing to protect color, aroma and nutrient content. Our study first attempted to unravel the complicated interaction between food color, food-grade TiO_2 and the antioxidant ascorbic acid (AA) added to the solution. A simulated sunlight induced study was carried out to evaluated CCS degradation with TiO_2 as influenced by AA. Fig. 6-7a shows the CCS degradation rate expressed as the ratio of light absorbance at different irradiation times verses the untreated sample (readings were taken at wavelength 625nm). The addition of 200 mg/L AA into the solution promoted CCS decomposition rather than protecting it from light. This result is interesting since AA has been reported to hinder light induced color degradation and to protect those active compounds from light illumination (Lee et al., 1998).

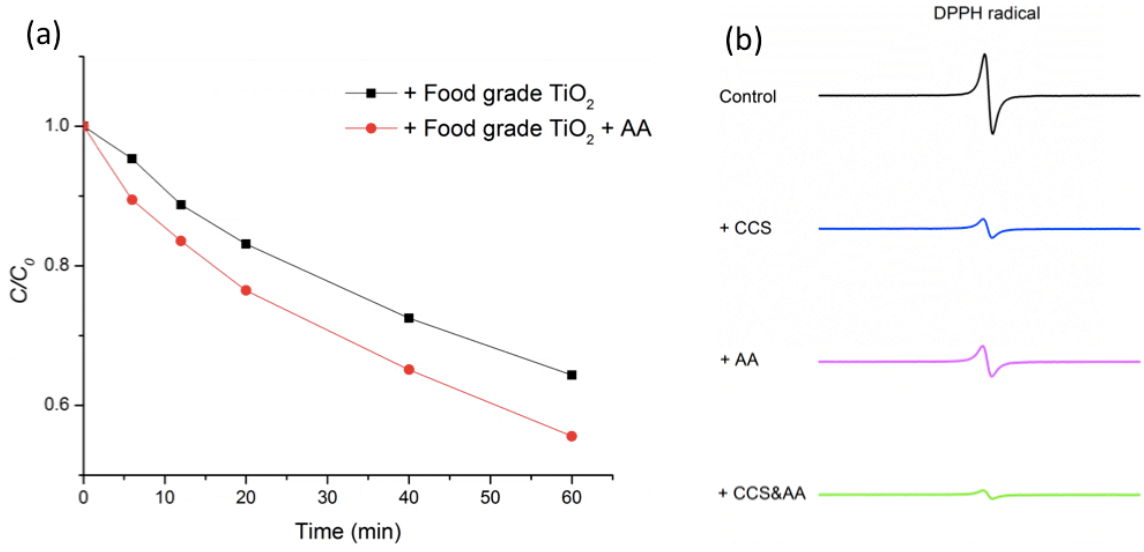

Figure 6-7 Effect of ascorbic acid (AA) on chlorophyllin copper sodium salted (CCS) degradation (a) and DPPH radical scavenging ability (b). Solutions in (a) contained 0.2 mg/mL food-grade TiO_2 and CCS with initial concentrations fixed at 200mg/L. Y axis in (a) represents the CCS concentration at corresponding simulated sunlight irradiation time versus the initial concentration. Control in (b) contained 25 mM DPPH radical and 10% ethanol. The ESR spectra were recorded at 2min after adding a final concentration at 200 mg/mL CCS, 100 mg/mL AA or both CCS and AA.

Since CCS and AA both function as antioxidants, we furthered investigated their radical scavenging effect using the stable radical 1,1-diphenyl-2-picryl-hydrazyl (DPPH•). DPPH radical scavenging is a commonly used simple and effective method to determine the overall radical quenching. The radical scavenging study is shown in Fig. 6-7b. Adding 200 mg/mL CCS to the reaction mixture 70% of DPPH• was quenched, while adding 100mg/mL AA lead to 61% DPPH• reduction. Adding AA and CCS together resulted in a higher radical quenching ability compared to adding them alone. This result indicates that adding AA to a solution containing CCS does not hinder the reaction between CCS and the radical. Therefore, AA did not promote the photocatalyzed degradation by direct damage to the dye molecule. It is very possible that surface modification of TiO_2 took place, in which the AA molecules bind to the OH site on TiO_2 surface, forming bidentate complexes through the *ortho*-substituted hydroxyl groups of furan ring. The AA molecules attached on the conduction band of TiO_2 accelerate superoxide radical formation via the one-electron reduction of dissolved oxygen by conduction band electrons (Yan et al., 2005).

6.4 Conclusion

To date, TiO_2 is used as food colorant without specific requirement on its phase composition. The sample food-grade TiO_2 particles we obtained were characterized as

nanoparticles, consisting only the photoactive anatase phase. Our results indicate that ROS promotion ability of TiO_2 is dramatically promoted when exposed to light irradiation. Food ingredient TiO_2 nanoparticles generate high levels of ROS. Even though current *in vitro* study demonstrates that nano-TiO_2 particles in food are relatively safe for gastrointestinal cells, the use of nano-sized TiO_2 should be used with caution due to their light induced activity. Upon sunlight irradiation, TiO_2 NPs can result degradation of synthetic azo dyes and in that way compromise food quality. Moreover, the TiO_2 surface consists of both hydrophobic and hydrophilic parts, which can be absorption sites that can trap active compounds, for example, the dietary antioxidant ascorbic acid. Such surface modification accelerates the decomposition of the green food color chlorophyllin copper sodium salt, potentially modulating its biological activity, compromising its antioxidant activity and thus reduces the beneficial antimutagenic activity.

Chapter 7 Conclusion and Future Recommendation

Nanotechnology brings promising applications that allow the production of better quality food by including new additives, enhancing nutrient delivery, improving hazard detection and fabricating novel packaging materials. However problems arise due to the lack of investigation on safety issues. Titanium dioxide nanoparticles (TiO_2 NPs) have been widely applied as a color agent to provide whiteness and/or opacity in paints, personal care products, as well as being used as food additives and drug delivery agents. The direct addition of engineered TiO_2 NPs as ingredient in food products has received attention because of its direct impact on food quality and public health. In addition to study the toxicity of TiO_2 NPs itself, effort should also be made to investigate the possible interaction between TiO_2 NPs and other active food ingredients such as food colors and antioxidants.

The results of this study suggest that potential problems may arise due to the interaction between dietary antioxidant and TiO_2 NPs in foods or other consumer related products. With the presence of TiO_2 NPs, the radical scavenging abilities of most antioxidants were compromised at different degrees. When exposed to sunlight, photoexcited TiO_2 NPs create electron/hole pairs as well as reactive oxygen species (ROS) known to result in oxidative damage. Oxidative damage could cause food quality deterioration including decomposition of color additives, such as the widely used azo dye FD&C Yellow No. 5 (tartrazine). When exposed to simulated sunlight, pH dependent generation of ROS, including hydroxyl radical (•OH), superoxide radical ($O_2^{-\bullet}$) and singlet oxygen ($^1O_2$) was detected in solutions containing TiO_2 NPs. The ROS generation of TiO_2 NPs was largely dependent on the crystal phase composition and the size of the particles. Food-grade TiO_2

powder was found to be in the nano-range and generated high level of ROS, resulting in the degradation of synthetic food dyes. Rutile phase TiO_2 promoted the least amount of ROS and did not show noticeable photo catalytic activity, suggesting that the use of rutile TiO_2 is safer when considering the possible oxidative quality deterioration of food products. The present study provided a systematic evaluation of the interaction between nanosized food ingredients and other food components. Conducted in aqueous solutions, this study simplified the reality where the food stuff is a complicated matrix that usually contains two or more ingredients.

Chapter 8 Appendix

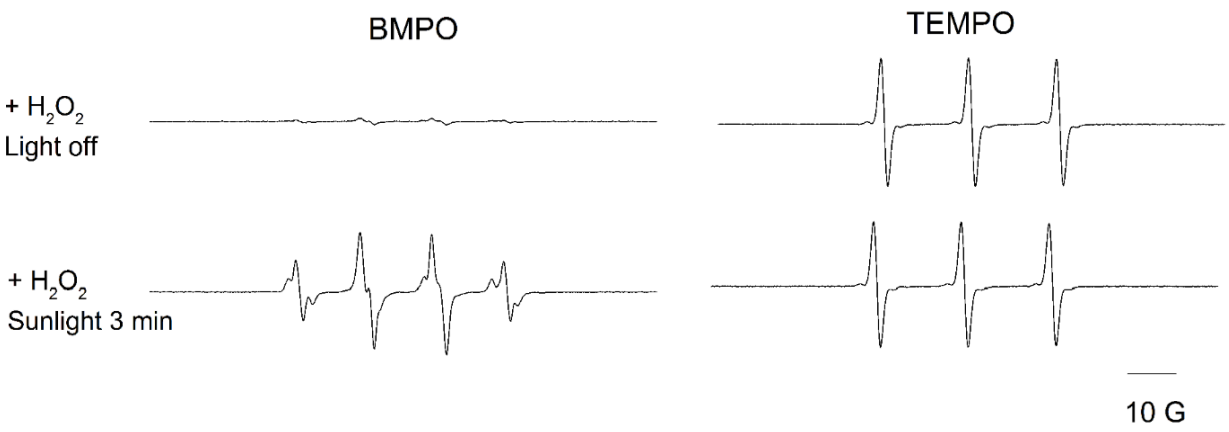

Figure A1 Effect of H_2O_2 on BMPO and TEMPO spin probes. ESR spectra were obtained from sample solutions containing 10mM H_2O_2 and spin probe BMPO (25 mM) or TEMPO (0.02 mM TEMPO), before or after 3 min exposure to simulated sunlight.

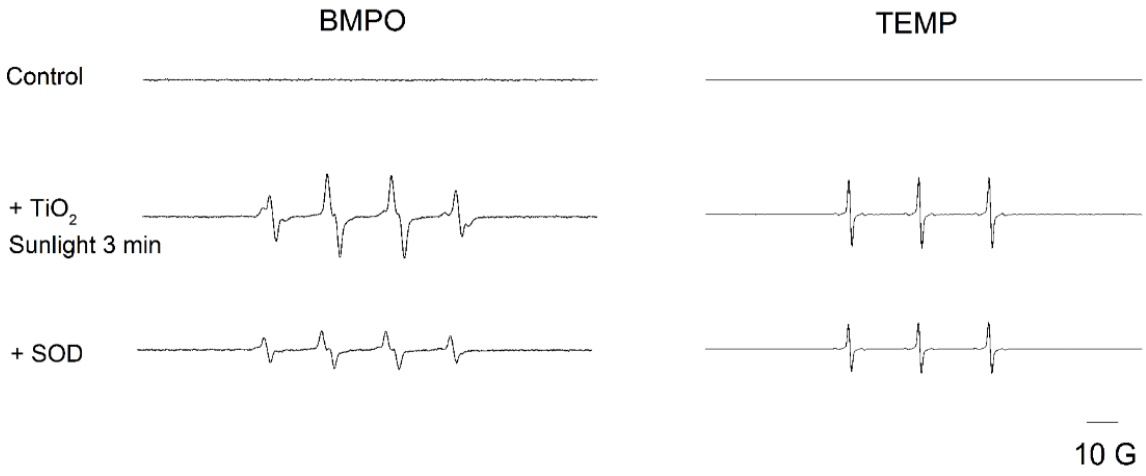

Figure A2 Effect of SOD on ESR signal generated from TiO_2 NPs solutions exposed to simulated sunlight. ESR spectra obtained from sample solutions contained 0.1 mg/mL TiO_2 NPs and 25 mM BMPO or 5mM TEMP spin probes, with or without addition of 0.2 U/mL SOD.

Sample: Sample 2-2

Type: Default

ID:

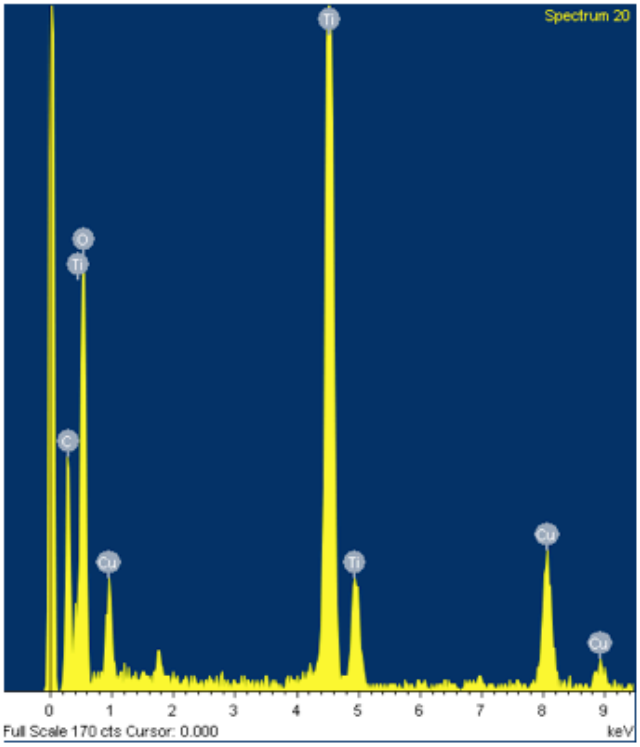

Spectrum processing :

Peak possibly omitted : 1.737 keV

Quantitation method : Cliff Lorimer thin ratio section.

Processing option : All elements analyzed (Normalised)

Number of iterations = 3

Standardless

Element	Weight%	Atomic%
C K	14.09	29.40
O K	26.08	40.85
Ti K	47.76	24.99
Cu K	12.07	4.76
Totals	100.00	

Figure B1 EDX analysis of anatase TiO_2 sample.

Reference

Agil A, Duran R, Barrero F et al. Plasma lipid peroxidation in sporadic Parkinson's disease. Role of the l-dopa. *J Neurol Sci* 2006; 240, 31-36.

Allahverdiyev AM, Abamor ES, Bagirova M et al. Investigation of antileishmanial activities of TiO_2@Ag nanoparticles on biological properties of *L. tropica* and *L. infantum* parasites in vitro. Exp Parasitol 2013; 135, 55-63.

Altenbach C, Flitsch SL, Khorana HG et al. Structural studies on transmembrane proteins. 2. Spin labeling of bacteriorhodopsin mutants at unique cysteines. *Biochemistry* 1989; 28, 19, 7806-12.

Altunkaya, A., Hedegaard, R. V., Harholt, J., Brimer, L., G. kmen, V., & Skibsted, L. H. Oxidative stability and chemical safety of mayonnaise enriched with grape seed extract. *Food Funct.,* 2013; 4, 1647-53

Alvarez, C. E., Alcover, S. R., Sainz, M. T., Anaya, T. M., & García, R. D. Especialidades farmacéuticas que contienen tartrazina. *Allergologia Et Immunopathologia,* 1981; 9, 1.

Aruoma, O. I., & Halliwell, B. *Free radicals and food additives*. London: Taylor & Francis. 1991

Banerjee, S., & Chattopadhyaya, M. C. Adsorption characteristics for the removal of a toxic dye, tartrazine from aqueous solutions by a low cost agricultural by-product. *Arabian Journal of Chemistry.*2013

Bar-Ilan O, Louis KM, Yang SP et al. Titanium dioxide nanoparticles produce phototoxicity in the developing zebrafish. Nanotoxicology. 2012; 6, 670-9.

Brand. W., Cuvelier, M., & Berset, C. Use of a free radical method to evaluate antioxidant activity. *Lwt - Food Science and Technology,* 1995; 28, 1, 25-30.

Brieger K, Schiavone S, Miller FJ Jr et al. Reactive oxygen species: from health to disease. *Swiss Med Wkly* 2012; 17, 142, 13659-72.

Buzea, C., Pacheco, I. I., & Robbie, K. Nanomaterials and nanoparticles, sources and toxicity. *Biointerphases,* 2007; 2, 4, 17-71.

Carlotti ME, Ugazio E, Gastaldi et al. Specific effects of single antioxidants in the lipid peroxidation caused by nano-titania used in sunscreen lotions. *J Photochem Photobiol B* 2009; 96, 2, 130-5.

Chang, W. T., Shao, Z. H., Yin, J. J., Mehendale, S., Wang, C. Z., Qin, Y., Li, J., Yuan, C. S.). Comparative effects of flavonoids on oxidant scavenging and ischemia-reperfusion injury in cardiomyocytes. *European Journal of Pharmacology,* 2007; 566, 58-66.

Chernomorsky, S., Rancourt, R., Virdi, K., Segelman, A., & Poretz, R. D. (January 01, 1998). Antimutagenicity, cytotoxicity and composition of chlorophyllin copper complex. *Cancer Letters, 120,* 2, 141.

Chen X, Mao SS Titanium Dioxide Nanomaterials: Synthesis, Properties, Modifications, and Applications. *Chem Rev* 2007; 107, 7, 2891-9.

Chen, X. X., Cheng, B., Yang, Y. X., Cao, A., Liu, J. H., Du, L. J., Liu, Y., Wang, H. Characterization and preliminary toxicity assay of nano-titanium dioxide additive in sugar-coated chewing gum. *Small (weinheim an Der Bergstrasse, Germany)* 2013; 9, 9-10.

Chen, Y.F., Lee, C.Y., Yeng, M.Y., & Chiu, H.T. The effect of calcination temperature on the crystallinity of TiO_2 nanopowders. *Journal of Crystal Growth,* 2013; 247, 3, 363.

Chu, W., Rao, Y., & Hui, W. Y. Removal of simazine in a UV/TiO_2 heterogeneous system. *Journal of Agricultural and Food Chemistry* 2009; 57, 15, 6944-9.

Cui Y, Liu H, Zhou M et al. Signaling pathway of inflammatory responses in the mouse liver caused by TiO_2 nanoparticles. *J Biomed Mater Res A* 2011; 96, 221–9.

Daimon T, Hirakawa T, Kitazawa M et al. Formation of singlet molecular oxygen associated with the formation of superoxide radicals in aqueous suspensions of TiO_2 photocatalysts. *Appl Catal A: Gen* 2008; 340, 169–175.

Daimon, T., & Nosaka, Y. Formation and Behavior of Singlet Molecular Oxygen in TiO_2Photocatalysis Studied by Detection of Near-Infrared Phosphorescence. *The Journal of Physical Chemistry C,* 2007; 111, 11, 4420-24.

Daimon, T., Hirakawa, T., Kitazawa, M., Suetake, J., & Nosaka, Y. Formation of singlet molecular oxygen associated with the formation of superoxide radicals in aqueous suspensions of TiO_2 photocatalysts. *Applied Catalysis A: General,* 2008; 340, 2, 169-175.

D'Arienzo M, Carbajo J, Bahamonde A et al. Photogenerated defects in shape-controlled TiO_2 anatase nanocrystals: a probe to evaluate the role of crystal facets in photocatalytic processes. *J Am Chem Soc*. 2011; 133, 17652-61

Deneke, S. M. Thiol-based antioxidants. *Current Topics in Cellular Regulation,* 2000; 36, 151-80.

Devasagayam, T. P. A., Tilak, J. C., Boloor, K. K., Sane, K. S., Ghaskadbi, S. S., & Lele, R. D. Free Radicals and Antioxidants in Human Health, Current Status and Future Prospects. *The Journal of the Association of Physicians of India,* 2004; 52, 794-808.

Dodd NJ, Jha AN. Photoexcitation of aqueous suspensions of titanium dioxide nanoparticles, an electron spin resonance spin trapping study of potentially oxidative reactions. *Photochem Photobiol*. 2011; 87, 632-40.

Dos Santos. T. C., Zocolo, G. J., Zanoni, M. V. B., Morales, D. A., & Umbuzeiro, G. D. A. Assessment of the breakdown products of solar/UV induced photolytic degradation of food dye tartrazine. *Food and Chemical Toxicology,* 2004; 68, 307-15.

Dragsted, L. O., Strube, M., & Larsen, J. C. Cancer-Protective Factors in Fruits and Vegetables: Biochemical and Biological Background. *Pharmacology & Toxicology,* 1993; 72, 116-135.

Dzwigaj S, Pezerat H. Singlet oxygen-trapping reaction as a method of $^1O_2$ detection: role of some reducing agents. *Free Radic Res* 1995; 23,103-15.

Echegoyen, Y., & Nerin, C. Nanoparticle release from nano-silver antimicrobial food containers. *Food and Chemical Toxicology,* 2013; 62, 16-22.

Ehrenshaft M, Mason RP. Protein radical formation on thyroid peroxidase during turnover as detected by immuno-spin trapping. *Free Radic Biol Med* 2006; 41, 422-30.

EU (1994). European Parliament and Council Directive on Colours, 94/36/EC. *Official J. Europ. Comm*., L237, 13-29.

FDA (2014). FDA Code of Federal Regulations, Title 21, Section 74.705, 74.1705, 74.2705, U.S., Washington, DC: Government Printing Office.

FDA (2014). FDA Code of Federal Regulations, Title 21, Section 73.575, U.S., Washington, DC: Government Printing Office.

Ferruzzi, M. G., & Schwartz, S. J. Thermal degradation of commercial grade sodium copper chlorophyllin. *Journal of Agricultural and Food Chemistry,* 2005; 53, 18, 7098-102.

Finkelstein E, Rosen GM, Rauckman EJ Spin trapping of superoxide and hydroxyl radical: Practical Aspects Arch Biochem Biophys 1980; 200, 1–16.

Frankel, E. N., & Meyer, A. S. The problems of using one-dimensional methods to evaluate multifunctional food and biological antioxidants. *Journal of the Science of Food and Agriculture,* 2000; 80, 13, 1925-1941.

Gago-Dominguez M, Castelao JE Role of lipid peroxidation and oxidative stress in the association between thyroid diseases and breast cancer. *Crit Rev Oncol Hematol* 2008; 68, 107-14.

Galano, A., & Alvarez-Idaboy, J. R. Glutathione: mechanism and kinetics of its non-enzymatic defense action against free radicals. *Rsc Advances,* 2011; 1, 9, 1763-1771.

Gallez B, Baudelet C, Jordan BF. Assessment of tumor oxygenation by electron paramagnetic resonance: principles and applications. *NMR Biomed* 2004; 17, 240-62.

Ghezzar, M. R., Ognier, S., Cavadias, S., Abdelmalek, F., & Addou, A. DBD"p"l"a"t"e-TiO"2 treatment of Yellow Tartrazine azo dye solution in falling film. *Separation and Purification Technology,* 2013; 104, 250-255.

Gomez, M., Arancibia, V., Rojas, C., & Nagles, E. Adsorptive stripping voltammetric determination of tartrazine and sunset yellow in gelatins and soft drink powder in the presence of cetylpyridinium bromide. *International Journal of Electrochemical Science,* 2012; 7, 8, 7493-7502.

González PM, Aguiar MB, Malanga G Electronic paramagnetic resonance (EPR) for the study of ascorbyl radical and lipid radicals in marine organisms. *Comp Biochem Physiol A, Physiol*. 2013; 165, 4, 439-47.

Goodeve CF, Kitchener JA The mechanism of photosensitisation by solids. Transactions of the Faraday Society 1938; 34, 902-8.

Gopal NO, Lo HH, Ke SC et al. A potential site for trapping photogenerated holes on rutile TiO_2 surface as revealed by EPR spectroscopy: An avenue for enhancing photocatalytic activity. *J Am Chem Soc*. 2005; 132, 32, 10982-3.

Guarini S, Bazzani C, Ricigliano G et al. Influence of ACTH-(1-24) on free radical levels in the blood of haemorrhage-shocked rats: direct ex vivo detection by electron spin resonance spectrometry. *Br J Pharmacol* 1996; 119, 1, 29-34.

Guzun R, Karu-Varikmaa M, Gonzalez-Granillo M et al. Mitochondria-cytoskeleton interaction: distribution of β-tubulins in cardiomyocytes and HL-1 cells. *Biochimica et Biophysica Acta* 2011, 1807, 4, 458-69.

Halliwell, B., & Gutteridge, J. M. C. (1999). *Free radicals in biology and medicine*. *Oxford: Clarendon Press*.

Hamal, D. B., Haggstrom, J. A., Marchin, G. L., Ikenberry, M. A., Hohn, K., & Klabunde, K. J. A multifunctional biocide/sporocide and photocatalyst based on titanium dioxide (TiO_2) codoped with silver, carbon, and sulfur. *Langmuir : the Acs Journal of Surfaces and Colloids,* 2010; 26, 4, 2805-10.

Hancock JT, Neill SJ, Wilson ID Nitric oxide and ABA in the control of plant function. *Plant Sci* 2011; 181, 5, 555-9.

Hansenne I., Lety A. *US Panten No. 5772987 A.* Washington, DC: U.S. Patent and Trademark Office. 1995

Hashimoto K, Irie H, Fujishima A TiO_2 Photocatalysis: A Historical Overview and Future Prospects. *Jpn J Appl Phys Part 1* 2005; 44, 12, 8269-85.

He C, Yu Y, Hu X et al. Influence of silver doping on the photocatalytic activity of titania films. *Appl Surf Sci* 2002; 200, 239-247.

He YY, Huang JL, Block ML et al Role of phagocyte oxidase in UVA-induced oxidative stress and apoptosis in keratinocytes. *J Invest Dermatol* 2005; 125, 560–6.

He, W., Kim, H.-K., Wamer, W. G., Melka, D., Callahan, J. H., & Yin, J.-J. Photogenerated Reactive Oxygen Species and Charge Carriers in ZnO/Au Hybrid Nanostructures Are Correlated with Enhanced Photocatalytic and Antibacterial Activity. *Journal of the American Chemical Society.* 2014; 136 (2) 750-757.

Hurum DC, Gray KA, Rajh T et al. Recombination pathways in the Degussa P25 formulation of TiO_2: surface versus lattice mechanisms. *J Phys Chem B* 2005; 109, 2, 977-80.

Hyde JS, Subczynski WK Spin label oximetry L.J. Berliner, J. Reuben (Eds.), Biological Magnetic Resonance, Vol 8: Spin Labeling: Theory and Applications, Plenum, New York 1989; 399–425.

India (2004(a)). Chewing gum and Bubble gum. In The Prevention of Food Adulteration Act and Rules, 1955, Appendix B, Section A.25.02.01, Directorate General of Health Services, Ministry of Health, New Deli.

India (2004(b)). Powdered concentrate mixes for fruit beverage drinks. In The Prevention of Food Adulteration Act and Rules, 1955, Appendix C, Table 3, Directorate General of Health Services, Ministry of Health, New Deli.

Jaeger A, Weiss DG & Jonas L Oxidative stress-induced cytotoxic and genotoxic effects of nano-sized titanium dioxide particles in human HaCaT keratinocytes. *Toxicology*. 2012; 296, 27-36.

Jaeger CD, Bard AJ Spin trapping and electron spin resonance detection of radical intermediates in photodecomposition of water at TiO_2 particulate systems. *J Phys Chem* 1979; 83, 3146–52.

James PE, Jackson SK, Grinberg OY et al. The effects of endotoxin on oxygen consumption of various cell types in vitro: an EPR oximetry study. *Free Radic Biol Med* 1995; 18, 4, 641-7.

Japan (2000). Titanium dioxide. In Japanese Specifications and Standards for Food Additives, 7th ed, Ministry of Health and Welfare, Tokyo.

Joseph, J. A., Shukitt-Hale, B., Denisova, N. A., Bielinski, D., Martin, A., McEwen, J. J., & Bickford, P. C. (January 01, 1999). Reversals of Age-Related Declines in Neuronal Signal Transduction, Cognitive, and Motor Behavioral Deficits with Blueberry, Spinach, or Strawberry Dietary Supplementation. *The Journal of Neuroscience: the Official Journal of the Society for Neuroscience, 19,* 18, 8114.

Kalyanaraman B, Perez-Reyes E, Mason RP The reduction of nitroso-spin traps in chemical and biological sysetms. A cautionary note. *Tetrahedron Letters* 1979, 20, 50, 4809-12.

Kavitha K, Sutha S, Prabhu M et al. *In situ* synthesized novel biocompatible titania-chitosan nanocomposites with high surface area and antibacterial activity. *Carbohydr Polym* 2013; 93,731-9.

Thamaphat K., Limsuwan P., Ngotawornchai B. Phase Characterization of TiO_2 Powder by XRD and TEM. *Kasetsart J. Nat. Sci.* 2008; 42 , 357 - 361

Kogo, A., Sakai, N., & Tatsuma, T. Photoelectrochemical analysis of size-dependent electronic structures of gold clusters supported on TiO_2. *Nanoscale,* 2012; 4, 14, 4217-21.

Konaka R, Kasahara E, Dunlap WC et al. Irradiation of titanium dioxide generates both singlet oxygen and superoxide anion. *Free Radic Biol Med* 1999; 27, 294-300.

Konstantinou, I. K., & Albanis, T. A. TiO_2-assisted photocatalytic degradation of azo dyes in aqueous solution: kinetic and mechanistic investigations - A review. *Applied Catalysis. B, Environmental,* 2004, 49, 1, 1.

Kuznetsov AV, Kehrer I, Kozlov AV et al. Mitochondrial ROS production under cellular stress: comparison of different detection methods. *Anal Bioanal Chem* 2011; 400, 2383-90.

Lacopini, P., Baldi, M., Storchi, P. & Sebastiani, L., 2008. Catechin, epicatechin, quercetin, rutin and resveratrol in grape: Content, in vitro antioxidant activity and interactions. J. Food Compos. Anal. 21, 589-598.

Lao, F., Zhao, Y., Qiu, Y., Liang, X.-J., Chen, C., Yin, J.-J., Wamer, W. G., ... Wang, P. C. The scavenging of reactive oxygen species and the potential for cell protection by functionalized fullerene materials. *Biomaterials,* 2009; 30, 4, 611-621.

Lavi, R., Sinyakov, M., Samuni, A., Shatz, S., Friedmann, H., Shainberg, A., Breitbart, H., ... Lubart, R. (January 01, 2004). ESR detection of 1O2 reveals enhanced redox activity in illuminated cell cultures. *Free Radical Research, 38,* 9, 893-902.

Lee, H. J., Seo, J. W., Lee, B. H., Chung, K. H., & Chi, D. Y. Syntheses and radical scavenging activities of resveratrol derivatives. *Bioorganic & Medicinal Chemistry Letters,* 2004; 14, 2, 463-6.

Lee, K. H., Jung, M. Y., & Kim, S. Y. Effects of Ascorbic Acid on the Light-Induced Riboflavin Degradation and Color Changes in Milks. *Journal of Agricultural and Food Chemistry,*1998; 46, 2, 407-410.

Li B, Ze Y, Sun Q et al. Molecular mechanisms of nanosized titanium dioxide-induced pulmonary injury in mice. *Plos One* 2013; 8, 2, e55563.

Li N, Duan Y, Hong M et al. Spleen injury and apoptotic pathway in mice caused by titanium dioxide nanoparticules. *Toxicol Lett* 2010; 195, 161–168.

Li, M., Yin, J. J., Wamer, W. G., & Lo, Y. M. Mechanistic characterization of titanium dioxide nanoparticle-induced toxicity using electron spin resonance. *Journal of Food and Drug Analysis*, 2014; 22, 1, 76-85.

Lion Y, Delmelle M, & Van de V. A. New method of detecting singlet oxygen production. *Nature* 1976; 263,442-3.

Lipovsky A, Levitski L, Tzitrinovich Z et al. The different behavior of rutile and anatase nanoparticles in forming oxy radicals upon illumination with visible light: an EPR study. *Photochem Photobiol* 2012; 88,14-20

Lipovsky, A., Gedanken, A., & Lubart, R. Visible Light-Induced Antibacterial Activity of Metaloxide Nanoparticles. *Photomedicine and Laser Surgery,* 2013; 31, 11, 526-530.

Liu S, Xu L, Zhang T, Ren G et al. Oxidative stress and apoptosis induced by nano-sized titanium dioxide in PC12 cells. *Toxicology* 2010; 267, 172-7.

Lobo, V., Patil, A., Phatak, A., & Chandra, N. Free radicals, antioxidants and functional foods: Impact on human health. *Pharmacognosy Reviews,* 2010; 4, 8, 118-26.

Lopez, M., Martinez, F., Del, V. C., Ferrit, M., & Luque, R. Study of phenolic compounds as natural antioxidants by a fluorescence method. *Talanta,* 2003; 60, 609-16.

Ma XY, Chen ZG, Hartono SB et al.. Fabrication of uniform anatase TiO_2 particles exposed by {001} facets. *Chem Commun*, 2010; 35, 6608-10.

Magnuson, B. A., Jonaitis, T. S., & Card, J. W. A brief review of the occurrence, use, and safety of food-related nanomaterials. *Journal of Food Science,* 2011, 76, 6.

Maness PC, Smolinski S, Blake DM et al. Bactericidal activity of photocatalytic TiO(2) reaction: toward an understanding of its killing mechanism. *Appl Environ Microbiol* 1999; 65, 9, 4094-8.

Mansfield, C. M., Alloy, M. M., Hamilton, J., Verbeck, G. F., Newton, K., Klaine, S. J., & Roberts, A. P. Photo-induced toxicity of titanium dioxide nanoparticles to Daphnia magna under natural sunlight. *Chemosphere,* 2014; 120, 206-210.

Maroga, M. V., Héquet, V., Andrès, Y., Pastrana-Martínez, L. M., Doña-Rodríguez, J. M., Silva, A. M., & Falaras, P. Photocatalytic degradation of endocrine disruptor compounds under simulated solar light. *Water Research,* 2013; 47, 12, 3997-4005.

Mason RP. Using anti-5,5-dimethyl-1-pyrroline N-oxide (anti-DMPO) to detect protein radicals in time and space with immuno-spin trapping. *Free Radic Biol Med* 2004; 36,1214-23.

Marmion, D. M. (1991). *Handbook of U.S. colorants: Foods, drugs, cosmetics, and medical devices*. New York: Wiley.

Meetani, M. A., Rauf, M. A., Hisaindee, S., Khaleel, A., AlZamly, A., & Ahmad, A. Mechanistic studies of photoinduced degradation of Orange G using LC/MS. *Rsc Advances,* 2011; 1, 3, 490-497.

Miller, R. J., Bennett, S., Keller, A. A., Pease, S., Lenihan, H. S., & Gilbert, J. A. TiO_2 Nanoparticles Are Phototoxic to Marine Phytoplankton. *Plos One,* 2012, 7, 1.

Mills, A. Oxygen indicators and intelligent inks for packaging food. *Chemical Society Reviews,* 2005; 34, 12, 1003-11.

Min, D. B., & Boff, J. M. Chemistry and Reaction of Singlet Oxygen in Foods. *Comprehensive Reviews in Food Science and Food Safety,* 2002; 1, 2, 58-72.

Mu, L., & Sprando, R. L. Application of Nanotechnology in Cosmetics. *Pharmaceutical Research,* 2010; 27, 8, 1746-1749.

Nagaveni K, Sivalingam G, Hegde MS et al. Photocatalytic degradation of organic compounds over combustion-synthesized nano-TiO_2. *Environ Sci Technol* 2004; 38, 5, 1600-4.

Ness, A. R., & Powles, J. W. Review article. Fruit and vegetables, and cardiovascular disease: a review. *International Journal of Epidemiology,* 1997; 26, 1, 1-13.

Nettis, E., Colanardi, M. C., Ferrannini, A., & Tursi, A. Suspected tartrazine-induced acute urticaria/angioedema is only rarely reproducible by oral rechallenge. *Clinical & Experimental Allergy,* 2003; 33, 12, 1725-1729.

Neverov, K. V., Krasnovsky, A. A., & Krasnovsky, A. A. Phosphorescence study of chlorophyll d photophysics. Determination of the energy and lifetime of the photo-excited triplet state. Evidence of singlet oxygen photosensitization. *Photosynthesis Research,* 2011; 108, 2-3.

Niki, E. Action of ascorbic acid as a scavenger of active and stable oxygen radicals. *The American Journal of Clinical Nutrition,* 1991, 54, 6.

NNI, 2014 http://www.nano.gov/about-nni/what/funding

Nosaka Y, Daimon T, Nosaka AY et al. Singlet oxygen formation in photocatalytic TiO_2 aqueous suspension. *J Phys Chem B* 2004; 6, 2917–8.

Nosaka, A. Y., Tanaka, G., & Nosaka, Y. The behaviors of glutathione and related amino acids in the TiO_2 photocatalytic system. *The Journal of Physical Chemistry. B,* 2012; 116, 36, 11098-102.

Ochiai, T., Masuko, K., Tago, S., Nakano, R., Niitsu, Y., Kobayashi, G., Horio, K., ... Fujishima, A. Development of a hybrid environmental purification unit by using of excimer VUV lamps with TiO_2coated titanium mesh filter. *Chemical Engineering Journal,* 2013; 218, 327-332.

Ou, Y., Lin, J.D., Zou, H.M., & Liao, D.W. Effects of surface modification of TiO 2 with ascorbic acid on photocatalytic decolorization of an azo dye reactions and mechanisms. *Journal of Molecular Catalysis. A, Chemical,* 2005; 241, 1, 59-64.

Packer, L., Rimbach, G., & Virgili, F. Antioxidant activity and biologic properties of a procyanidin-rich extract from pine (pinus maritima) bark, pycnogenol. *Free Radical Biology and Medicine,* 1999; 27, 704-724.

Park, H., Neppolian, B., Jie, H. S., Ahn, J. P., Park, J. K., Anpo, M., & Lee, D. Y. Preparation of bimetal incorporated TiO2 photocatalytic nano-powders by flame method and their photocatalytic reactivity for the degradation of diluted 2-propanol. *Current Applied Physics*, 2007; 7, 2, 118-123.

Perez-Vincente, A., Serrano, P., Abellan, P., & Garcia-Viguera, C. Influence of packaging material on pomegranate juice colour and bioactive compounds, during storage. *Journal of the Science of Food and Agriculture,* 2004; 84, 639-644.

Popov, A. P., Priezzhev, A. V., Lademann, J., & Myllylä, R. TiO_2 nanoparticles as an effective UV-B radiation skin-protective compound in sunscreens. *Journal of Physics D: Applied Physics,* 2005; 38, 15, 2564-2570.

Poul, M., Jarry, G., Elhkim, M. O., & Poul, J. M. Lack of genotoxic effect of food dyes amaranth, sunset yellow and tartrazine and their metabolites in the gut micronucleus assay in mice. *Food and Chemical Toxicology,* 2009; 47, 2, 443-448.

Poulios, I., & Tsachpinis, I. Photodegradation of the textile dye Reactive Black 5 in the presence of semiconducting oxides. *Journal of Chemical Technology & Biotechnology,* 1999; 74, 4, 349-357.

Ranguelova K, Bonini MG, Mason RP (Bi)sulfite oxidation by copper, zinc-superoxide dismutase: Sulfite-derived, radical-initiated protein radical formation. *Environ Health Perspect* 2010; 118, 970-5.

Ray PC, Yu H, Fu, PP Toxicity and environmental risks of nanomaterials: Challenges and future needs. *J Environ Sci Health C Environ Carcinog Ecotoxicol Rev* 2009; 27, 1, 1-35.

Reeves JF, Davies SJ, Dodd NJ et al. Hydroxyl radicals (•OH) are associated with titanium dioxide (TiO_2) nanoparticle-induced cytotoxicity and oxidative DNA damage in fish cells. *Mutat Res*. 2008; 640,113-22.

Regnström J, Nilsson J. Lipid oxidation and inflammation-induced intimal fibrosis in coronary heart disease. *The Journal of Laboratory and Clinical Medicine* 1994; 124, 2, 162-8.

Rehn B, Seiler F, Rehn S et al. Investigations on the inflammatory and genotoxic lung effects of two types of titanium dioxide: untreated and surface treated. *Toxicol Appl Pharmacol* 2003; 189, 2, 84-95.

Rembold, M., & Kramer, H. Singlet Oxygen as an Intermediate in the Catalytic Fading of Dye Mixtures. *Journal of the Society of Dyers and Colourists,* 1978; 94, 1, 12-17.

Robichaud, C. O., Uyar, A. E., Darby, M. R., Zucker, L. G., & Wiesner, M. R. Estimates of upper bounds and trends in nano-TiO_2 production as a basis for exposure assessment. *Environmental Science & Technology,* 2009; 43, 12, 4227-33.

Roco, M. C., Mirkin, C. A., Hersam, M. C., & SpringerLink (Online service). (2011). *Nanotechnology research directions for societal needs in 2020: Retrospective and outlook*. United States: World Technology Evaluation Center.

Rosenthal IC, Murali K, Yang GC et al. A new approach for EPR detection of hydroxyl radicals by reaction with sterically hindered cyclic amines and oxygen. *FEBS Lett* 1987; 222, 75–78.

Roubaud, V., Sankarapandi, S., Kuppusamy, P., Tordo, P., & Zweier, J. L. Quantitative Measurement of Superoxide Generation and Oxygen Consumption from Leukocytes Using Electron Paramagnetic Resonance Spectroscopy. *Analytical Biochemistry,* 1998; 257, 2, 210-217.

Sabliov, C. M., Astete, C. E., Astete, C. E., Khachaturyan, M., Khachatryan, L., & Leonardi, C. Effects of Temperature and UV Light on Degradation of ÎĦ-Tocopherol in Free and Dissolved Form. *Journal of the American Oil Chemists' Society,* 2009; 86, 9, 895-902.

Sadeghipour, M., Terreux, R., & Phipps, J. Flavonoids and tyrosine nitration: structure-activity relationship correlation with enthalpy of formation. *Toxicology in Vitro,* 2005; 19, 2, 155-165.

Sharma, P., Ganti, S., & Bhate, N. Effect of surfaces on the size-dependent elastic state of nano-inhomogeneities. *Applied Physics Letters,* 2003; 82, 535-537.

Sakai, N., Wang, R., Fujishima, A., Watanabe, T., & Hashimoto, K. PHYSISORPTION, INTERFACIAL FILMS, MEMBRANES - Effect of Ultrasonic Treatment on Highly Hydrophilic TiO_2 Surfaces. *Langmuir : the Acs Journal of Surfaces and Colloids,* 1998; 14, 20, 5918.

Salem, M. A., Abdel-Halim, S. T., El-Sawy, A. E., & Zaki, A. B. Kinetics of degradation of allura red, ponceau 4R and carmosine dyes with potassium ferrioxalate complex in the presence of H2O2. *Chemosphere,* 2009; 76, 8, 1088-1093.

Sanders K, Degn LL Mundy WR et al. In vitro phototoxicity and hazard identification of nano-scale titanium dioxide. *Toxicol Appl Pharmacol* 2011; 258, 2, 226-36.

Sarkar A, Das J, Manna P et al. Nano-copper induces oxidative stress and apoptosis in kidney via both extrinsic and intrinsic pathways. *Toxicology* 2011; 290, 208-17.

Sawada T, Yoshino F, Kimoto K et al. ESR detection of ROS generated by TiO_2 coated with fluoridated apatite. *J Dent Res* 2010; 89, 848-53.

Sayes CM, Wahi R, Kurian PA et al. Correlating nanoscale titania structure with toxicity: a cytotoxicity and inflammatory response study with human dermal fibroblasts and human lung epithelial cells. *Toxicol Sci* 2006; 92, 174-85.

Scherz-Shouval R, Elazar Z Regulation of autophagy by ROS, physiology and pathology. *Trends in Biochemical Sciences* 2011; 36, 1, 30-8.

Scott, N., & Chen, H. Nanoscale Science and Engineering for Agriculture and Food Systems. *Industrial Biotechnology,* 2013; 9, 1, 17-18.

Servili, M., & Montedoro, G. F. Contribution of phenolic compounds to virgin olive oil quality. *European Journal of Lipid Science and Technology,* 2002; 104, 602-613.

Sha, B., Gao, W., Han, Y., Wang, S., Wu, J., Xu, F., & Lu, T. Potential application of titanium dioxide nanoparticles in the prevention of osteosarcoma and

chondrosarcoma recurrence. *Journal of Nanoscience and Nanotechnology, 2013,* 2, 1208-11.

Sharma VK Aggregation and toxicity of titanium dioxide nanoparticles in aquatic environment-a review. *J Environ Sci Health Part A* 2009; 44, 14, 1485-95.

Sökmen M, Değerli S, Aslan A Photocatalytic disinfection of Giardia intestinalis and Acanthamoeba castellani cysts in water. *Exp Parasitol* 2009;119, 44-8.

Solomon, O., Svanberg, U., & Sahlström, A. Effect of oxygen and fluorescent light on the quality of orange juice during storage at 8°C. *Food Chemistry* 1995 53, 4, 363-368.

Sumithra, M., & Vasugi, R. N. Micro-encapsulation and nano-encapsulation of denim fabrics with herbal extracts. *Indian Journal of Fibre and Textile Research,* 2012, 37, 4, 321-325.

Sun Q, Tan D, Ze Y et al. Pulmotoxicological effects caused by long-term titanium dioxide nanoparticles exposure in mice. *J Hazard Mater* 2012; 235–236, 47–53.

Tada M, Yokoyama H, Ito O et al. Evaluation of the hepatic reduction of a nitroxide radical in rats receiving ascorbic acid, glutathione or ascorbic acid oxidase by in vivo electron spin resonance study. *J Gastroenterol Hepatol* 2004; 19, 99-105.

Tanaka, A., Ogino, A., Iwaki, M., Hashimoto, K., Ohnuma, A., Amano, F., Ohtani, B., ... Kominami, H. Gold-titanium(IV) oxide plasmonic photocatalysts prepared by a colloid-photodeposition method: correlation between physical properties and photocatalytic activities. *Langmuir : the Acs Journal of Surfaces and Colloids,* 2012; 28, 36, 13105-11.

Tournebize J, Sapin-Minet A, Bartosz G et al Pitfalls of assays devoted to evaluation of oxidative stress induced by inorganic nanoparticles. *Talanta* 2013; 116,753-63.

Unnithan J, Rehman MU, Ahmad FJ et al. Aqueous synthesis and concentration-dependent dermal toxicity of TiO_2 nanoparticles in Wistar rats. *Biol Trace Elem Res*. 2011;143, 1682-94.

Unno, T., Sugimoto, A., & Kakuda, T. Scavenging effect of tea catechins and their epimers on superoxide anion radicals generated by a hypoxanthine and xanthine oxidase system. *Journal of the Science of Food and Agriculture,* 2000; 80, 5, 601-606.

Vachirapatama, N., Mahajaroensiri, J., & Visessanguan, W. Identification and determination of seven synthetic dyes in foodstuffs and soft drinks on monolithic C18 column by high performance liquid chromatography. *Journal of Food and Drug Analysis,* 2008; 16, 5, 77-82.

Vamathevan V, Amal R, Beydoun D et al. Photocatalytic oxidation of organics in water using pure and silver-modified titanium dioxide particles. *J Photochem Photobiol A* 2002, 148, 233-245.

Vamvakaki, V., & Chaniotakis, N. A. Pesticide detection with a liposome-based nano-biosensor. *Biosensors and Bioelectronics,* 2007; 22, 12, 2848-2853.

Wamer WG, Yin JJ, Wei RR. Oxidative damage to nucleic acids photosensitized by titanium dioxide. *Free Radic Biol Med* 1997; 23, 851-8.

Wamer WG, Yin JJ. Photocytotoxicity in human dermal fibroblasts elicited by permanent makeup inks containing titanium dioxide. *J Cosmet Sci* 2011; 62, 535-47.

Wang CC, Wang S, Xia Q et al. Phototoxicity of zinc oxide nanoparticles in HaCaT keratinocytes-generation of oxidative DNA damage during UVA and visible light irradiation. *J Nanosci Nanotechnol* 2013; 13, 3880-8.

Wang J, Ma J, Dong L et al. Effect of anatase TiO_2 nanoparticles on the growth of RSC-364 rat synovial cell. *J Nanosci Nanotechnol* 2013;13, 3874-9.

Wang, G., Xu, L., Zhang, J., Yin, T., & Han, D. Enhanced Photocatalytic Activity of Powders (P25) via Calcination Treatment. *International Journal of Photoenergy,* 2012; 50, 1-9.

Wang, J., Zhang, Y., Yan, N., Chen, J., & Rittmann, B. E. Enhanced phenol bioavailability by means of photocatalysis. *Biodegradation,* 2013; 24, 5, 597-602.

Wang, S. Y., Chen, C. T., & Yin, J. J. Effect of allyl isothiocyanate on antioxidants and fruit decay of blueberries. *Food Chemistry,* 2010; 120, 1, 199-204.

Wang, X., Zhang, J. ., Zhu, W. ., & Shi, L. Preparation and properties of nano-TiO_2 modified interior wall paint. *Journal- Shanghai University,* 2007; 11, 4, 432-436.

Weir, A., Westerhoff, P., Fabricius, L., Hristovski, K., & von, G. N. Titanium dioxide nanoparticles in food and personal care products. *Environmental Science & Technology,* 2012; 46, 4, 2242-50.

Weisz, A., Ridge, C. D., Roque, J. A., Mazzola, E. P., & Ito, Y. Preparative separation of two subsidiary colors of FD&C Yellow No. 5 (Tartrazine) using spiral high-speed counter-current chromatography. *Journal of Chromatography A,* 2013; 1343, 91-100.

Wennermark, B., Ahlmen, H., & Jaegerstad, M. Improved Vitamin E Retention by Using Freshly Milled Whole-Meal Wheat Flour during Drum-Drying. *Journal of Agricultural and Food Chemistry,* 1994; 42, 6, 1348.

Wu, N., Wang, J,Tafen DN et al. Shape-Enhanced Photocatalytic Activity of Single-Crystalline Anatase TiO_2 (101) Nanobelts. *J Am Chem Soc* 2010; 132, 19, 6679-85.

Wu, P., Xie, R., Imlay, K., & Shang, J. K. Visible-light-induced bactericidal activity of titanium dioxide codoped with nitrogen and silver. *Environmental Science & Technology,* 2010; 44, 18, 6992-7.

Xue C, Wu J, Lan F et al. Nano titanium dioxide induces the generation of ROS and potential damage in HaCaT cells under UVA irradiation. *J Nanosci Nanotechnol* 2010; 10, 12, 8500-7.

Yadav, D. K., & Pospíšil, P. Evidence on the formation of singlet oxygen in the donor side photoinhibition of photosystem II: EPR spin-trapping study. *Plos One,* 2012; 7, 9.

Yan, J., Wu, G., Guan, N., Li, L., Li, Z., & Cao, X. Understanding the effect of surface/bulk defects on the photocatalytic activity of TiO_2: anatase versus rutile. *Physical Chemistry Chemical Physics,* 2013; 15, 26, 10978.

Yang, Y., Doudrick, K., Bi, X., Hristovski, K., Herckes, P., Westerhoff, P., & Kaegi, R. Characterization of food-grade titanium dioxide: the presence of nanosized particles.*Environmental Science & Technology,* 2014; 48, 11, 6391-400.

Yilmaz, Y., & Toledo, R. T. Major flavonoids in grape seeds and skins: antioxidant capacity of catechin, epicatechin, and gallic acid. *Journal of Agricultural and Food Chemistry,* 2004; 52, 2, 255-60.

Yin JJ, Fu PP Magnetic resonance in food science: Challenges in a changing world. Eds. Gudjonsdottir M, Belton P, Webb G, *The Royal Society of Chemistry* 2009, 213.

Yin JJ, Liu J, Ehrenshaft M, et al. Phototoxicity of nanotitanium dioxides in HaCaT keratinocytes--generation of reactive oxygen species and cell damage. *Toxicol Appl Pharmacol* 2012; 263, 81-8.

Yin JJ, Mossoba MM, Kramer JK et al. Effects of conjugated linoleic acid on oxygen diffusion-concentration product and depletion in membranes by using electron spin resonance spin-label oximetry. *Lipids* 1999; 34, 10, 1017-23.

Yin JJ, Zhao B, Xia Q et al. Electron Spin Resonance Spectroscopy for Studying the Generation and Scavenging of Reactive Oxygen Species by Nanomaterials in Nanopharmaceutics: The potential application of nanomaterials. *Singapore: World Scientific Pub. Co.* 2012; 375-400.

Yin, J. J., Lao, F., Fu, P. P., Wamer, W. G., Zhao, Y., Wang, P. C., Qiu, Y., Chen, C. The scavenging of reactive oxygen species and the potential for cell protection by functionalized fullerene materials. *Biomaterials,* 2009; 30, 4, 611-21.

Yu, K. P., Huang, Y. T., & Yang, S. C. The antifungal efficacy of nano-metals supported TiO_2 and ozone on the resistant Aspergillus niger spore. *Journal of Hazardous Materials,* 2013; 261,155-62.

Yuan Y, Ding J, Xu J et al. TiO_2 nanoparticles co-doped with silver and nitrogen for antibacterial application. *J Nanosci Nanotechnol* 2010; 10, 8, 4868-74.

Zhan, H., Chen, K., & Tian, H. Photocatalytic degradation of acid azo dyes in aqueous TiO_2 suspensionII. The effect of pH values. *Dyes and Pigments,* 1998; 37, 3, 241-7.

Zhang, D., & Hamauzu, Y. Phenolics, ascorbic acid, carotenoids and antioxidant activity of broccoli and their changes during conventional and microwave cooking. *Food Chemistry,* 2004; 88, 4, 503-9.

Zhao, H., Joseph, J., Zhang, H., Karoui, H., & Kalyanaraman, B. Synthesis and biochemical applications of a solid cyclic nitrone spin trap: a relatively superior trap for detecting superoxide anions and glutathiyl radicals. *Free Radical Biology and Medicine,* 2001; 31, 5, 599-606.

Zhou, Y.T., He, W., Yin, J., Lo, Y. M., Hu, X., & Wu, X. Effect of silver nanomaterials on the activity of thiol-containing antioxidants. *Journal of Agricultural and Food Chemistry,* 2013; 61, 32, 7855-62.

Zhu, X., Zhou, J., & Cai, Z. The toxicity and oxidative stress of TiO_2 nanoparticles in marine abalone (Haliotis diversicolor supertexta). *Marine Pollution Bulletin,* 2011, 63, 334-8.